Doctor of Philosophy

Fault Diagnosis of a Helical Gearbox based on Empirical Wavelet Transform

The Graduate School

of the University of Ulsan

Department of Mechanical and Automotive Engineering

Peng Wang

Fault Diagnosis of a Helical Gearbox based on Empirical Wavelet Transform

Supervisor: Professor Chang-Myung Lee

Author: Peng Wang

Department of Mechanical and Automotive Engineering
University of Ulsan

A dissertation submitted to the faculty of the University of Ulsan in partial fulfillment the requirement for the degree of Doctor of Philosophy in the Department of Mechanical and Automotive Engineering.
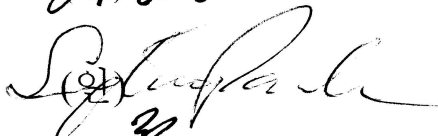
Ulsan, Korea
May 30th, 2019
Approved by

Professor Chang-Myung Lee

Peng Wang 의 공학박사학위 논문을 인준함

심사위원장   김도중

심사위원   이병룡

심사위원   박성태   (인)

심사위원   전두환   (인)

심사위원   이장명   (인)

울산대학교 대학원

2019 년 5 월

ABSTRACT

Fault Diagnosis of a helical gearbox based on empirical wavelet transform

Peng Wang
Department of Mechanical and Automotive Engineering
The Graduate School
University of Ulsan

A gearbox is an essential power transmission component for the rotating machine systems, in which working conditions will directly affect the performance of the whole mechanical equipment. The development of condition monitoring and fault diagnosis systems for Gearboxes has received considerable attention in recent years. Extracting fault feature information from a gearbox's vibration signal by using the signal processing methods has been the key to the fault diagnosis for the gearbox. Therefore, reliable fault detection is necessary to ensure productive and safe operations.

Generally, when a gearbox is damaged, accurate identification of the side-band features can be used to detect the condition of machinery equipment to reduce financial losses. However, the side-band features of damaged gears that are constantly disturbed by strong jamming are embedded in the background noise. In this paper, a hybrid signal-processing method is proposed based on a spectral subtraction (SS) denoising algorithm combined with an empirical wavelet transform (EWT) to extract the side-band feature of gear faults. Firstly, SS is used to estimate the real-time noise information, which is used to enhance the fault signal of a helical gearbox from a vibration signal with strong noise disturbance. The empirical wavelet transform can extract amplitude-modulated/frequency-modulated (AM-FM) components of a signal using different filter bands that are designed in accordance with the signal properties.

Secondly, the fault signal is obtained by building a multi-body dynamics model of the gearbox system with ADAMS software. The influence of flexible body deformation is considered in the process of dynamic simulation, so a flexible gear is used to simulate the gear fault dynamic characteristics. The experiment shows the feasibility and availability of the multi-body dynamics model with different algorithms.

Then, the signal processing techniques viz empirical decomposition (EMD), local mean decomposition (LMD) and discrete wavelet transform (DWT) for diagnostics of a gearbox, are majorly employed. The spectral subtraction-based adaptive empirical wavelet transform (SS-AEWT) method was applied to estimate the gear side-band feature for different tooth breakages and the strong background noise. The verification results show that the proposed method gives a clearer indication of gear fault characteristics with different tooth breakages and the different signal-noise ratio (SNR) than the conventional EMD and LMD methods. Finally, the fault characteristic frequency of a damaged gear suggests that the proposed SS-AEWT method can accurately and reliably diagnose faults of a gearbox. Furthermore, the simulated model is an efficient approach to test the performance of a new algorithm working in the different conditions, in which the variables would be limited and the model is easy to be modified. Therefore, this simulation model would be useful in the development of new algorithms.

ACKNOWLEDGMENTS

First of all, I would like to express my sincere gratitude to Prof. Chang-Myung Lee, my supervisor, for his invaluable guidance, encouragement, and living supporting during my Ph.D. program. Sincere gratitude is also expressed to the members of the advisory committee in the graduate school of the University of Ulsan, who are Prof. Byung-Ryong Lee, Prof. Do-Joong Kim, Prof. Jung-Soo Ryue, and Prof. Du-Hwan Chun and the other professors who had taught me and helped me in the fields of mechanical, automotive Engineering, sound and vibration.

Specifically, I wish to thank Prof. Hui He, the supervisors of my M.D. program in the Liaoning University of Technology, for their encouragement, guidance, and help during the period of the graduate study. I wish to express my thanks to senior brothers Zhen-Hua Xu, Hao Liu and Zhi Qiu, for their recommendations, encouragements and help during my study in Korea.

Special thanks are extended to the members in the Sound and Vibration laboratory of the University of Ulsan, especially to Huan-Yu Dong, Guang-Quan Hou, Qi Wu, Min Chen and Hang Su for their advice on this manuscript and the help of life in Korea. I would like to thank the members of the SCIEN company, who are Woo-Jin Kim, Chae-Rok Lim, and Young-Wook Bae, for their guidance and help for experiments implementation during my Ph.D. program. Same thanks are also regarded to my friends, Ya-Li Yang, Jing Liu, Jin-Cheng Wang, Ji Liu, Tian-Jun Zhou, Ying-Xiao Yu, etc., for their help in my daily life.

Finally, I would like to express my sincere gratitude to my parents for their understanding and encouragement.

CONTENTS

LIST OF FIGURES

LIST OF TABLES

ABBREVIATIONS

AE	Acoustic emission
TSA	Time-domain synchronous average
ANC	Adaptive noise canceling
SNR	Signal noise ratio
TSA	Time synchronous averaging
STFT	Short-time Fourier transform
WVD	Wigner-Ville distribution
WA	Wavelet analysis
EMD	Empirical mode decomposition
LMD	Local mean decomposition
HHT	Hilbert-Huang transform
IMF	Intrinsic mode function
DWT	Discrete wavelet transforms
SVM	Support vector machines
EEMD	Ensemble empirical mode decomposition
ITD	Intrinsic time-scale decomposition
LCD	Local characteristic-scale decomposition
MBD	Multibody dynamics
IDFT	Inverse discrete Fourier transform
EWT	Empirical wavelet decomposition
SES	Squared envelope spectrum
HS	Hilbert Spectral

ECG	Electrocardiogram
PFs	Product functions
FEM	Finite Element Method
MNF	Modal neutral file
MBS	Multibody System Simulation
2D	Trilateral
3D	Tetrahedron

NOMENCLATURES

$x(t)$	Complex signal
$X(f)$	Fourier transform of complex signal
$\text{Im}[\bullet]$	Imaginary part
$\text{Re}[\bullet]$	Real part
$STFT(t, f)$	Short-time Fourier transform
$g(t)$	A window function
$WT(a, b)$	Wavelet transform
$W(t, \omega)$	Wigner-Ville distribution
a	Scaling factor
b	Time shift factor
$\psi_{a,b}(t)$	Mother wavelet
$z(m)$	Measured mixed-signal
$s(m)$	Vibration signal of the gear
$n(m)$	Additive noise
m	Discrete-time index
$Z(k)$	Discrete Fourier transform of $z(m)$
$S(k)$	Discrete Fourier transform of $s(m)$
$N(k)$	Discrete Fourier transform of $n(m)$
$\mathcal{F}\{y(m)\}$	Discrete Fourier transform of a time signal
k	Discrete-frequency index
$\left|\hat{N}(k)\right|^2$	Estimate of the noise power spectrum

$\left\|\hat{S}(k)\right\|^2$	Enhanced signal power spectrum
α	Over-subtracting multiplication factor
SNR	Signal noise ratio
β	Spectral flooring parameter
$\phi(k)$	A phase function
$\beta(x)$	An arbitrary function
$\hat{s}(m)$	Estimated value of the faulty signal obtained by the spectral subtraction method
$\phi(k)$	Phase function
Λ_n	Bandpass filter
$\hat{\phi}_n(\omega)$	Empirical scaling function
$\hat{\psi}_n(\omega)$	Empirical wavelet
$W_s^\varepsilon(n,t)$	Detail coefficient of empirical wavelet transform
$DW(j,k)$	Discrete wavelet
M	Equivalent mass of gear pair
C	Gear meshing damping
$k(t)$	Gear meshing stiffness
$F(t)$	Dynamic load
E_1	Average static elastic deformation
$v_{sg}(t)$	Gear vibration signal
$A_{sgm}(\overline{L},\theta_s)$	The amplitude due to tooth deflection
$\overline{E}_{sgm}$	The mean amplitude
N_{sg}	The number of teeth on the gear

$\beta_{sg}(\theta_s)$	The phase modulation due to torque fluctuations
ϕ_{sgm}	The phase of harmonic
$A_{sgm}(\bar{L}, \theta_s)$	Fluctuating load periodic
$\bar{L}$	The mean load
$\bar{A}_{sgm}(\bar{L})$	The amplitude due to the mean load
$\alpha_{sg}(\theta_s)$	The amplitude modulation due to fluctuating load
β_{sg}	Load dependant phase modulation
α_{sg}	Amplitude modulation effects
ξ_{sgk}	The phase of harmonic

Chapter 1 Introduction

1.1 Research background

Gearboxes are common mechanical equipment that is used to change the rotation speed and transmit power. Due to the advantages of the high driving torque, high transmission accuracy and compact structure, it is widely used in automobile, aircraft, gas turbine, and heavy machinery. Accounting with the increase in high operating speed, large carried load, and light weight, the premature failures due to excessive wear and material fatigue occur in components of transmission systems. Because the working conditions of gearboxes are very terrible, they are vulnerable to damage and failure, so the fault diagnosis of a gearbox is one of the most important issues since people are concerned with maintaining equipment [1]. It is a benefit that the gearbox fault is detected at its early stage, so corrective action can be taken promptly. The preventive maintenance can also be made in advance for replacement in a damaged part.

The importance of gears in the gearbox system cannot be overstated. They provide essential power transfer in configurable directions at remarkably high efficiency (70-99% depending upon gear type and relative angles of the axels) [2]. These high efficiencies are likely why so little progress has been made in the development of new advanced manufacturing and novel processing methods. Even so, as we strive to make more durable machinery at lower costs, with greater specific power outputs, there is a growing need to provide insight on the mechanistic underpinnings of wear and failure of gears. Gears are so essential and prevalent in our machine systems that the failure of a single tooth could cause catastrophic failures. In this thesis, it was carried out by combining the experiment and the multi-body dynamics simulation to identify the changes in vibration spectrum that occur with the breakage tooth on a single tooth on

an individual gear embedded in a multi-stage gearbox.

Rotational reduction systems, including gears, have played a major role in energy conversion since the dawn of the industrial age. The need to impart rotation from one axis to another, to change the orientation of the axes, and to reduce/upgrade the rotational velocity of shafts led to the development of a host of gear systems. These include spur, helical, bevel, and worm gears, shown in figure 1-1. Spur gears, simplest of the gear types, have teeth parallel to the axis of rotation and are used to transmit motion from one shaft to a parallel shaft. Helical gears have teeth inclined to the axis of motion and can be used in the same types of applications as spur gears but were designed to run more quietly at higher RPMs. Even though helical gears are often less noisy than spur gears, the inclined teeth develop thrust and bending couples that spur gears do not experience. Bevel gears have teeth formed on conical surfaces and are generally used for applications that involve transmitting rotary motion between intersecting shafts. Lastly, worm gears are used to transmit rotary motion between nonparallel and nonintersecting shafts. [3]

Figure 1-1. Gear types: spur gear, helical gear, bevel gear, worm gear [4].

A helical gearbox system such as reduction gearbox is widely used in industrial machinery, and its faults directly cause large mechanical equipment to stop service and increase production costs. Early identification of faults in a helical gearbox is helpful for preventing equipment failure to avoid catastrophic losses. The types of gear fault include tooth surface pitting and wear [5-10], fatigue and crack [11-14], which can be described by measuring the vibration acceleration response of the gearbox.

Presently, the prevention and management of premature failures in equipment have become a vital part of the maintenance program. Many kinds of research have done for finding a reliable monitoring strategy in gear transmission systems. A variety of fault detection procedures have been developed. The mostly impractical procedure could be visual inspection because it is not easy to visualize faults in micro-scale unless costly, specialized equipment is used. However, it is quite impossible to examine gear transmissions during operation. Practically, visual inspection is used mainly after machine failure has been experienced. One of the most promising procedures for detecting incipient faults in gear-rotor and bearing system is the vibration analysis. The advantage of vibration signature analysis is no requirement of machinery shutdown and it can be carried out online by a computer-based on machine health monitoring.

The vibration signals of a gearbox caused by gear impact, resonation, or mutual interference are very complex in actual working conditions. It is difficult to apply the conventional test and diagnosis methods effectively. The faulty characteristics for the diagnosis of a gearbox are different for different sizes of the cracking tooth, rotation speed, misalignment of gears, and so on [15-17]. Many researchers have established dynamical simulation models to analyze gear faults [18]. Brethee et al. [19] established an 18-degree-of-freedom vibration system to study the different degrees of tooth-surface wear. However, their analytical equations are very complex and inconvenient to use.

When a certain degree of shaft deflection or gear wear occurs, the impacted component may be visible in the gear's vibration signal. The spectrum of the response is characterized by the different levels of amplitude modulation and frequency modulation. The meshing frequency, modulation signal, and side-band information are very important features for the gear vibration signal [20]. Therefore, during the fault diagnosis, the impacted component and the frequency interval of the side-band can be used as the main basis for judging whether a fault happens in the gear system. When a

gear failure that has the frequency bandwidth characteristics is measured by an acceleration sensor, high noise is distributed throughout the frequency spectrum. As a result, the frequency bands overlap with each other. Vibration signals also contain high-energy background signals related to the rotational speed.

When a gearbox fails, the actual measured signals are generally non-stationary and non-Gaussian signals, that usually contain strong noise. Therefore, it is difficult to eliminate the background signals and noise signals retaining fault information when using only conventional filtering methods. Wang et al. [21] presented an optimal demodulation subband selection method that can detect a gear fault by using envelope analysis, but the subband frequency features are not obvious in the environment with different noise levels.

1.2 The common methods of gearbox fault diagnosis

Presently, there are many methods of gearbox fault diagnosis, mainly include vibration analysis, oil analysis, acoustic emission analysis, torsional vibration analysis, temperature and energy consumption monitoring, et al. Thereinto, vibration analysis [22-23], oil analysis [24-25] and acoustic emission analysis [26-27] are commonly used for the gearbox fault diagnosis.

1.2.1   Vibration analysis

Vibration analysis method started earlier in the 1960s, and its information carrier is the vibration signal of the gearbox. Because the unbalance of each radial section of the gearbox components (such as shaft, gear) caused by asymmetric shapes, heterogeneous material density, machining or assembly errors lead to change the center position of rotating parts, the rotating equipment produces vibration. The vibration signal of the

gearbox system contains abundant working information. The energy distribution and frequency component of the vibration signal will change if the gearbox breaks down, the extraction of fault sensitive features in vibration signals can provide an important basis for a gearbox fault diagnosis. Because the vibration analysis method has many advantages, such as fast diagnosis speed, high accuracy, accurate fault location and on-line detection, it has become the most widely used and effective method in the research of gearbox fault diagnosis.

1.2.2   Oil analysis

Oil analysis is also a common fault diagnosis method for a gearbox. The method is based on lubricating oil in the gearbox as an information carrier. During the operation of gearbox, each friction pair of gear and rolling bearing will produce friction in the process of contact, which causes the abrasive particles of friction pair to fall off and enter the lubricating oil. The severity of wear is different, and the number, size and shape of the abrasive grains entering the oil are different. Therefore, the fault of the gearbox can be monitored and diagnosed by analyzing the concentration, shape and composition of the abrasive particles in the lubricating oil. According to the working principle, the common oil analysis method mainly includes the physical and chemical analysis, the spectrum analysis and the ferrography analysis. The application range of the oil analysis method is still limited due to the high monitoring cost and difficulty in locating the fault.

1.2.3   Acoustic emission analysis

Acoustic emission (AE) is a dynamic non-destructive testing technique developed in the 1960s, which utilizes particles (including atoms, molecules, and particle swarm) inside matter to identify the internal state of a substance or structure by releasing strain

energy in the form of elastic waves. When a metal component is subjected to internal or external forces resulting in deformation or crack propagation, the phenomenon that the strain energy of the metal component is released in the form of an elastic wave is called acoustic emission [28]. Acoustic emission technology is a detecting and testing technique that takes elastic wave as an information carrier, detects and analyzes acoustic emission signal by instrument to infer acoustic emission source, so as to locate fault location. Presently, acoustic emission technology can only diagnose some obvious faults, but its diagnostic accuracy is low for complex or inconspicuous faults.

Above the three analytical methods, vibration analysis is the most important analytical method in the field of mechanical fault diagnosis because it is easy to measure and sensitive to faults. Therefore, this paper mainly studies the fault diagnosis method of gearbox based on vibration signal processing.

1.3 Summary of vibration signal processing methods in Gearbox fault diagnosis

The purpose of mechanical equipment fault diagnosis is to identify and classify the working state or working mode of mechanical equipment in order to distinguish it as a normal state or abnormal state. In general, mechanical equipment fault diagnosis can be divided into three steps: 1), the acquisition of fault signals; 2) the extraction of fault features; 3) the pattern recognition and the fault diagnosis. Thereinto, the extraction of fault features is the most important and difficult. In a sense, the extraction of fault features is the bottleneck problem in the current research of mechanical fault diagnosis. The signal processing is the most commonly used method of fault feature extraction. The signal processing method can be divided into a time-domain analysis method, frequency-domain analysis method and time-frequency analysis method according to the different signal analysis field.

1.3.1 *Time-domain analysis method*

The time-domain analysis method is a simple diagnosis method in gearbox fault diagnosis. It is mainly used in fault diagnosis with an obvious harmonic component, periodic component or transient impact component. The time-domain analysis method is also called waveform analysis or time-domain statistical analysis. It calculates its statistical parameter index through the time-domain waveform of the signal. The commonly used statistical parameter indexes can be divided into two parts: the non-dimensional parameter index and dimensional parameter index.

The non-dimensional parameters include kurtosis index, impulse index, peak value index, waveform index, margin index and so on. Thereinto, kurtosis index, impulse index and peak value index are sensitive to the impact fault type and can be used for early diagnosis of faults. According to the difference kurtosis index of periodic component, transient impact component and noise component in the signal, Hong H et al. adopt the wavelet denoising method based on hybrid thresholding to separate the fault impact component from the bearing fault vibration signal [29].

The dimensional parameters include maximum, minimum, peak and peak value, mean square value, variance and skewness, etc. The variance directly reflects the intensity of the vibration signal. The skewness reflects the asymmetry degree of the density of signal amplitude distribution. The dimensional parameters are related not only to the operating state of the gearbox but also to the operating parameters of the gearbox (such as speed, load, etc.). Therefore, the dimensional parameter index is not comparable for different types, sizes and operating conditions of the gearbox.

In addition to the statistical parameters, the time-domain synchronous average (TSA), correlation analysis and adaptive noise cancelling (ANC) are also commonly used in the time-domain analysis. TSA, also known as coherent detection, is used to

sum and average data segments with the same phase. It can effectively suppress asynchronous components and random noise and is widely applicated in denoising processing of vibration signals. Braun S uses the TSA method to extract periodic components from noisy vibration signals [30]. McFadden P D adopts TSA method to eliminate noise components in gear vibration signals to highlight gear fault characteristics [31]. Correlation analysis reflects the linear or dependence relationship of signals, which can be divided into cross-correlation analysis and autocorrelation analysis. The cross-correlation analysis describes the degree of similarity between the two signals, and the auto-correlation analysis reflects the self-similar degree of the signal itself at different times. The noise is mainly composed of a large number of random components, which has the wide spectrum, the uniform distribution and the smaller auto-correlation, but the frequency spectrum of the periodic signal is narrow and the auto-correlation is strong. Therefore, the auto-correlation function is often used to analyze the periodic components and noise cancellation of the detection signal, which is interfered by noise. It is also more effective to enhance the periodic fault characteristics of rotating machinery equipment during the early failure. ANC is also a commonly used noise cancellation method, which can effectively extract the feature information of masking in noise.

The time-domain analysis method is direct and simple, and can be used in some simple diagnosis. However, the time-domain analysis method is difficult to locate the fault for the vibration signal with early fault or low signal noise ratio (SNR), so it is only used for the preliminary analysis at present.

1.3.2   Frequency-domain analysis method

The frequency-domain analysis is one of the most commonly used and basic methods in signal processing. It is an important method in the fault diagnosis of the gearbox. The

main frequency components, such as rotation frequency, meshing frequency and the high harmonic can be obtained by analyzing the vibration signal of gearbox in the frequency-domain analysis. Therefore, it provides an important basis for analyzing and judging the location of gearbox fault, the type of obstacle and the cause of failure. The most commonly used frequency-domain analysis methods are the spectrum analysis, the demodulation spectrum analysis and the high-order spectrum analysis in gearbox fault diagnosis. In this section, the progress of these three analysis methods will be briefly described.

1.3.2.1 The spectrum analysis

In order to describe the distribution of the signal in the frequency domain, spectrum analysis can provide more direct characteristic information compared with time-domain analysis. Spectrum analysis originated from Fourier series proposed by Fourier in 1807, that is any periodic signal can be decomposed into a superposition of complex sine signals. In 1822, Fourier transform is proposed by Fourier for the non-periodic signal decomposition. The Fourier transform and its inverse transformation are shown in formula (1.1) and formula (1.2), respectively.

$$X(f) = \int_{-\infty}^{+\infty} x(t)e^{-i2\pi ft}dt \tag{1.1}$$

$$x(t) = \int_{-\infty}^{+\infty} X(f)e^{i2\pi ft}df \tag{1.2}$$

where $x(t)$ is the original signal, $X(f)$ is the Fourier transform of $x(t)$. The frequency spectrum is obtained by Fourier transform. The amplitude spectrum and phase spectrum of the signal are (1.3) and (1.4), respectively.

$$|X(f)| = \sqrt{\mathrm{Re}^2[X(f)] + \mathrm{Im}^2[X(f)]} \tag{1.3}$$

9

$$\varphi(f) = \arctan \frac{\mathrm{Im}\left[X(f)\right]}{\mathrm{Re}\left[X(f)\right]} \qquad (1.\,4)$$

where $\mathrm{Im}\left[\bullet\right]$ is imaginary part, $\mathrm{Re}\left[\bullet\right]$ is real part.

The relationship between time-domain and frequency-domain is established by Fourier transform. Through the Fourier transform of the signal, the time-domain function can be converted into the frequency-domain function to observe the frequency distribution of the signal, and the frequency-domain function can be transformed into the time-domain function through its inverse transformation to observe the waveform of the signal. For the fault diagnosis of a gearbox, the operating state of the gearbox can be judged by monitoring the amplitude change of each frequency component and the generation of new frequency components.

1.3.2.2　The demodulation spectrum analysis

The demodulation spectrum analysis is also called envelope demodulation analysis. It can extract the low-frequency information modulated on the high-frequency signal, which is an envelope signal. When the components in the gearbox (such as gears, rolling bearings) have local faults, there will be modulation phenomena in the vibration signals. When the gear has broken teeth or cracks, its meshing frequency will be modulated by the rotating frequency. There are side frequency bands spaced by the rotation frequency on both sides of meshing frequency. The fault location and the damage degree in the gearbox can be judged by demodulating the modulation information from the signal and analyzing its intensity and frequency features. At present, the commonly used demodulation methods are the generalized detection filter demodulation (square demodulation, the detection filter demodulation and the high-pass absolute value demodulation), Hilbert demodulation, cyclostationary demodulation, energy operator demodulation, and so on. As an important tool for gearbox fault diagnosis, the

demodulation analysis is often used to extract modulation information from gearbox vibration signals.

1.3.2.3 The high-order spectrum analysis

A higher-order spectrum is a powerful tool for analyzing nonlinear, non-Gaussian signals. It can effectively compensate for the defect of second-order statistics (power spectrum) which does not contain phase information. It can quantificationally describe the nonlinear phase coupling which is closely related to the fault in the signal, and it can completely suppress the influence of Gaussian noise in theory. The mechanical vibration signal contains a large number of non-linear and non-Gaussian signals. Especially, when the mechanical equipment fails, the nonlinearity increases with the severity of the fault. Therefore, many researchers have studied the use of high-order spectrum to diagnose mechanical faults in recent years. McCormick A C et al. used bispectrum and trispectrum to detect bearing fault [32]. Fonollosa J R et al. used Wigner bispectrum and Wigner-Ville distribution to monitor transient signals. The results show that Winger bispectrum is superior to Wigner-Ville distribution [33]. Barker R W et al. used a high-order spectrum to monitor the wear condition of machining tools [34].

In addition, spectrum analysis methods such as detailed spectrum analysis, cepstrum analysis and holographic spectrum analysis are also used in the fault diagnosis of a gearbox, and some achievements have been obtained.

1.3.3 The time-frequency analysis

Fourier transform has become an important tool in signal analysis and processing. A frequency-domain analysis is based on Fourier transform and is widely used in radar, medicine, mining and other fields. However, it has some shortcomings in the practical

application.

(1) The frequency-domain analysis method lacks the time localization function. The frequency-domain analysis method cannot determine the frequency components at some point. Conversely, this method cannot determine when the particular frequency component appear in the signal.

(2) The frequency-domain analysis method is not suitable for non-stationary signal analysis. As shown in formula (1.1) and formula (1.2), the response functions are univariate (time or frequency), so it cannot describe the frequency variation on the time axis. Therefore, the frequency-domain analysis method can only be used to analyze stationary signals. Actually, most of the signals are non-stationary signals varying with time, such as the bat's echolocation, earthquake waves, and so on. Therefore, in order to overcome the shortcomings of time-domain and frequency-domain analysis methods, the time-frequency analysis method is studied by some researchers. The time-frequency analysis method can not only describe the frequency components and the variation of the frequency components with time, but also reflect the distribution of the energy in the time-frequency plane of the signal. Therefore, the time-frequency analysis method has become a powerful analytical tool for nonlinear and non-stationary signals.

The vibration signals of mechanical equipment are commonly nonlinear and non-stationary. When the mechanical equipment fails or the working condition changes, the nonlinearity and non-stationarity are especially prominent. Therefore, the time-frequency analysis method has been applicated in the field of mechanical fault diagnosis for the analysis of mechanical fault signals in recent years. At present, the time-frequency analysis methods in the field of mechanical faults mainly include short-time Fourier transform, Wigner-Ville distribution, wavelet analysis and Hilbert-Huang transform.

1.3.3.1 The short-time Fourier transform

Short-time Fourier transform (STFT) is a linear time-frequency analysis method, which is an extension of Fourier transform. Therefore, it is also called window Fourier transform. The expression of short-time Fourier transform is as follows:

$$STFT(t,f) = \int_{-\infty}^{+\infty} [x(\tau)g^*(\tau-t)]e^{-i2\pi\tau}d\tau \qquad (1.5)$$

where $*$ represents a conjugate. $g(t)$ is a window function. When the rectangular window function takes the infinite length ($g(t)=1$), the STFT transform is the traditional Fourier transform. The STFT principle: Assume that the signal is stationary in the given analysis window moved along the time axis. The signal is divided into a series of short signal segments, then the spectrum of each signal segment is calculated, so the time-frequency localization of the signal can be achieved. Because STFT can highlight the local characteristics of the signal, it has been applied in the field of mechanical fault diagnosis. Wang W J et al. used time-frequency distribution diagram to diagnose gear fault based on STFT [35]. Stazewski W J et al. used moving window to diagnose gear fault in gearbox [36].

However, there are many shortcomings for STFT method, which affect its further application in mechanical fault diagnosis. Firstly, due to the limitation of the Heisenberg uncertainty principle, STFT method cannot obtain high temporal resolution and frequency resolution at the same time, so the time-frequency resolution is lower. Secondly, STFT method is based on the stationary signal in the analysis window. STFT method is not applicable for the non-stationary signal with fast frequency change, so STFT method can only be used for the analysis of stationary signal or quasi-stationary signal.

1.3.3.2 The Wigner-Ville distribution

Wigner distribution was proposed by Wigner in 1932 with studying quantum mechanics, then it was introduced into the signal analysis by Ville, so it is called Wigner-Ville distribution (WVD). WVD is the instantaneous correlation function of the Fourier transform of the signal $x(t)$. The expression is:

$$W(t,\omega) = \int_{-\infty}^{+\infty} x(t + \frac{\tau}{2}) x^*(t - \frac{\tau}{2}) e^{i\omega\tau} d\tau \tag{1.6}$$

WVD does not use any window function, which avoids the restriction of time-frequency resolution, so it has high time-frequency aggregation. Because WVD has many advantages such as time-shift invariance, translation invariance, high time-frequency aggregation and so on, especially it can directly and accurately define the instantaneous frequency for the linear frequency modulation signal, so it has been applied in mechanical fault diagnosis. Meng Q F et al. used Wigner distribution to analyze the rotor vibration signal [37]. The results indicate that the vibration signal of cracked rotor has different time-frequency distribution compared with normal rotor vibration signal. Chillaz M et al. used WVD to analyze the engine noise [38]. Baydar N et al. had compared and analyzed the pseudo WVD of the acoustic and vibration signals in the different conditions such as gear broken teeth, cracks and local wear faults [39]. The results show that it is more sensitive for the time-frequency distribution of the acoustic signal in early faults.

1.3.3.3 The wavelet analysis

Wavelet analysis (WA), which provides a good filtering characteristic, is used widely in various subfields of mathematics, science and engineering. Through the decomposition and reconstruction of a signal, WA can be used to determine the transient

trait of a signal in the time-frequency domain, therefore, is regarded as an effective approach for non-stationary data processing. WA is the process of decomposing or reconstructing a signal using wavelets, a family of orthogonal functions of type

$$WT(a,b) = \frac{1}{\sqrt{a}} \int_{-\infty}^{+\infty} x(t) \psi^* (\frac{t-b}{a}) dt = \langle x(t), \psi_{a,b}(t) \rangle \quad a > 0 \tag{1.7}$$

where a is the scaling factor,

b is the time shift factor,

$\psi_{a,b}(t)$ is the mother wavelet.

WA is different from the STFT method, which uses the time-frequency window function to analyze the signal. In other words, the time-frequency window with higher time resolution and lower frequency resolution are used in the high-frequency region of the signal, and the time-frequency window with higher frequency resolution and lower time resolution is used in the low-frequency region of the signal. Therefore, wavelet analysis is also known as a mathematical microscope.

WA cannot only provide localized time-frequency information of the signals, but also has the advantages of the multi-resolution analysis. Therefore, it is widely used in mechanical fault diagnosis. In general, the application of wavelet in mechanical fault diagnosis can be divided into two aspects: 1) Fault feature extraction based on wavelet analysis; 2) Pattern recognition based on wavelet analysis and artificial intelligence. Lin J et al. proposed a morlet wavelet analysis method based on soft threshold denoising for the low SNR signal, and applied it to extract the fault features of rolling bearing [40]. Due to the shortage of the time-frequency clustering of wavelet scale spectrum, Peng Z K et al. proposed the redistribution of the wavelet scale spectrum [41]. Cheng J S et al. constructed impulse response wavelet and used the continuous wavelet transform to extract the fault characteristics of the rolling bearing fault vibration signal.

Therefore, the scale-wavelet energy spectrum comparison method and the wavelet energy spectrum autocorrelation method are proposed [42]. Fan X F et al. combine wavelet packet with Hilbert demodulation method to detect the fault diagnosis of gearbox [43].

In recent years, many new wavelets have been used in the mechanical fault diagnosis field with the development of wavelet analysis, such as lifting wavelet frame, chirp wavelet, quality factor adjustable wavelet and so on. Presently, WA is still a hot topic in the mechanical fault diagnosis field.

1.3.3.4 The Hilbert-Huang transform

Hilbert-Huang transform (HHT) is a nonlinear and non-stationary adaptive time-frequency analysis method proposed by Norden E Huang. Firstly, the signal is decomposed by empirical mode decomposition (EMD), then a series of the intrinsic mode function (IMF) is obtained. secondly, each IMF is transformed by Hilbert, and the instantaneous spectrum of each IMF is obtained. Finally, the time-frequency distribution of the whole signal can be obtained by combining the instantaneous spectrum of each IMF. EMD is a very important step in the HHT method. It makes the instantaneous frequency of the Hilbert transform have a clear physical meaning.

Due to the advantages of the EMD method, such as orthogonality, completeness and self-adaptability, it is very suitable for analyzing non-linear and non-stationary signals. Therefore, it has been widely used in the field of mechanical fault diagnosis. Loutridis S J determines the crack severity of gear tooth root based on the instantaneous energy density of each IMF component [44]. On the basis of introducing Hilbert-Huang transform, Yu D J et al. proposed the local Hilbert spectrum and the local Hilbert marginal spectrum, and applied them to detect the fault diagnosis of the roller bearing [45]. Yang Y et al. combined HHT with Support vector machines (SVM) to classify and

identify the rolling bearing fault [46].

HHT method has been widely used in many fields such as geophysics, biomedicine, electric power communication and so on. However, HHT also has some deficiencies as a new time-frequency analysis method, such as mode confusion [47], negative frequency [48-49] and so on. For this reason, many scholars have studied it and derived many improved methods, such as local mean decomposition (LMD) method [50-51], ensemble empirical mode decomposition (EEMD) method [52], intrinsic time-scale decomposition (ITD) method and local characteristic-scale decomposition (LCD) method, et al. The research of HHT method and its improved method is an important research direction in the field of mechanical fault.

1.4 ADAMS software

Multibody dynamics (MBD) is a very powerful tool used in many engineering and science fields with the objective of analyzing the kinematic and dynamic behavior of a system composed of different interconnected bodies. It has many applications in various fields such as mechanical engineering, aerospace, biomechanics, robotics, particle simulation, vehicle dynamics and so on. MBD models are computational models of interconnected rigid bodies, used to simulate and predict the dynamics of physical and bio-mechanical systems. The interconnected rigid bodies are allowed to undergo large translational and rotational displacements. Recent MBD models of gearbox consider shaft and gear mesh flexibility [53–56]. Current commercial MBD programs also support component and joint flexibility in the presence of large overall motion as well as complex interaction with other modeling elements. Dynamic studies conducted on virtual MBD models of mechanical systems are time efficient and much cheaper than the more complicated, time consuming and expensive experimental analysis. For example, MBD gearbox models are used for research and design purposes [53-55,57].

MBD models have also been effectively used by implant designers and researchers in the area of bio-mechanics, for example MBD model has been used to predict wear for knee replacements and to study the reliability of implanted total knee replacement systems [58-60].

When designing a mechanical system, designers need to understand how various components such as motors, rigid and flexible bodies interact as well as what forces those components generate during operation. ADAMS is a dynamic motion simulation solution for analyzing the complex behavior of mechanical assemblies. ADAMS allows one to test virtual prototypes and optimize designs for performance, speed, and durability without having to build and test numerous physical prototypes.

ADAMS is a family of interactive motion simulation software modules, which allows one to import geometry from CAD systems. There is also an opportunity to build a solid model from scratch. After defining the joints, constraints, motions etc. the dynamic model is completed. Then ADAMS offers wide variety of simulations and graphical representation of the results. The most important part is one can export these data in a desired type. There is also an option to save the animation and visually inspect the simulation. Another property of this software is the ability of communicating with finite element analysis programs.

Several modules that are part of ADAMS can be used to accomplish specialized tasks. For example, ADAMS/Flex can be used to examine the effect of flexible links on a mechanism and ADAMS/Controls can be used to model control systems such as hydraulics, pneumatics, electronics and more. ADAMS also offers a range of modules tailored to industry specific applications. Several CAD interface modules allow you to explore the motion of CAD designs without having to leave a familiar CAD interface or transfer data into ADAMS.

The benefits of the ADAMS software could be listed as below:

(1) Work in a secure virtual environment, without the fear of losing critical data due to instrument failure or of falling behind schedule due to poor weather conditions, common elements that accompany real-world testing.

(2) Reduce risk by getting better design information at every stage of the development process.

(3) Analyze design changes much faster and at a lower cost than physical prototype testing requires.

(4) Improve product quality by exploring numerous design variations in order to optimize full-system performance.

(5) Explore system variations without having to modify physical instrumentation, test fixtures, and test procedures.

1.5 *Main contents and organization of this dissertation*

This dissertation is aimed to develop a new signal processing method for gear fault diagnosis system. The dynamical model is established to verify the validity and limits of the algorithms in the different conditions. The remainder of this dissertation is organized as follows.

Chapter 2 studies the basic theory of the spectral subtraction method combining EWT technique, then the side-band frequency features are obtained by the envelop spectrum analysis. Meanwhile, for explaining the advantages of the SS-AEWT method, the theory of EMD, LMD and DWT method is introduced, respectively.

Chapter 3 focuses on the main failure types of the gear fault based on the analysis of the failure proportion of the components in the gearbox system. The theory and vibration characteristics of the gear are introduced in detail. Finally, the experimental results for the gear fault signal are validated by using the different algorithms.

Chapter 4 mainly establishes the multi-body dynamical model of the gearbox system by using the ADAMS software in detail. Meanwhile, in order to make the simulation more authentic, the flexible gear is used for the simulated model. The fault type of the gear is a breakage tooth included small, middle and big size.

Chapter 5 carries out the simulation experiment of multi-body dynamic model. The simulated results are analyzed and summarized in the different conditions. Comparing the advantages of the different algorithms, the result indicates that the performance of the SS-AEWT method is more effective and valuable.

Chapter 6 concludes this dissertation and future work.

Chapter 2   Theoretical algorithm research based on gearbox fault diagnosis

2.1 Introduction

Signal processing and data analysis is the main stage in the gearbox fault diagnosis. This step is to refine and get rid of impurity from the raw signals in order to clarify signal specifications and details. The raw signals captured by sensors commonly contain a high level of noise and some random signals carrying a characteristic of fault components in the gearbox system. Feature extraction of the vibration signal plays important roles in the health monitoring and fault diagnosis of rotating machinery. When a gear has a local fault, the vibration signal of the gearbox may contain amplitude and phase modulations that are periodic with the rotation frequency of the gear. The modulation of the meshing frequency, as a result of faulty teeth, generates side-bands, which are frequency components equally spaced around a center frequency. The center frequency called the carrier frequency may be the gear meshing frequency, multiples of bearing ball pass frequency, the resonant frequency of a machine component/structure, or the resonant frequency of an accelerometer. Side-bands are either the shaft rotational speed or one of its multiples. It is well known that the most important components in gear vibration spectra are the tooth meshing frequency and their harmonics, together with side-bands. Amplitude modulations are present when a gear meshes an eccentric gear or a gear riding on a bent or misaligned shaft. If there is a local gear fault, the gear angular velocity could change as a function of the rotation. As a result of the speed variation, frequency modulations occur. In many cases, both amplitude and frequency modulations are present. The increasing in the number and the amplitude of such side-bands often indicates faulty conditions [61]. Since modulating frequencies are caused

by certain faults of machine components including gear, bearing, and shaft, the detection of the modulating signal is very useful to detect gearbox fault.

A new signal-processing scheme is proposed to detect gearbox faults at a constant speed. A flow chart of the fault diagnosis method is shown in figure 2-1. To improve the side-band frequency features of fault information, the spectral subtraction technique is first used to remove the partial noise of the signal. The impacted component of the gear fault signal is obtained with the EWT method, and then the side-band frequency of the fault features is obtained with the square envelope spectrum method.
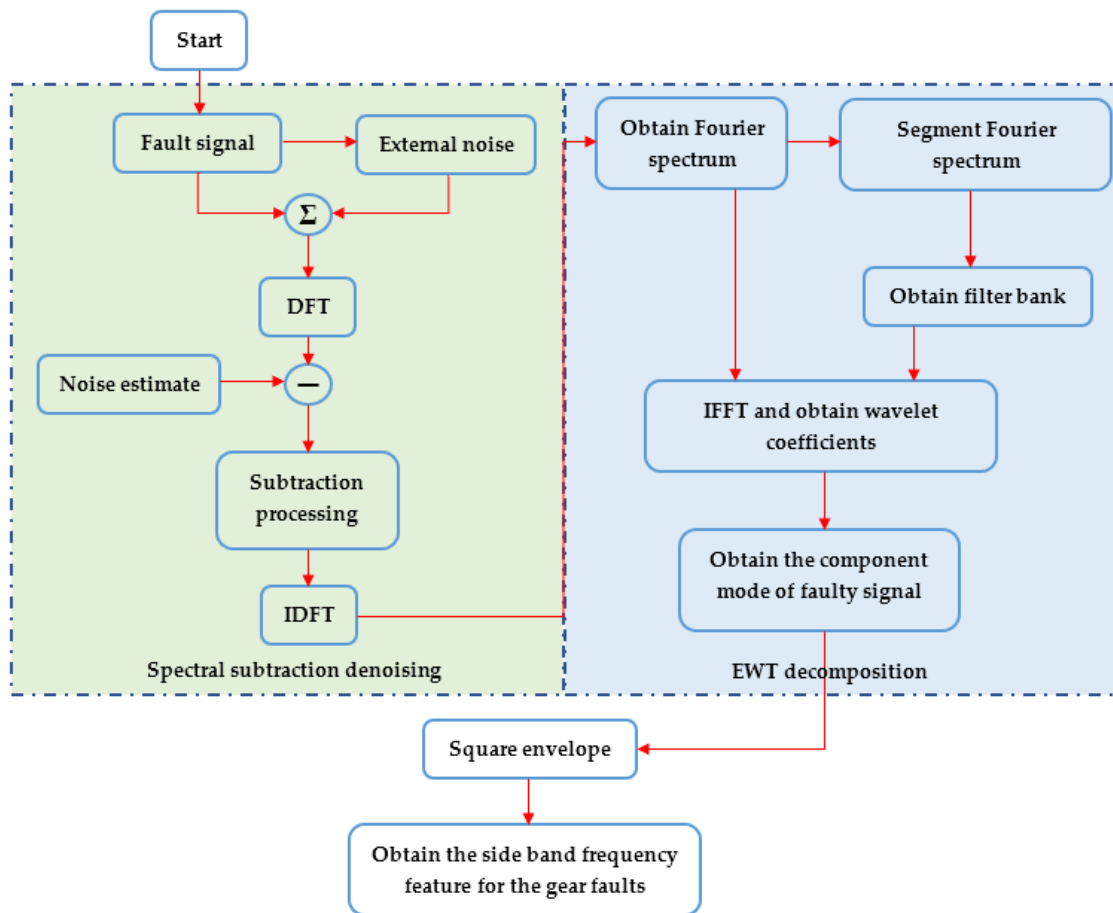
Figure 2-1. Flow chart of the fault diagnosis method.

2.2 The theory of SS-AEWT algorithm for extracting gear fault features

2.2.1 Spectral subtraction methods

The spectral subtraction method is widely employed in signal processing for speech enhancement in order to remove acoustic noise [62-64]. The figure 2-2 illustrates a block diagram configuration of the spectral subtraction method.
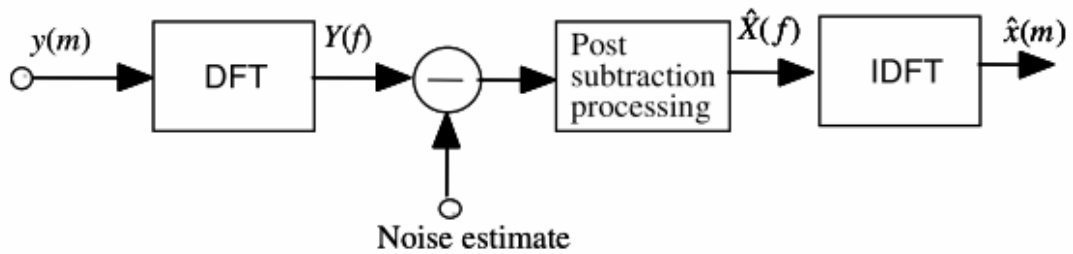
Figure 2-2. A block diagram illustration of spectral subtraction.

Spectral subtraction is usually used as a denoising method for fault detection. The proposed technique is appropriate for the fault diagnosis of rotating machinery in steady-state at a constant speed. It is only applied to stationary signals, which means the frequency content is independent of time. In this context, a new denoising scheme is employed to enhance the useful information of the vibration signals measured from a faulty gearbox. It is assumed that the vibration signal is disturbed by random noise, which can be removed by subtracting of an estimation of the mean of the noise spectrum from the noisy signal spectrum. The measured signal model in the time domain is given by:

$$z(m) = s(m) + n(m) \qquad (2.\ 1)$$

where $z(m)$ is the measured mixed-signal (include the vibration signal and noise

signal), $s(m)$ is the vibration signal of the gear, $n(m)$ is the additive noise and m is the discrete-time index. The frequency domain representation of the relation is given by

$$Z(k) = \mathcal{F}\{y(m)\} = S(k) + N(k) \tag{2.2}$$

where $Z(k)$, $S(k)$, $N(k)$ are the discrete Fourier transform of $z(m)$, $s(m)$, $n(m)$, respectively. k is the discrete-frequency index. Therefore, the expression of the power spectrum is

$$|Z(k)|^2 = |S(k)|^2 + |N(k)|^2 + S^*(k)N(k) + S(k)N^*(k) \tag{2.3}$$

where $*$ denote the complex conjugate.

In the fault detection of gearbox, most corrupting noise signals, which are uncorrelated with the gear vibration signal, are generated from the vibration of other components impact (e.g. bearing fault, shaft imbalance, motor and braking system vibration) on the constant speed condition. Therefore, the cross products $X^*(k)S(k) + X(k)S^*(k)$ in Equation (2.3) could be ignored, and the simplified power spectrum is

$$|Z(k)|^2 = |S(k)|^2 + |N(k)|^2 \tag{2.4}$$

The interfering noise is assumed to be short-term stationary, so that the time-averaged noise spectrum can be obtained from the periods

$$|\hat{N}(k)|^2 = \frac{1}{L}\sum_{i=0}^{L-1}|N_i(k)|^2 \tag{2.5}$$

In the spectral subtraction method, the estimate of the original signal power spectrum can be obtained with the variation of parameters. It includes an over-subtracting estimate of the noise power spectrum and a lower limiting value for the

resulting spectrum. The form of the enhanced signal power spectrum is as follow

$$|\hat{S}(k)|^2 = \max\{|Z(k)|^2 - \alpha|\hat{N}(k)|^2, \beta|\hat{N}(k)|^2\} \qquad (2.\,6)$$

where α is the over-subtracting multiplication factor and the value is greater than or equal to 1, and it determined the degree of distortion for the fault signal, β is the spectral flooring parameter and the value is between 0 and 1,and it control the effect of residual noise. The multiplication factor of α in proposed method is defined by the function of segmental SNR (signal-noise ratio) and SNR is estimated in the frame and defined by

$$\alpha = \begin{cases} 5 & SNR < -5 \\ 4 - \dfrac{1}{5}SNR & -5 \le SNR \le 20 \\ 1 & SNR > 20 \end{cases} \qquad (2.\,7)$$

$$SNR = 10\log 10\left(\dfrac{\sum\limits_{k=0}^{L-1}|Z(k)|^2}{\sum\limits_{k=0}^{L-1}|N(k)|^2} \right) \qquad (2.\,8)$$
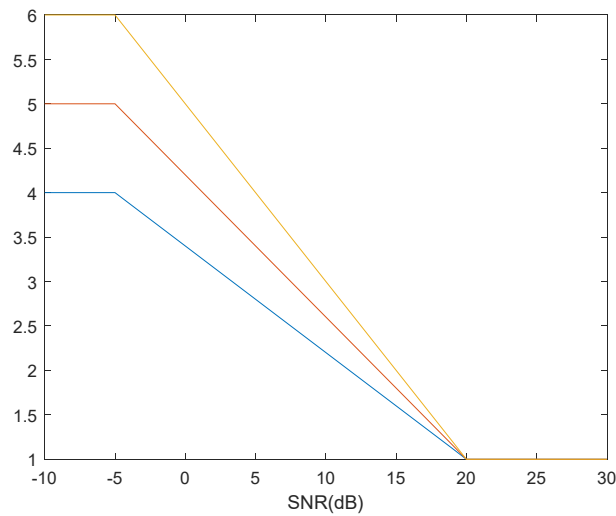
Figure 2-3. Multiplication factor with SNR.
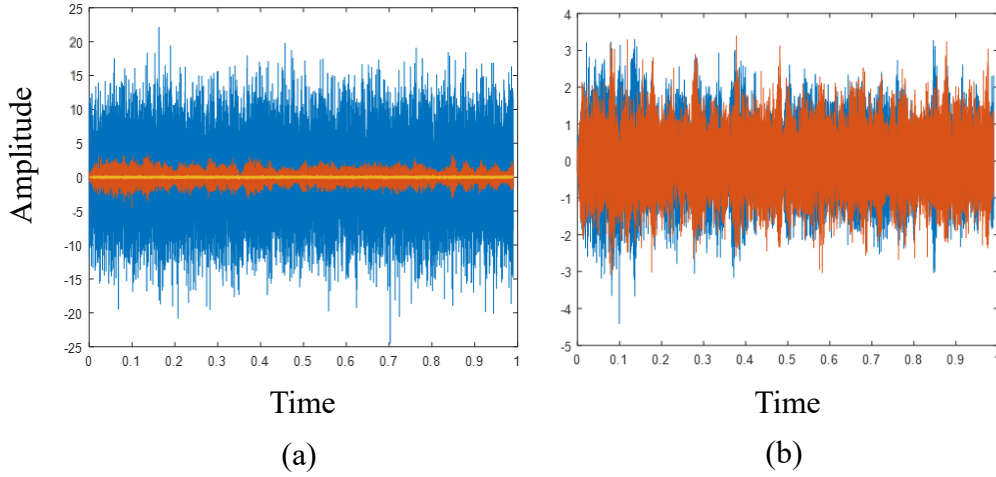
Figure 2-4. The results for (a) α=5 or 26; (b) α=2 or 5.

Form figure 2-3 (a), α=5, the noise reduction effect is very good (red line), α=26, the valid signal is distorted (yellow line); from figure 2-3 (b), α=2, the noise is equivalent to the body noise, so the result trend has not changed, and the fault signal cannot be obtained. In order to clearly obtain the sidelobe characteristic of the meshing frequency, the value (α=5) is selected based on the a lot of experimental results.

Finally, the enhanced signal is obtained by inverse discrete Fourier transform (IDFT).

$$\hat{S}(k) = |\hat{S}(k)| e^{j\phi(k)} \tag{2.9}$$

$$\hat{s}(m) = \mathcal{F}^{-1}\{\hat{S}(k)\} \tag{2.10}$$

where $\phi(k)$ is the phase function of the DFT of the input signal.

According to the basic theory of spectral subtraction, the vibration noise is estimated over the whole spectrum by adjusting the multiplication factor α [65]. By using the spectral subtract technique, the faulty signal is enhanced. However, it cannot extract the mono-component information. To identify the side-band frequency feature, EWT is used to analyze the faulty signal.

26

2.2.2 *Empirical wavelet decomposition*

EWT is a new signal processing algorithm to detect the different vibration modes based on the EMD method and wavelet analysis theory. It can effectively extract the different modes from the mixed vibration signal, through adaptively establishing the appropriate filter bank based on the Fourier spectrum. EMD can adaptively decompose a signal into intrinsic mode functions (IMFs) and obtain a time-frequency resolution to extract the fault features, but it is lacking mathematic theory support. In contrast, EWT has not only the frequency resolution but also the clear mathematical theoretical basis and high computation speed of discrete WT. EWT procedure as the follow
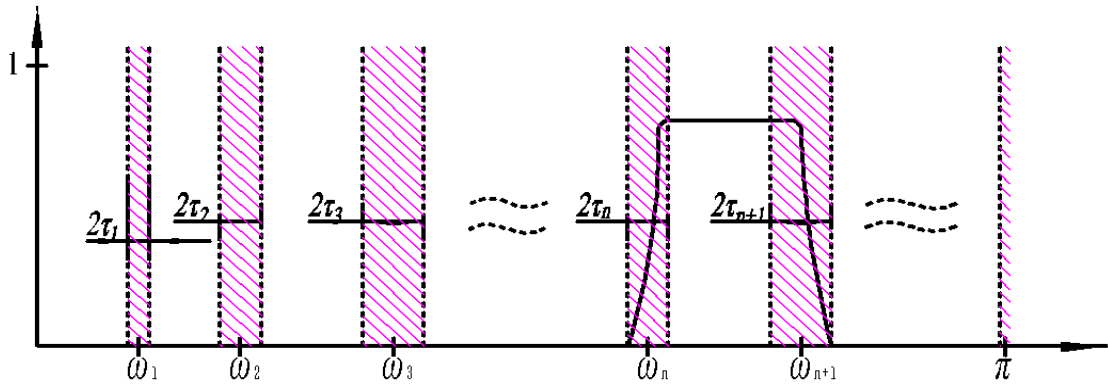
Figure 2-5. Segmenting Fourier spectrum into N contiguous segments.

Firstly, accordingly to Shannon criteria, the frequency limit is defined as $[0, \pi]$ in a normalized Fourier axis of a periodicity 2π. The initial Fourier support $[0, \pi]$ is segmented into N contiguous segments containing the spectra of definite modes. The boundary of each segment is denoted ω_n, hence, the bandpass filter is obtained $\Lambda_n = [\omega_{n-1}, \omega_n]$. In order to realize EWT on the segmental support Λ_n, the transition phase T_n of width $2\tau_n$ is defined with centered around each ω_n. Empirical filter bank is provided in figure 2-5. The simplest of τ_n is proportional to ω_n : $\tau_n = \gamma\omega_n$,

where the range of γ is $0 < \gamma < \min_n \dfrac{\omega_{n+1} - \omega_n}{\omega_{n+1} + \omega_n}$.

Next, the empirical wavelets are defined as bandpass filters on each Fourier support Λ_n. The empirical scaling function and empirical wavelets are established by using the idea of the construction of both Littlewood-Paley and Meyer's wavelets, respectively. The simplifying form is as follows

$$\hat{\phi}_n(\omega) = \begin{cases} 1 & |\omega| \leq (1-\gamma)\omega_n \\ \cos[\dfrac{\pi}{2}\beta(\dfrac{1}{2\gamma\omega_n}(|\omega| - (1-\gamma)\omega_n))] & (1-\gamma)\omega_n \leq |\omega| \leq (1+\gamma)\omega_n \\ 0 & otherwise \end{cases} \tag{2.11}$$

$$\hat{\psi}_n(\omega) = \begin{cases} 1 & (1+\gamma)\omega_n \leq |\omega| \leq (1-\gamma)\omega_{n+1} \\ \cos[\dfrac{\pi}{2}\beta(\dfrac{1}{2\gamma\omega_{n+1}}(|\omega| - (1-\gamma)\omega_{n+1}))] & (1-\gamma)\omega_{n+1} \leq |\omega| \leq (1+\gamma)\omega_{n+1} \\ \sin[\dfrac{\pi}{2}\beta(\dfrac{1}{2\gamma\omega_n}(|\omega| - (1-\gamma)\omega_n))] & (1-\gamma)\omega_n \leq |\omega| \leq (1+\gamma)\omega_n \\ 0 & otherwise \end{cases} \tag{2.12}$$

where $\beta(x)$ is an arbitrary function with an independent variable x, and the value is determined by

$$\beta(x) = \begin{cases} 0 & x \leq 0 \\ x^4(35 - 84x + 70x^2 - 20x^3) & 0 < x < 1 \\ 1 & x \geq 1 \end{cases} \tag{2.13}$$

According to the theoretical framework of wavelet transform, the empirical wavelet transform is built by the constructed bandpass wavelet filter bank. The detail coefficient of empirical wavelet transform is the inner product between the analyzed signal and the empirical wavelet in the time domain, and is the inverse Fourier transform of the frequency function production, as following

$$W_s^\varepsilon(n,t) = \langle s(t), \psi_n(t) \rangle = \int s(\tau)\overline{\psi_n(\tau-t)}d\tau = \mathcal{F}^{-1}\left(\hat{S}(\omega)\overline{\hat{\psi}_n(\omega)} \right) \qquad (2.14)$$

and the approximation coefficient of empirical wavelet transform is the inner product between the analyzed signal and the scaling function in the time domain, and is the inverse Fourier transform of the of the frequency function production, as following

$$W_s^\varepsilon(0,t) = \langle s(t), \phi_1(t) \rangle = \int s(\tau)\overline{\phi_n(\tau-t)}d\tau = \mathcal{F}^{-1}\left(\hat{S}(\omega)\overline{\hat{\phi}_n(\omega)} \right) \qquad (2.15)$$

Finally, the mono-component modes are obtained through the detail and approximation coefficient of empirical wavelet transform. The construction of the original signal is obtained by

$$s(t) = W_f^\varepsilon(0,t)*\phi_1(t) + \sum_{n=1}^{N}W_f^\varepsilon(n,t)*\psi_n(t) = \mathcal{F}^{-1}\left(\hat{W}_f^\varepsilon(0,\omega)\hat{\phi}_1(\omega) + \sum_{n=1}^{N}\hat{W}_f^\varepsilon(n,\omega)\hat{\psi}_n(\omega) \right)$$

$$(2.16)$$

The mono-component modes are as follow

$$s_0(t) = W_s^\varepsilon(0,t)*\phi_1(t) \qquad (2.17)$$

$$s_k(t) = W_s^\varepsilon(k,t)*\psi_k(t) \qquad (2.18)$$

2.2.3   The proposed SS-AEWT for extracting gear fault features

If the fault information can be enhanced by using the spectral subtraction method, the mono-component mode of the faulty signal is clearly obtained by EWT. The mono-

component mode is described by:

$$L(m) = \hat{s}(m) * \Gamma \qquad (2.19)$$

where $\hat{s}(m)$ denotes the estimated value of the faulty signal obtained by the spectral subtraction method, and Γ represents the decomposition band width of EWT.

Envelop analysis is an effective technique for rolling element bearing diagnostics in recent decades, and it has the advantage of the application simplicity and low computational effort required. This algorithm can demodulate the multi-component signal to obtain the representation of the mono-component signal for a cyclostationay impulse signal. The squared envelope spectrum (SES) analysis is the simpler efficient algorithm, and its process as follow.

Step 1: The useful information is much clearer than others, the square for the vibration signal is operated.

Step 2: The filtered signal is obtained by the bandpass filtering, and its purpose is to preserve only the frequency band feature of the impulse signal for gear faulty information. In this context, the simple Butterworth filter is used for designing the process easily.

Step 3: The filtered signal is taking the square root.

Step 4: The SES is obtained as the absolute amplitude of FFT.

In this process, it is used for taking square and square root to eliminate some hidden information more efficiently.

2.3 The based theory of EMD

As previously, Hilbert-Huang transformation (HHT) is an analyzing method with combining EMD and Hilbert Spectral (HS) analysis [66], and is designed to work

well for time-series data that are non- stationary and nonlinear. HHT uses EMD to decompose a multi-component signal into several mono-component signals called Intrinsic Mode Function (IMF), and then IF can be extracted from each IMF.

IMF is a mono-component signal, which contains only one oscillatory mode at any time instance. The concept of IF is applicable only to mono-component signals, therefore, to obtain IF of a signal any complex (multi-component) signal needs to be decomposed to some IMFs. Any IMF should satisfy the following two criteria:

(1) The numbers of local extrema and the numbers of zero crossings must be equal or differ by at most 1.

(2) At any time point, the mean value of the "upper envelope" (defined by local Maxima) and the "lower envelope" (defined by the local minima) must be zero.

EMD is an algorithm that can decompose a complex signal into several IMFs. The first step is Hilbert-Huang Transform for EMD method. EMD empirically reduces a time series to several sub-signals (IMFs), each of which is input to the same time-frequency environment via the Hilbert transform. EMD uses the characteristics of the signal itself to adaptively decompose it into several Intrinsic Mode Functions (IMFs).

$$x(t) \qquad \boxed{EMD \qquad \boxed{IMF}} \qquad x(t) = \sum_{j=1}^{C} IMF_j(t) + r_C(t)$$
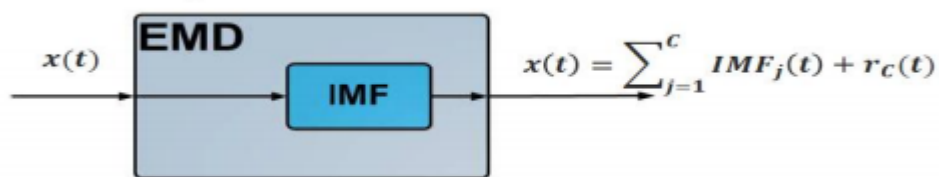
Figure 2-6. Schematic of signal decomposition into set of IMFs and residue using EMD [67].

EMD algorithm for a complex signal $x(t)$ can be summarized as follows [68]:

(1) Identifying all the extrema (including maxima and minima) of the signal $x(t)$.

(2) The upper and lower envelope is generated by a cubic spline interpolation of

the extrema points.

(3) Calculating the mean function of the upper and lower envelope, $m(t)$.

(4) Calculating the difference signal $d(t) = x(t) - m(t)$.

(5) If $d(t)$ is a zero mean process (i.e an IMF), then the criteria stops and $d(t)$ is the first IMF, named $c_1(t)$.

(6) Calculating the residue signal $r(t) = x(t) - c_1(t)$.

(7) Repeating the procedure from steps (1) to (6) to obtain IMF 2. Continuing the iterations for n times leads to obtaining $c_n(t)$. This procedure stops when the final residue signal $r(t)$ is a monotonic function.

At the end of this procedure we have a collection of n IMFs from $c_1(t)$ to $c_n(t)$ and the residue $r(t)$. Thus, the signal $x(t)$ can be written as

$$x(t) = \sum_{i=1}^{n} c_i(t) + r(t) \tag{2.20}$$

The number of decomposition levels (IMFs and residue) is also determined by the length of the input signal $x(t)$, according to the formula [68]

$$N = \log_2(length(x)) \tag{2.21}$$

An illustration of EMD decomposition of a normal rhythm electrocardiogram (ECG) signal $x(t)$ is shown in figure 2-7. This decomposition resulted in 8 IMFs and a residue. It is clear that lower order IMFs carry high frequency components of the original signal $x(t)$ and as the order of the IMFs increases, the corresponding frequency decreases.
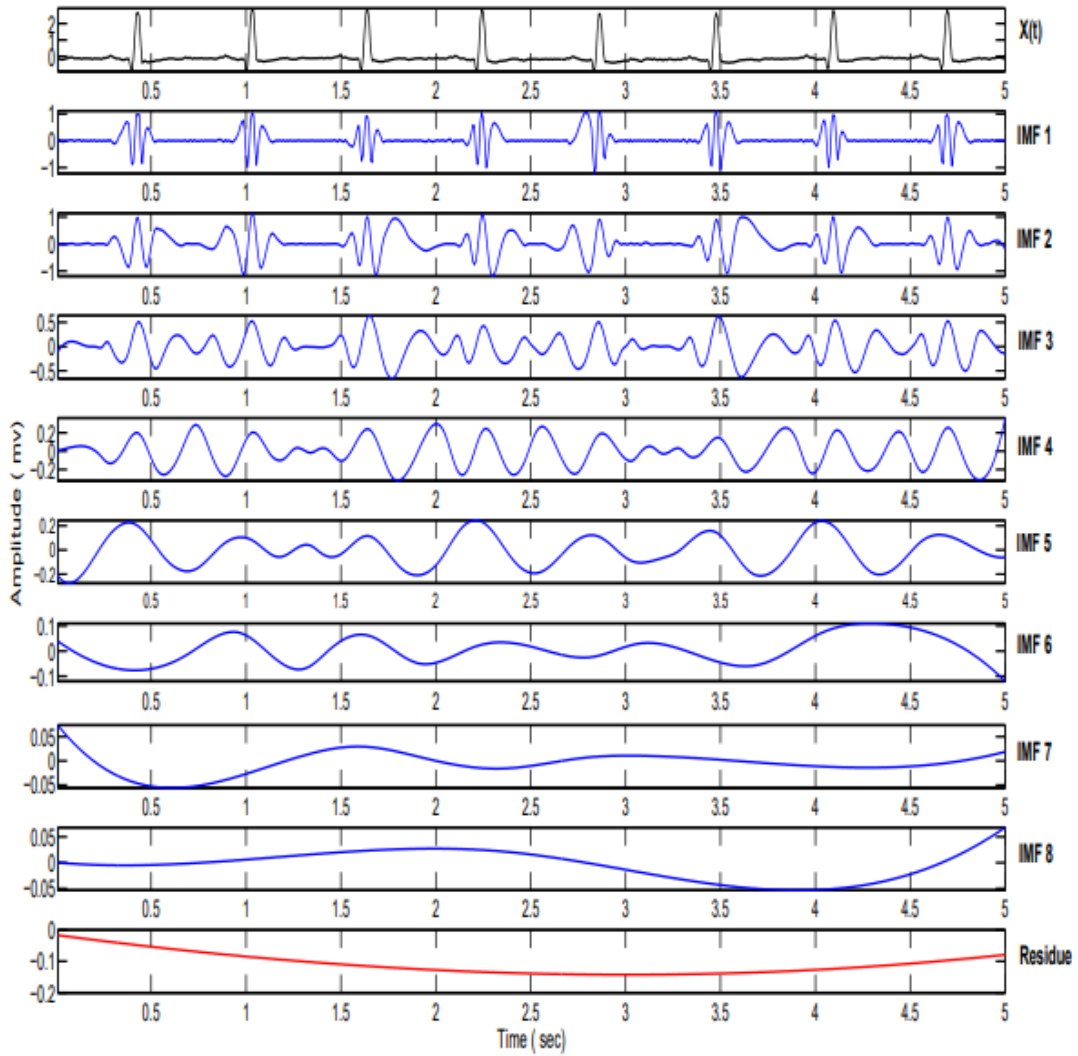
Figure 2-7. A 5- sec normal rhythm ECG signal x(t) in black; IMF distribution from scale 1 to scale 8 in blue; and the residue signal in red. ECG recording is from PhysioNet [69].

2.4 The based theory of LMD

A series of product functions (PFs) can be obtained by the LMD processing method, each of PFs represents a mono-component of the original signal which contains multi-components. The LMD method has been widely used to extract fault features for diagnosing rolling element bearing faults [70-72]. It can also be used to extract the fault component by selecting an appropriate PF which contains the fault component signal.

The LMD decomposition procedure are shown as following steps for an original

33

signal $u(t)$ [73]:

(1) Extracting the extrema $z_i(i=1,\cdots,M)$ of the original signal $u(t)$.

(2) Calculating the local mean value m_i and the amplitude envelope estimate a_i via the two successive extrema.

$$m_i = \frac{z_i + z_{i+1}}{2}, i=1,2,\cdots,M-1 \tag{2.22}$$

$$a_i = \frac{|z_i + z_{i+1}|}{2}, i=1,2,\cdots,M-1 \tag{2.23}$$

These local means are connected by straight lines with extending between adjacent extrema. The continuous local mean function $m_{11}(t)$ are formed through moving averaging. The local magnitude envelope function $a_{11}(t)$ can be obtained by the same smoothing procedure as the local means.

(3) The continuous local mean function is subtracted from the original signal $u(t)$:

$$h_{11}(t) = u(t) - m_{11}(t) \tag{2.24}$$

The demodulated amplitude $s_{11}(t)$ is obtained with the envelope function $a_{11}(t)$:

$$s_{11}(t) = \frac{h_{11}(t)}{a_{11}(t)} \tag{2.25}$$

Ideally, if $s_{11}(t)$ was a pure frequency modulated signal, its envelope function $a_{12}(t)$ should satisfy the condition: $a_{12}(t)=1$. If $a_{12}(t) \neq 1$, $s_{11}(t)$ is taken as the new signal, and the procedures are repeated steps (1)-(3). The process will stop until $s_{1n}(t)$ is the pure frequency modulated signal. The iteration can be shown as follows:

$$\begin{cases} h_{11}(t) = x(t) - m_{11}(t) \\ h_{12}(t) = s_{11}(t) - m_{12}(t) \\ \quad\vdots \\ h_{1n}(t) = s_{1(n-1)}(t) - m_{1n}(t) \end{cases} \tag{2.26}$$

where the $s_{1n}(t)$ is:

$$\begin{cases} s_{11}(t) = h_{11}(t) / a_{11}(t) \\ s_{12}(t) = h_{12}(t) / a_{12}(t) \\ \quad\vdots \\ s_{1n}(t) = h_{1n}(t) / a_{1n}(t) \end{cases} \tag{2.27}$$

(4) The envelop signal can be obtained as:

$$a_1(t) = a_{11}(t) a_{12}(t) \cdots a_{1n}(t) = \prod_{p=1}^{n} a_{1p}(t), \lim_{n \to \infty} a_{1n}(t) = 1 \tag{2.28}$$

Thus, the envelope function $a_1(t)$ is expressed as the instantaneous amplitude. The instantaneous phase is:

$$\theta_1(t) = arc\,\cos\left(s_{1n}(t)\right) \tag{2.29}$$

The instantaneous frequency can be defined as:

$$f_1(t) = \frac{1}{2\pi} \frac{d\theta_1(t)}{dt} \tag{2.30}$$

(5) The first $PF_1(t)$ can be obtained from the product envelope function $a_1(t)$ and frequency modulated signal $s_{1n}(t)$:

$$PF_1(t) = a_1(t) s_{1n}(t) \tag{2.31}$$

(6) New data $u(t)$ can be obtained by subtracting $PF_1(t)$ from the original data.

35

Then, steps (1)-(5) are repeated k times until $u_k(t)$ is a constant or doesn't contain oscillations. Finally, the original signal can be reconstructed:

$$x(t) = \sum_{p=1}^{k} PF_p(t) + u_k(t) \qquad (2.\ 32)$$

As previously introduced, LMD has the end effect problem. Researchers have proposed some improvement methods and have been applied to eliminate it.

Huang et al. [74] proposed a mirror periodic method to extend the two ends data to deal with the end effect. In this method, the data was only extended by using the extreme values which close to the ends, the characteristics of data were not considered. Considering the tendency of the data, Gai et al. [75] proposed a wave matched processing method. However, a choppy signal was generated near the ends. By using the neural network, Yong-jun et al. [76] extended the data by the adaptive prediction method. But parameter selection and long computation time should be considered on the applications. An adaptive extending method based on the spectral coherence was proposed for handing the end effect on the LMD [77]. However, it just separated the signal into a number of segments, some information of the signal missed when the segment was very large. Wang et al. [78] used the mean local extrema on the ends to process the boundary effect of LMD. However, the matched signal may be not revealing the similarity of original signal.

2.5 The based theory of DWT

Wavelet transform is classified as the continuous and discrete wavelet transforms (DWT). The continuous wavelet transform is calculated by the convolution of the signal and a wavelet function. A wavelet function is a small oscillatory wave, which contains both the analysis and the window function. However, the discrete wavelet transform

uses filter banks for the analysis and synthesis of a signal. This technique, in fact, provides powerful multi-resolution analysis in the time and frequency domain, which becomes a very useful tool to extract the transitory features of non-stationary vibration signals generated by the gear fault. In order to extract the fault features of signals more effectively, it is necessary to select the appropriate wavelet base function. The discrete wavelet transform is based on the discretization of continuous wavelet transform, and the dyadic scale and translation are used to reduce the computational time and can be expressed after [79] by the following equation:

$$DW(j,k) = \frac{1}{\sqrt{2^j}} \int_{-\infty}^{+\infty} s(t)\psi^* \left(\frac{t - 2^j k}{2^j} \right) dt \qquad (2.33)$$

where j, k are integers, 2^j and $2^j k$ are the scale and translation parameter, ψ is the mother wavelet, ψ^* is the complex conjugate of mother wavelet.

Four kinds of wavelets from the wavelet family are show in the figure 2-6. The wavelet analysis has a good adaptability, which provides a high time resolution for high frequency, meanwhile, a high frequency resolution for low frequency. To show the adaptability of wavelet, the 'Symmlet 8' wavelet at various scales and locations is show in figure 2-6.
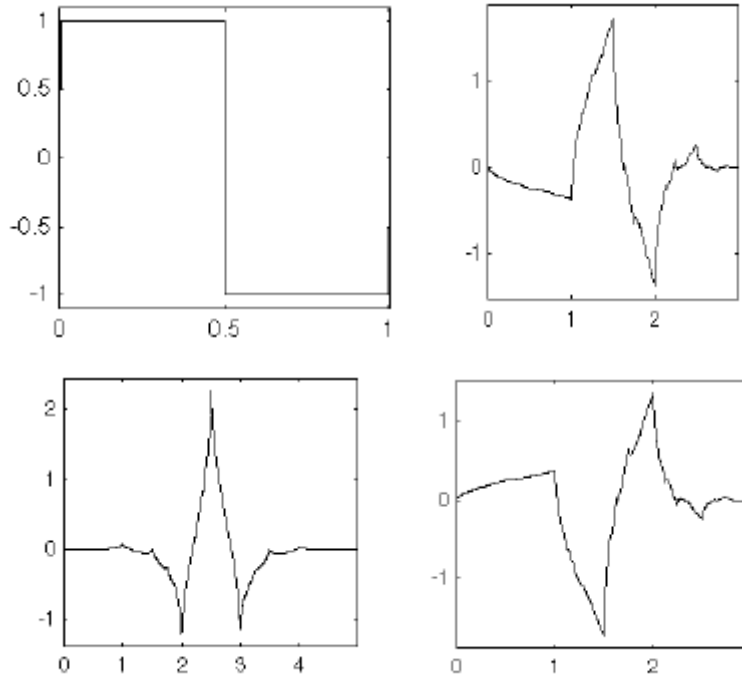
Figure 2-8. Mother wavelets of wavelet family.
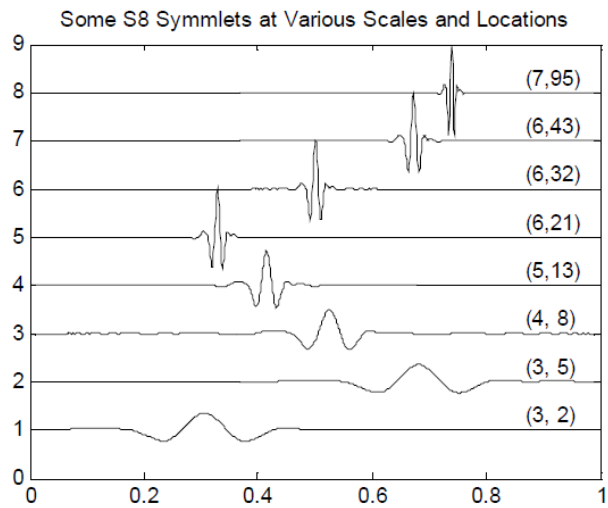
Figure 2-9. 'Symmlet 8' wavelet at various scales and locations.

In particular, it decomposes the signal in its high-scale, low-frequency components, named approximations (A) and its low-scale, high-frequency components, which is called details (D). The filtering process, with the approximation and detail components,

is represented in figure 2-8. This decomposition process can be iterated, and the successive approximations are decomposed in turn: a signal is decomposed into several lower-resolution components, and the so-called wavelet decomposition tree is obtained. As it could be imagined, the analysis process is iterative, so it can be continued indefinitely in theory. Because of its good ability to deal with non-stationary signals, it has been applied widely in fault diagnosis of rotating machinery [80-84]. However, in reality, the decomposition can proceed only until a certain suitable number of levels based on the nature of the signal, or on a suitable criterion such as entropy.
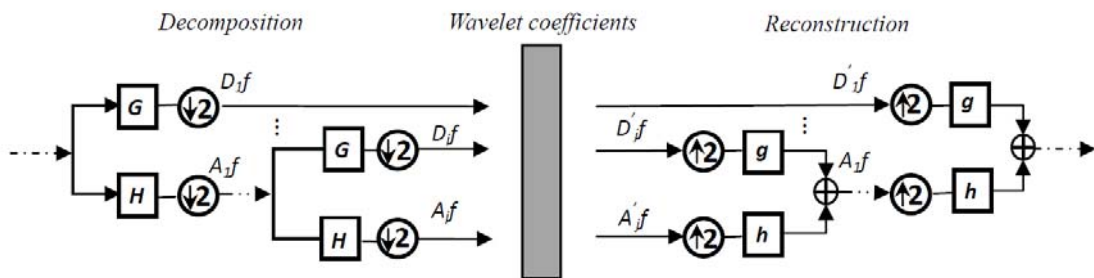
Figure 2-10. A multi-level analysis and synthesis process of DWT [85].

2.6 Conclusions

In this chapter, the approach using the spectral subtraction method combined with empirical wavelet transform has been proposed for gear fault diagnostic. The side-band frequency features for the gear fault signal are a very important indicator, so it can be calculated by using the envelope spectrum analysis. In order to compare the advantages of the SS-AEWT method, the signal processing method for EMD, LMD and DWT technique is also introduced respectively in this chapter.

Chapter 3 Modelling Gearbox vibration responses

3.1 Introduction

As an indispensable connection and power transmission device in mechanical equipment, the normal operation of gearbox directly determines whether the whole mechanical equipment can run normally or not. The gearbox system is a complex system composed of gear pairs, shafts, bearings and other parts. The failure of the components in the system can directly lead to the abnormal operation of the gearbox. Therefore, it is very important to study the common failure types, vibration mechanism and the fault signal model for the gearbox. It is a great significance to clarify the dynamic characteristics of the gearbox fault by using a computer to simulate the typical fault vibration signal.

This chapter focuses on the main failure types of the gear fault based on the analysis of the failure proportion of the components in the gearbox. The vibration mechanism and vibration signal model of local fault is described in detail in order to lay a foundation for the next fault diagnosis of the gearbox.

3.2 The types of the gearbox

Gearboxes usually contain components such as gears, rolling bearings, and rotary shafts. Gears and bearings are the two main components in the gearbox. The gears play the role of transmitting speed and power, and the rolling bearings support the rotating parts of the gearbox. Because the structure of the gearbox is complex and the working strength is high, the components inside the gearbox are easy to break down due to fatigue wear. The common faults in gearbox include gear fault, bearing fault, rotating shaft fault and so on. Failure ratio of each part in the gearbox.

Table 3-1. Failure ratio of each part in gearbox.

Component	Gear	Bearing	Shaft	Box	Fastener	Oil seal
Ratio	60%	19%	10%	7%	3%	1%

The failure of the gear and the rolling bearing is 60% and 19%, respectively. The failure of the gear is the main failure mode of the gearbox. Therefore, it is great significance to study the fault features, the vibration mechanism and the failure form of the gear.

3.3 The vibration characteristic analysis of the gear

3.3.1 The types of the faulty gear

In the process of gear operation, the phenomenon that the gear loses its working capacity or its working parameter value exceeds the maximum allowable range due to some reasons, is called gear fault. There are many causes of gear failure, such as manufacturing error, assembly error, bad lubrication, overload, fatigue wear and so on. According to the cause of gear failure, gear fault can be divided into two types

(1) Static gear failure due to a manufacturing process or installation errors, etc. Such as gear tooth error, gears and holes are not concentric, the axis of each part is misalignment or unbalanced, and so on. The poor assembly of gear will cause serious mechanical loss. Especially, when the assembly error is large, the gear transmission will turn quickly and slowly inconsistently, which will lead to the impact in meshing, and cause greater vibration and noise.

(2) Dynamic gear failure caused by the operation. Generally, the tooth surface of the gear is subjected to a large load. In the meshing process of the gear, there are both relative rolling and sliding between the teeth of the gear pair. During the rolling process,

the positive pressure in the contact region of the gear tooth surface causes shear stress. The relative sliding of the tooth surface will produce tensile stress (or compressive stress), which will lead to pitting, breakage teeth, wear and other dynamic gear failures during the continuous running of the gear. The occurrence proportion of gear failure.

Table 3-2. Proportion of common gear failure.

| Types	Breakage	Pitting	Wear	Scratch	others
Proportion	41%	31%	10%	10%	8%

Breakage teeth, pitting and wear account for a large proportion of gear faults. The reasons and vibration performance of these three faults will be explained below.

(1) Gear breakage tooth. Breakage tooth is a kind of serious fault, which is mainly included the fatigue breakage tooth and overloaded breakage tooth. Fatigue breakage tooth is the propagation form of gear crack fault. The main reason is that when the gear tooth is subjected to alternating load, the root of the gear tooth will be subjected to periodic bending stress. When the bending stress exceeds the bending fatigue limit of gear material, fatigue breakage tooth will occur. Gear breakage teeth usually produce more energy, and there will be a regular impact for the vibration signal in the time domain. Therefore, the impact frequency equals to the rotating frequency of the shaft in which the breakage gear is located for a single breakage tooth fault. On the other hand, there is a side-band frequency, which is spaced by the rotational frequency and its multiple frequencies of the shaft where the gear is broken, around the meshing frequency of the gear and its multiple frequency in the frequency domain.
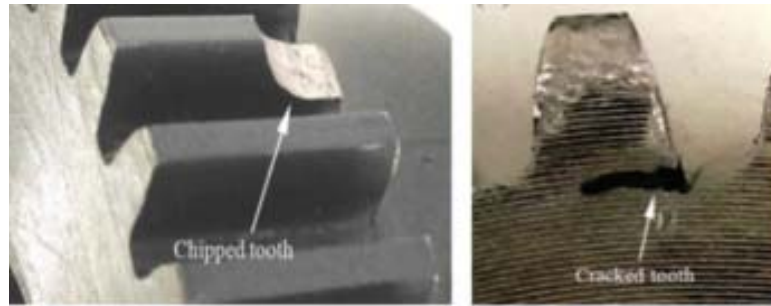
Figure 3-1. the type of gear: breakage tooth [86].

(2) Gear pitting. Gear pitting is a common fault in engineering practice. Pitting is a surface fatigue failure of the gear tooth. It occurs due to repeated loading of tooth surface and the contact stress exceeding the surface fatigue strength of the material. The material in the fatigue region gets removed and a pit is formed. When a pitting appears on the surface of the gear tooth, the periodic impact component will be produced for the vibration signal in the time domain, and the kurtosis value will increase with the development of the fault. The spectrum amplitude will gradually increase in the frequency domain with the development of gear fault, the increment for the medium or high frequency will be more obvious, and the side-band of rotational frequency modulation will be generated around the meshing frequency.
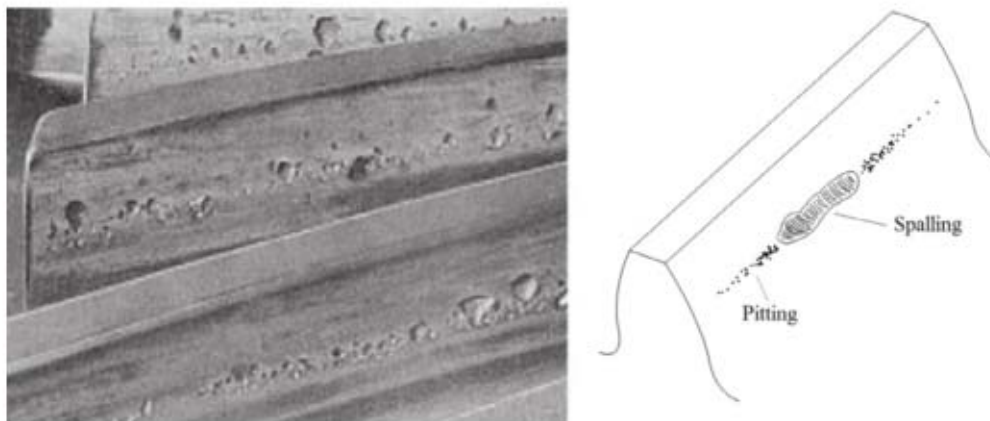
*Figure 3-2. Gear tooth pitting and spalling.*

(3) Gear wear. Gear wear refers to the phenomenon of material friction damage on the surface of gear teeth. Gear wear that does not affect the normal operation of the gear

is called normal wear. The normal wear gear tooth surface is shiny and smooth, no obvious abrasion, and all tolerances are within the allowable range. However, severe wear will thin the tooth thickness, increase vibration noise, so it leads to gear failure. The main forms of gear wear failure include abrasive wear, corrosion wear and section impact wear. The abrasive wear is caused by the abrasive entering the tooth surface meshing region. The corrosion wear is caused by the chemical reaction between the lubricant and gear material. The section impact wear is caused by the impact load. If each gear tooth is worn out, it is called uniform wear. When the gear appears the uniform wear, the amplitude value of the meshing frequency and the higher harmonic increases, but the amplitude value of the higher harmonic increases much faster. Therefore, the vibration signal waveform gradually approaches the square wave.

In the static and dynamic gear faults, the static gear faults can be corrected before or during installation, however, the dynamic gear faults are inevitable, which occur in the running gears. Therefore, dynamic gear failure is studied in this paper.

3.3.2   The gear vibration mechanism

Gear vibration system is a very complex nonlinear system. It is difficult to establish a complete nonlinear dynamic model. Therefore, gear drive pairs are usually simplified and Simplified gear meshing vibration model
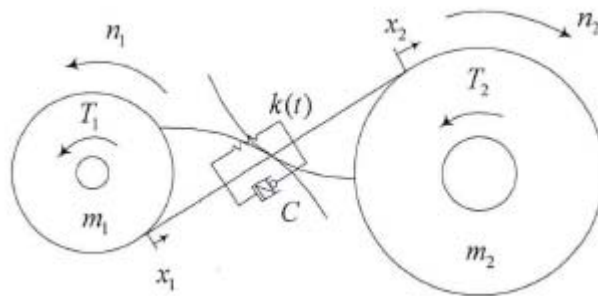
Figure 3-3. The vibration model of gear meshing.

The dynamical equation is

$$M\ddot{x} + C\dot{x} + k(t)x = F(t) \tag{3.1}$$

where, the equivalent mass of gear pair is defined by $M = \dfrac{m_1 m_2}{m_1 + m_2}$. m_1, m_2 is the mass of two gears. x is the relative displacement along the gear meshing line. $x = x_2 - x_1$. C is the gear meshing damping. $k(t)$ is the gear meshing stiffness. $F(t)$ is the dynamic load, and it contains the excitation generated by the failure defect. $F(t)$ is not only affected by the tooth stiffness and transmission error, but also by the direction of the friction force on the tooth surface. However, the friction force on the tooth surface has a little effect on $F(t)$ under the well lubrication condition and low tooth surface roughness. Therefore, the friction force can be ignored.

$$M\ddot{x} + C\dot{x} + k(t)x = k(t)E_1 + k(t)E_2(t) \tag{3.2}$$

where, E_1 is the average static elastic deformation of the gear after being loaded. $E_2(t)$ is the relative displacement of two gear teeth caused by gear error and gear fault. $k(t)E_1$ is the vibration in normal gear operation. $k(t)E_2(t)$ depends on the gear stiffness $k(t)$ and the fault function $E_2(t)$. This part can explain the existence of the side-band frequency in gear fault signal and the relationship between them and fault.

3.4 The mathematical model of the gear vibration

Conventionally, vibration is expressed as a stationary function of time, having fixed frequency components with the phase of a particular component increasing linearly with time at a slope proportional to its frequency. In order to clearly express the inherent periodicities and angular dependencies in the gearbox vibration, the vibration is expressed in the following derivation as a non-stationary function of time with phase

45

expressed in terms of the angular position of the underlying rotating element. The instantaneous frequency of a particular component is given by the time derivative of its phase θ(t) [87]

$$f(t) = \frac{1}{2\pi} \frac{d\theta(t)}{dt}$$

(3. 3)

The angular position of a rotating element at time t is given by the integral of its instantaneous frequency since time $t = 0$ [88]

$$\theta(t) = \theta_0 + 2\pi \int_0^t f(\tau) d\tau$$

(3. 4)

where θ_0 is the angular position at time $t = 0$.

In the following, where a function is said to be periodic with an angular variable, it repeats with the modulo 2π value of the variable.

3.4.1   Gear Vibrations

The gear vibration is periodic with the angular position of the gear, which is represented in the following by the angular position of the shaft on which the gear is mounted, $\theta_s(t)$. The vibration due to gear g on shaft s, can be described as the sum of the load dependant tooth-meshing vibration and additive vibrations caused by geometric errors:

$$v_{sg}(t) = v_{sg}^{(1)}(t) + v_{sg}^{(2)}(t)$$

(3. 5)

3.4.1.1 Tooth meshing vibration

The gear vibration signal has components at the tooth-meshing frequency and its harmonics with the amplitudes dependent on the mean load and load fluctuations

periodic with the shaft rotation (load and amplitude modulation effects) plus a nominally constant amplitude due to mean geometric errors on the tooth profiles (machining errors and wear). The frequency modulation effects due to periodic torque fluctuations and tooth spacing errors are more appropriately described as phase modulation as they only affect the instantaneous frequency of the vibration, not the mean frequency over the period of rotation

For the first M harmonics, the vibration at harmonics of tooth-meshing for gear g on shaft s, can be expressed as:

$$v_{sg}^{(1)}(t) = \sum_{m=1}^{M}[A_{sgm}(\bar{L},\theta_s) + \bar{E}_{sgm}]\cos(mN_{sg}(\theta_s + \beta_{sg}(\theta_s)) + \phi_{sgm}) \qquad (3.6)$$

Where $\theta_s = \theta_s(t)$ is the shaft angular position;

$A_{sgm}(\bar{L},\theta_s)$ is the amplitude due to tooth deflection;

$\bar{E}_{sgm}$ is the mean amplitude at harmonic m due to machining errors and wear;

N_{sg} is the number of teeth on the gear;

$\beta_{sg}(\theta_s)$ is the phase modulation due to torque fluctuations;

ϕ_{sgm} is the phase of harmonic m at angular position $\theta_s(t) = 0$.

The amplitude due to tooth deflection is a function of both the mean load, $\bar{L}$, and fluctuating load periodic with the angular position $\theta_s(t)$

$$A_{sgm}(\bar{L},\theta_s) = \bar{A}_{sgm}(\bar{L})(1 + \alpha_{sg}(\theta_s)) \qquad (3.7)$$

Where $\theta_s = \theta_s(t)$ is the shaft angular position;

$\bar{L}$ is the mean load;

47

$\overline{A}_{sgm}(\overline{L})$ is the amplitude due to the mean load;

$\alpha_{sg}(\theta_s)$ is the amplitude modulation due to fluctuating load.

The load dependant phase modulation, β_{sg} in equation (3.6), and amplitude modulation effects, α_{sg} in equation (3.7), are periodic with the shaft rotation $\theta_s(t)$ and therefore they can be expressed as Fourier series

$$\beta_{sg}(\theta) = \sum_{k=1}^{K} b_{sgk} \cos(k\theta + \gamma_{sgk})$$
(3. 8)

$$\alpha_{sg}(\theta) = \sum_{k=1}^{K} a_{sgk} \cos(k\theta + \lambda_{sgk})$$
(3. 9)

Where γ_{sgk} and λ_{sgk} are the phases at $\theta = 0$. Note that these modulation effects both have a mean value of zero.

3.4.1.2 Additive vibration

In addition to the vibration at harmonics of tooth-meshing and modulations due to load fluctuations, other vibrations related to gear meshing are those caused by geometric profile errors (including 'ghost components') which are not identical for each tooth and those due to additive impulses. The amplitude of these additive errors are not significantly affected by load or rotational speed and are expressed as K harmonics of the shaft rotation:

$$v_{sg}^{(2)} = \sum_{k=0}^{K} E_{sgk} \cos(k\theta_s(t) + \xi_{sgk})$$
(3. 10)

Where ξ_{sgk} is the phase of harmonic k at shaft angular position $\theta_s = 0$.

Note that a DC component ($k = 0$) is included in the above, indicating that the

48

additive vibration does not necessarily have a mean value of zero.

3.4.1.3 *Additive vibration*

Although the tooth-meshing vibration has been expressed above as if it were due solely to, and periodic with, a single gear, it is obvious that tooth-meshing vibrations can only be produced by the interaction between meshing gears. This results in a combined periodicity of the meshing vibration, which is only repeated when the angular position of both gears return to the starting point (i.e., when the same tooth pair returns to mesh). In general, for meshing gears, the vibration will repeat over a period equal to the rotational period of one of the gears times the number of teeth on its mating gear. An exception to this is when there is a common factor in the number of teeth on the gears, in which case the normally expected period will be reduced by the value of the common factor.

The tooth-meshing vibration defined in equation (3.6) represents the mean vibration for one gear over the tooth-to-tooth meshing period. The unmodulated portion of this vibration (i.e., the mean tooth-meshing component) will be identical for both gears, with the modulated portion being contributed by the variations between teeth on the individual gears. For simplicity, the gears have been treated as separate entities here (with the mean tooth-meshing vibration being divided between the two gears). The combination of the vibrations by addition is acceptable where small phase modulations are involved. Where large phase modulations are involved, the tooth-meshing vibration can be treated as the mean vibration with both the amplitude and phase modulations being the mean of those for the two gears.

3.4.1.4 Additive vibration

The meshing vibrations defined above relate to the meshing action of the gear teeth with those of a mating gear. In the situation where a gear meshes with more than one other gear (i.e., a multi-mesh gear), a set of meshing vibrations will be produced for each of the gear meshes. However, it cannot be assumed that the vibration characteristics are identical for each of the gear meshes; loading conditions, depth of mesh and even the tooth surface which is in contact can be different for each of the mating gears.

Even though the basic periodicities will be the same for each of the gear meshes, the vibration waveforms may be quite different and the simplest, and most effective, means of modelling multi-mesh gears is to treat each gear mesh as if it were a separate gear. For instance, a gear having 22 teeth and meshing with two other gears would be modelled as if it were two separate 22 tooth gears.

## 3.5 The experimental results and discussion

This subsection presents the design of a gearbox test rig, and the corresponding experiments conducted for the gear wear monitoring. The data acquisition system that used in the vibration measurement is shown in figure 3-4.
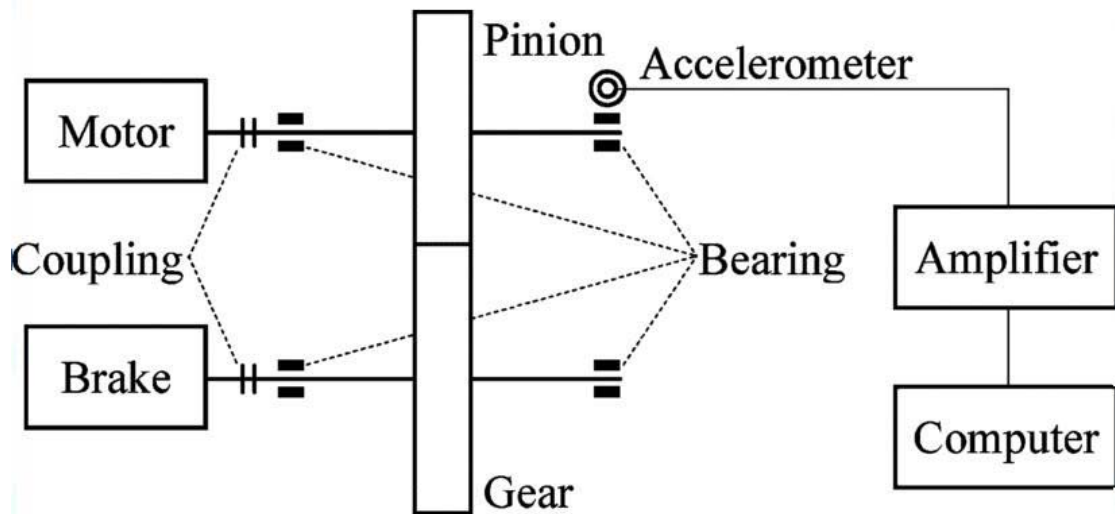
Figure 3-4. Test bench diagram.

3.5.1   *The specification of gearbox experiment*

In this subsection, the experimental data of CETIM (Centre des Etudes Techniques des Industries Mécaniques de Senlis) [89] is used to extract the side-band frequency features with the SS-AEWT method. The experimental device includes a motor, brake, gearbox, and bearing. The figure 3-5 shows the gearbox experimental setup.
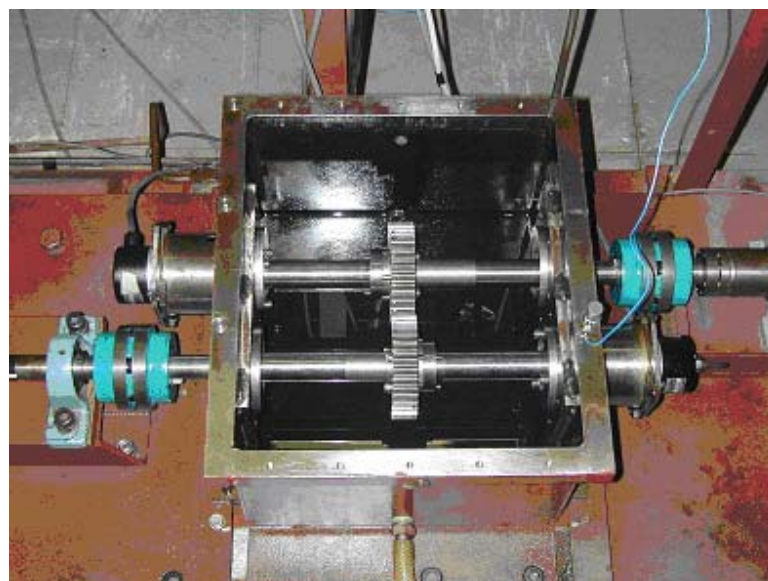

*Figure 3-5. The gearbox experimental setup.*

An accelerometer is mounted on top of the gearbox casing. The single-stage reducer for the gearbox includes a pinion with 20 teeth and a gear with 21 teeth. During the experiment, the motor runs at a stable speed of 1000 rpm (i.e. approximately 16.667 Hz), the driven gear speed is 15.873 Hz, and the meshing frequency is 333.333 Hz. During the experiment, the accelerometer signals are acquired at a sampling frequency of 20 kHz and each record lasts for 1 s. While under the faulty status, one of the pinion teeth is spalled. The spectral subtraction denoising method is applied to obtain the processed signal and compare it to the original signal. The figure 3-6 shows that the impulse response of the fault information is much clearer.
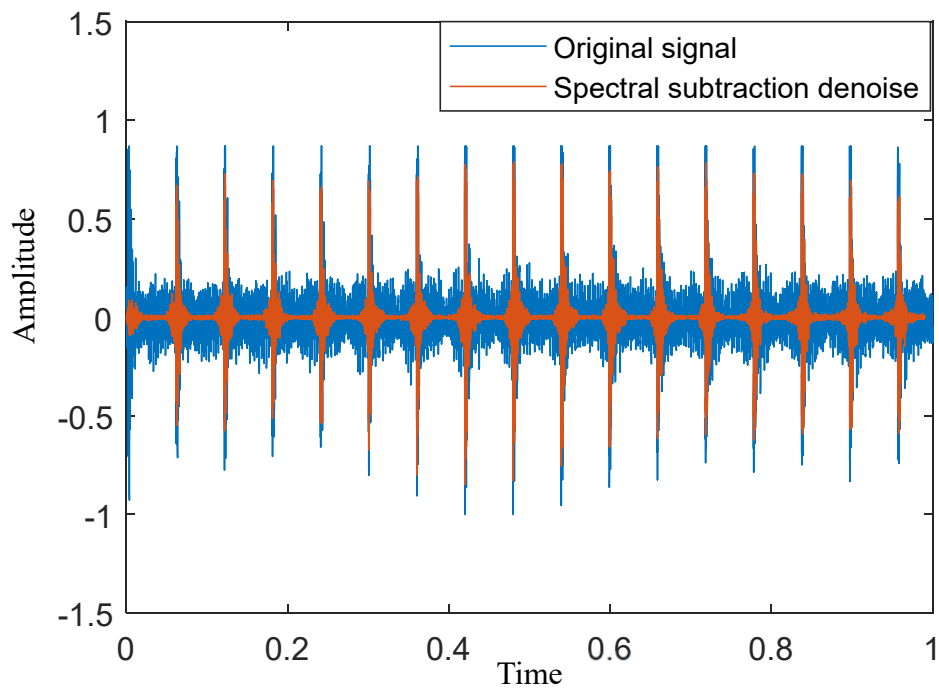
Figure 3-6. The compared results with spectral subtraction denoising.
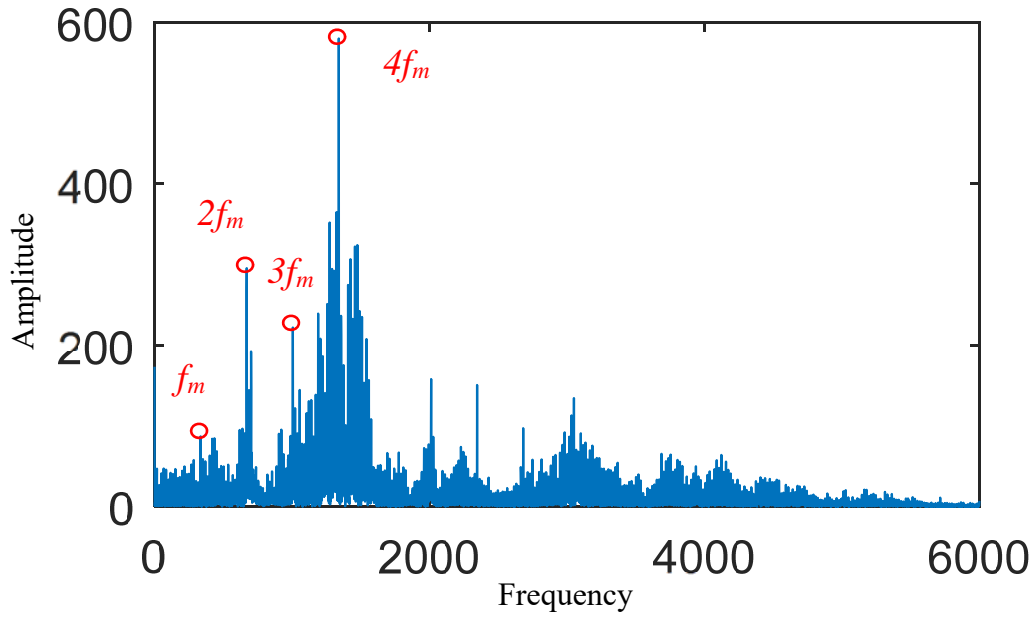
(a) Frequency spectrum of the original signal.
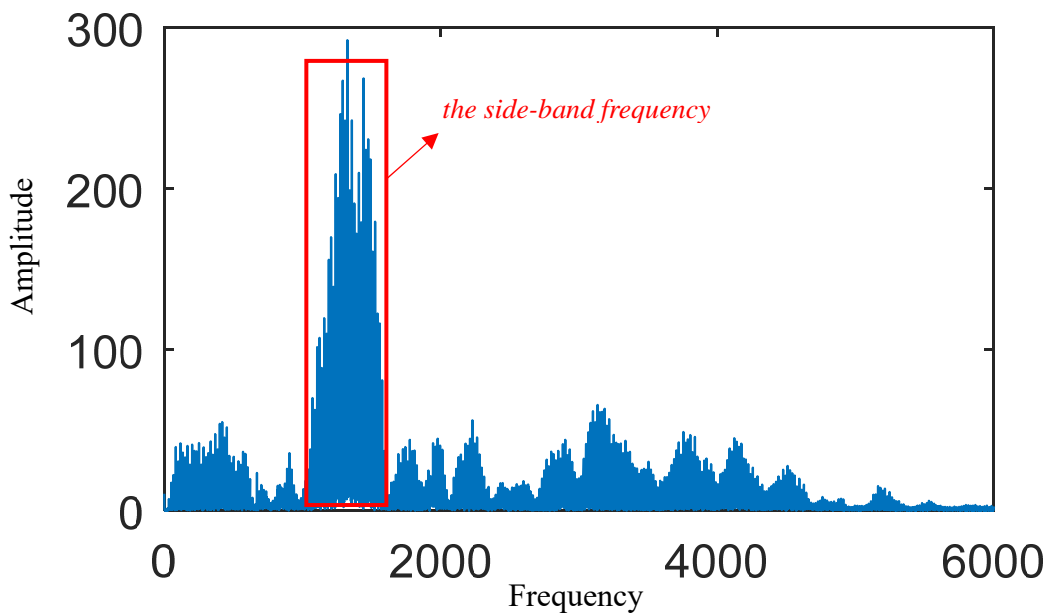
(b) Frequency spectrum of the processed signal.

**Figure 3-7. Frequency spectrum results with spectral subtraction denoising.**

The frequency spectrum results are compared in figure 3-7. The gear meshing frequency is clearer than the side-band frequency in the frequency spectrum of the original signal, as shown in figure 3-7 (a). However, the side-band frequency features are enhanced by the spectral subtraction method, as shown in figure 3-7 (b). The results

indicate that the noise can be effectively removed by the spectral subtraction method to obtain the processed signal, which is beneficial for extracting the fault features by the EWT method.
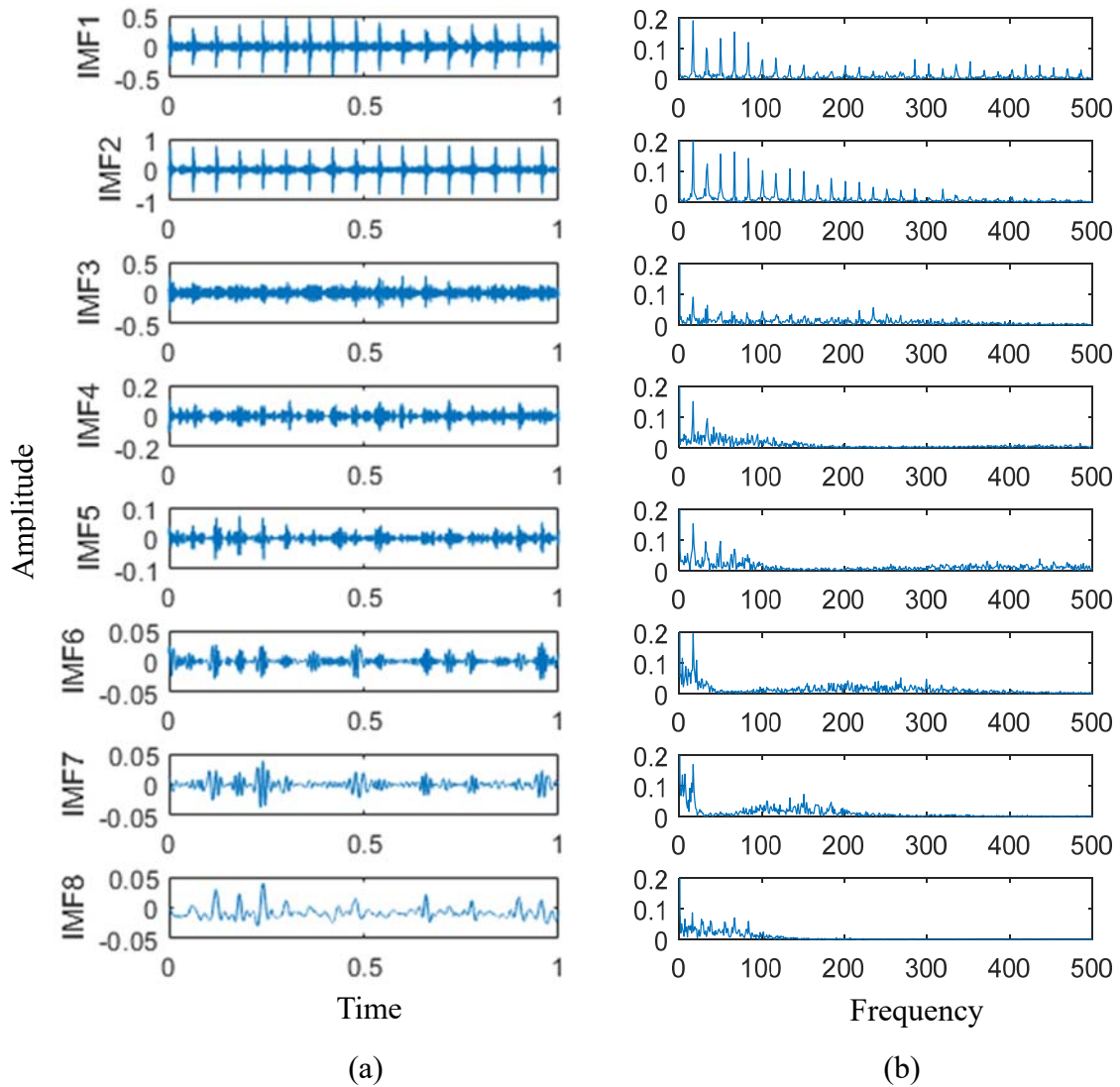
Figure 3-8. IMF distribution and envelope spectrum results with EMD.

For comparison, EMD, LMD and DWT methods are used to decompose the simulated signal, respectively. Firstly, EMD is employed to decompose the observation signal into eight IMFs, and the result of each IMF is showed in figure 3-8 (a). The frequency characteristics of first and second IMF are significantly extracted with the envelope spectrum, which shows in figure 3-8 (b).

54
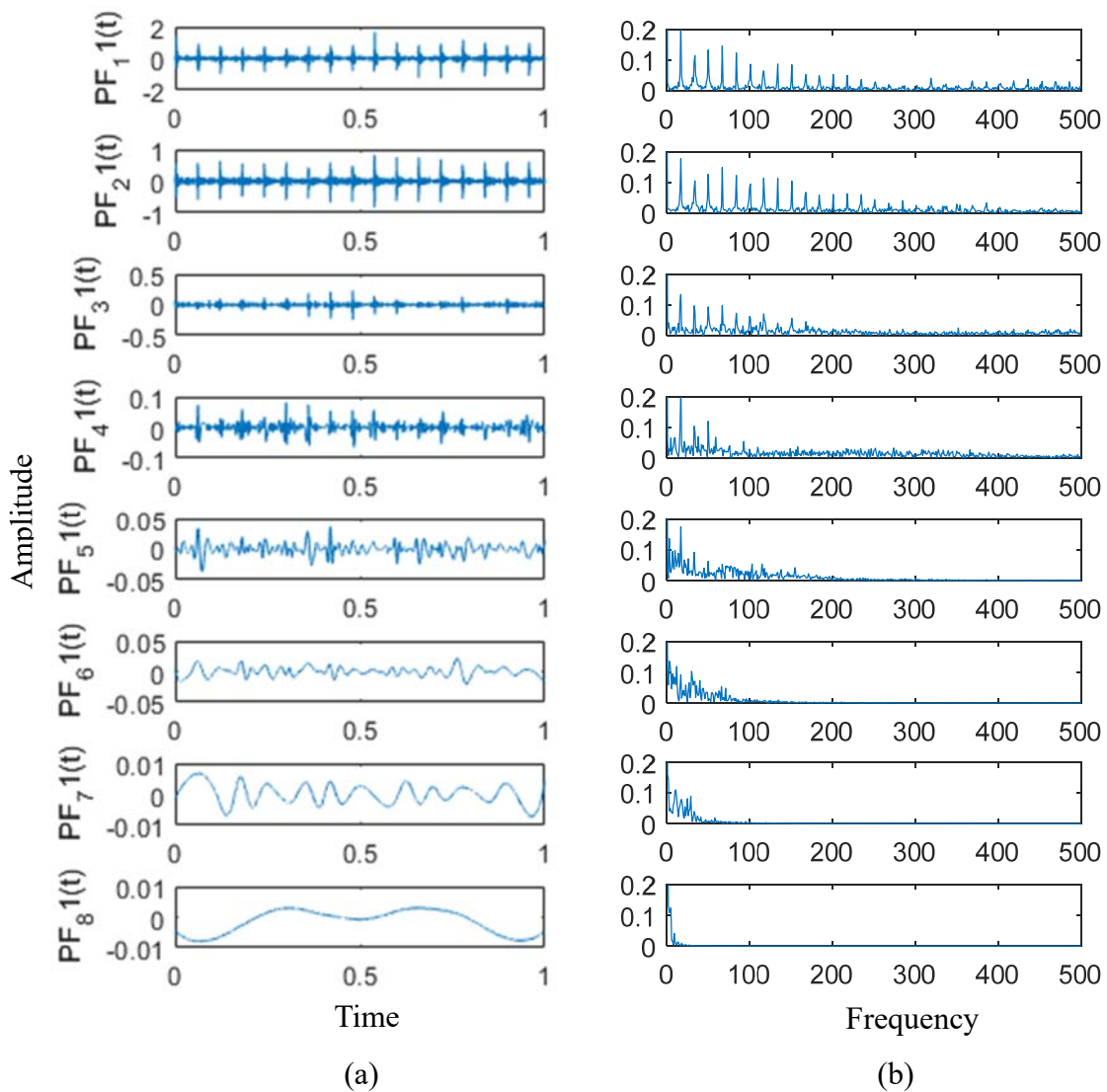
Figure 3-9. LMD decomposition results and envelope spectrum.

The LMD is applied to adaptively decompose the fault signal into several PFs from high frequency band to the low one. Several PFs can be obtained with the LMD process. The LMD decomposition results and the envelope spectrums are shown in figure 3-9. The first PF is selected for further analysis, because it has the biggest correlation coefficient value and keeps the most of information from the fault signal.
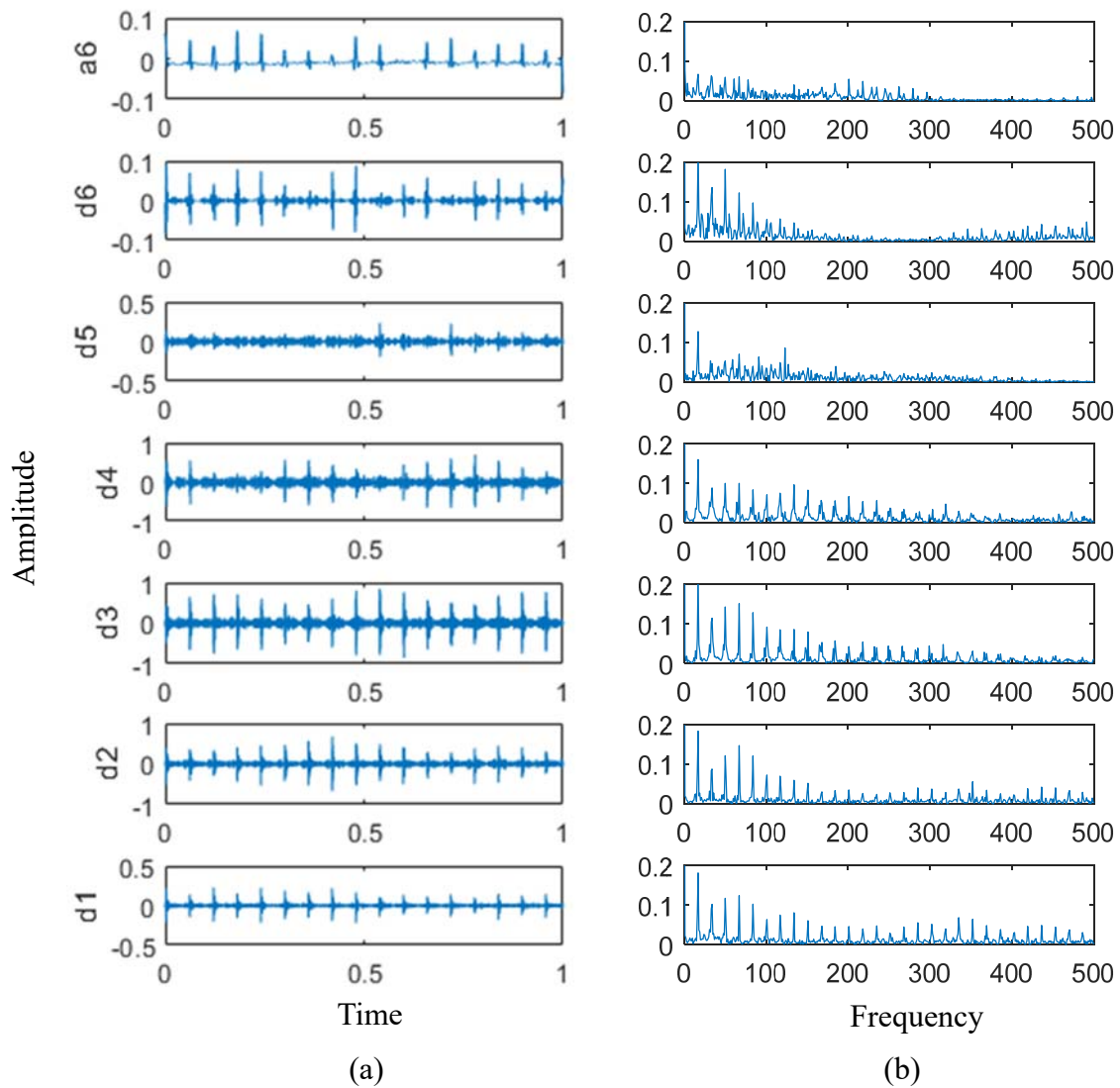
Figure 3-10. DWT decomposition results and envelope spectrum.

In this section, The DWT decomposes the fault signal to extract the main information of the fault features, and the results of DWT decomposition and the envelope analysis of each level wavelet coefficients are shown in figure 3-10. The wavelet correlation of the d_3 level is much bigger than others, so it can be used as the features of the fault information.
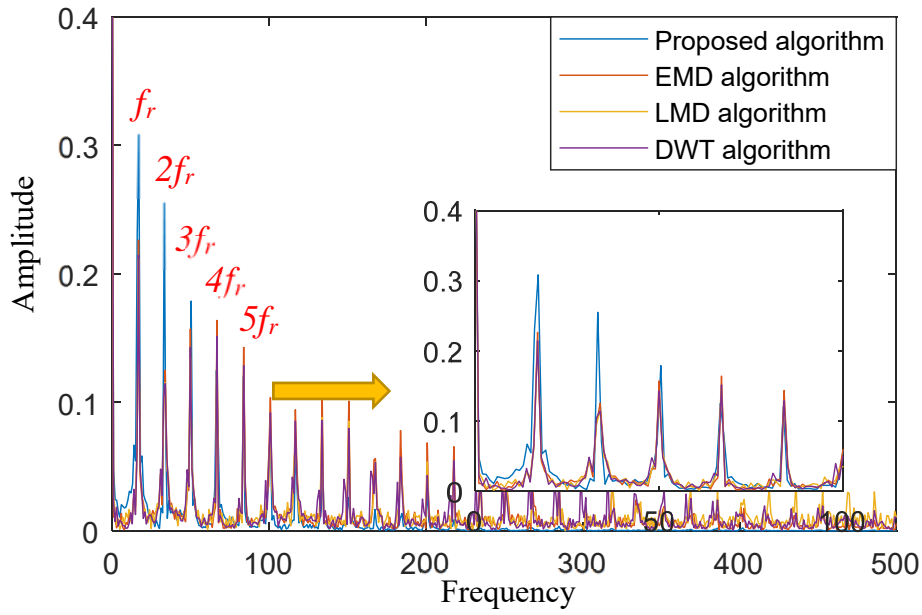
Figure 3-11. The fault features with square envelope analysis

Table 3-3. The side-band amplitudes for different analysis methods.

Analysis type	Amplitude of fr	Amplitude of 2fr	Amplitude of 3fr	Amplitude of 4fr	Amplitude of 5fr
EMD algorithm	0.2264	0.1252	0.1572	0.1639	0.1435
LMD algorithm	0.212	0.1154	0.1341	0.1468	0.1245
DWT algorithm	0.2144	0.1147	0.1429	0.1515	0.1287
Proposed algorithm	0.3085	0.255	0.1789	0.1248	0.1203

The SS-AEWT method can extract a greater amplitude of the side-band frequency for the gear fault feature. The figure 3-11 and table 3-3 show the detailed information. The amplitude values of the first and second-order frequency are better for the SS-AEWT method than the others. The amplitude values of the first-order frequency are improved by 36.26%, 45.52% and 43.89% with EMD, LMD and DWT, respectively. The amplitude value is not improved by more than 50%, because the external noise is very low. Furthermore, the calculated frequency is 16.17Hz, which approximately equals the theoretical value (15.87Hz). Hence, we can conclude that the first-order

frequency in the side-band frequency features equals the rotation frequency of the input shaft. This demonstrates that the SS-AEWT method is effective for gearbox fault diagnosis.

3.6 Conclusions

This chapter has carried on the detailed analysis to the gear fault type. The mathematical model of the gear vibration is built, and the components of its vibration signal are introduced in detail. Finally, the side-band frequency of the gear fault signal is obtained with the experimental data by using the different methods. The results indicate that the SS-AEWT method can more clearly extract the fault frequency features than the EMD, LMD and DWT method.

Chapter 4 Description of the rigid model

4.1 Introduction

In this chapter, the gear dynamical model will be investigated for gear pairs operating at fixed center distance. The utilization of multi-body dynamics programs such as ADAMS make complex dynamical simulations possible. ADAMS [90] is a multi-body dynamics simulation application. Many dynamical systems can be modelled in Adams from simple cranes and conveyor belts to full systems like cars, aircraft and wind turbines with most detailed complexity from a dynamical viewpoint. Even other from FEM analysis and CFD calculations can be coupled to the software. This thesis concerns the gearbox vibration with the flexible body of the gear. The most important property of this work is using of a finite element and dynamic simulation program together.

HyperwWorks is a software product for solving physical problems through the Finite Element Method (FEM). ADAMS is also a software product, applied among others for static, kinematic and dynamic analysis of mechanisms, usually with rigid members, but it also enables to calculate generally with non-rigid links between the members or between a mechanism and its surroundings. The flexibility of such bodies in the data files communicating with the ADAMS environment was presented in a previously prepared form, and Modal neutral file (MNF) has been chosen as such a form, which results from the realized analyses in FEM and contains information about geometry, weight characteristics and modal shapes of a flexible body. MNF is generated by using HyperwWorks software.

4.2 Establishment of gearbox simulation model

The gearbox is used in this study, and it is a double stage reduction gearbox developed for a crane. This gearbox has two gear pairs composed by helical gears, and the number of teeth is 17, 81, 23 and 109, respectively. The reduction gearbox also includes input shaft, middle shaft and output shaft. We can see a model of the gearbox in the figure below.
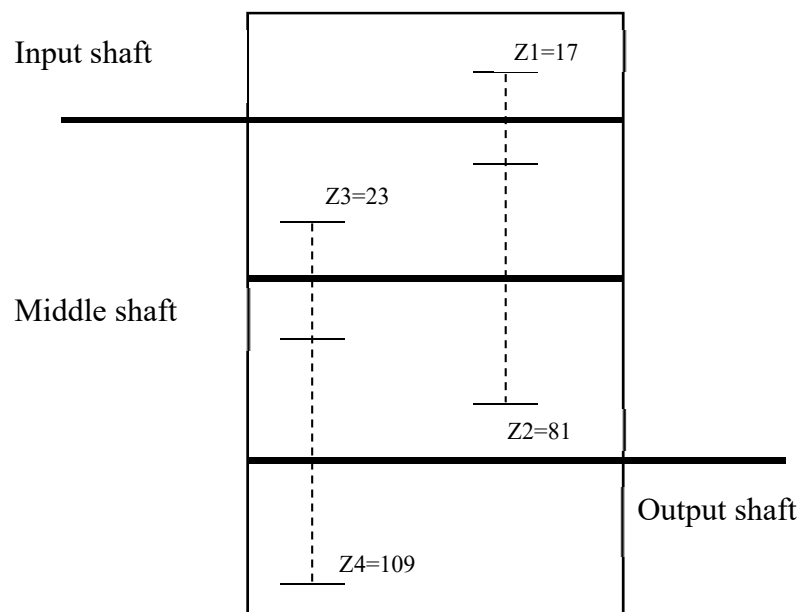

Figure 4-1. The model of gearbox.

4.2.1 The gearbox model

ADAMS provides the measured data for the strategy of the faulty gear in various test environments, which are important for the modes and intensities of the monitored gears. All gears modeled in this thesis are done in SolidWorks and then transferred to ADAMS. SolidWorks was used greatly due to its ability to model the involute profile of gear teeth very accurately as well as create complex gear damage such as pitting and root damage. The models could be used for ADAMS by modeling everything in SolidWorks. Several

steps are necessary before obtaining the simulation signal. Firstly, ADAMS applies gravity to all the parts and leads all the solid models (including the gearbox body, the gear shafts and gears).
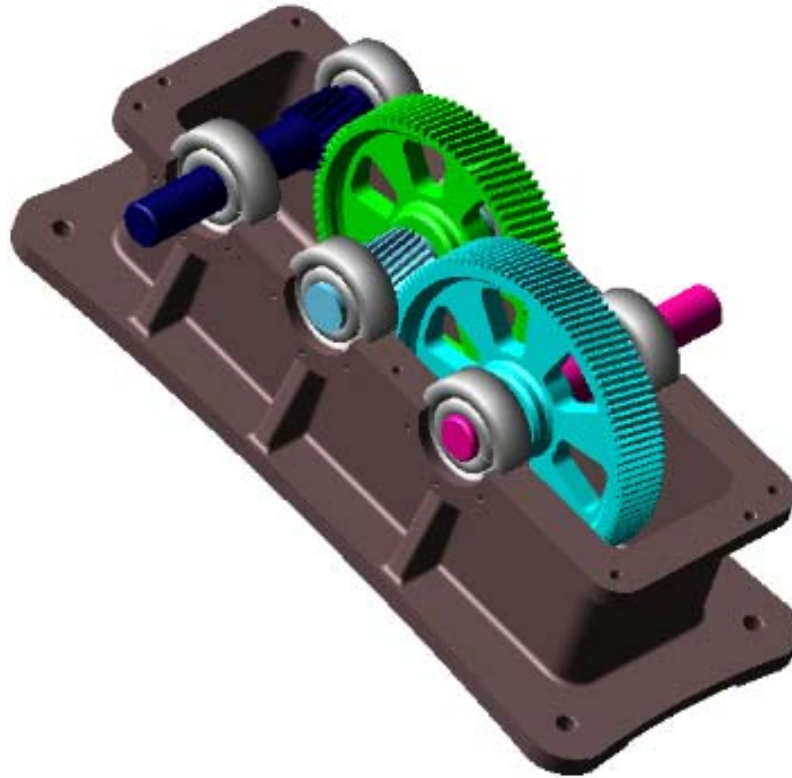
Figure 4-2. The configuration and dynamical model of the gearbox system

We can select the material type of the gear, which will be steel, and the program will calculate its mass and inertia matrix according to the geometry defined, or we can also input the matrix number by number if we knew its values. In this step, the system automatically generates information such as the mass of the components, the mass center, and the moment inertia of the components, etc. according to the parameter set of the steel material properties.

In ADAMS software, the dynamic mesh force of gear pairs is essentially a contact force simulated by the impact function. The formulation of a contact kinetics in ADAMS is summarized from [91] as follows. During a dynamic simulation, the first step is to find out whether the contact occurs between the geometry pairs identified in

the contact statements. If there is no contact, there is no force. If there is a contact, the geometry modeling system calculates the location of the individual contact points and the outward normal to the two geometries at the contact point. In theory, the contact between rigid bodies requires that the two bodies do not permeate each other, which can be expressed as a unilateral constraint. The contact force is the force associated with the enforcement of this constraint. There are usually two ways to deal with this auxiliary constraint, one is to introduce Lagrange multiplier, the other is penalty regularization. For contact problems in ADAMS, the latter technique is adopted. The impenetrability of two approaching bodies is measured with a gap function, p where zero indicates no contact and positive value of p indicates penetration. The normal contact force magnitude is denoted by F_n, where a positive value indicates there is contact and quantifies a separation force between the contacting bodies. Combining some auxiliary contact constraints ($p \geq 0; F_n \geq 0$ and $F_n p = 0$), it is possible to get

$$F_n = kp^e \tag{4.1}$$

where k (stiffness) is a scalar penalty parameter and e is the contact coefficient.

The selection of k and e is up to the user and needs experience an tuning until you get good results with minimized noised levels. This is the disadvantage of penalty regularization technique. You can also approximate the compliance of a body by correlating k to its material and geometric parameters. For example, Hertzian Contact Theory can be used to estimate contact stiffness from material and geometric properties [92-93]. As can be seen from the figure 4-3, a very high degree of non-linearity will be experienced during a transition from non-contact ($p = 0$) to a contact ($p > 0$) if the contact coefficient $e \leq 1$. As it is the case with other numerical method, this will adversely affect the calculation time of impact force. Hence, Adams/Solver performance will be enhanced if e is selected to be greater than one. The transition

into contact using the exponential function shown on the figure 4-3 with a green dashed line will always be the best option.

In an effort to incorporate general material constitutive relationships for the contacting bodies, as well as facilitate time integration, Adams/Solver extends the previous expression by using nonlinear displacement-dependent, cubic viscous damping terms. The general form of the impact function model used in ADAMS is given by

$$F_n = kp^e + step(p,0,0,d_{max},C_{max})\dot{p}$$
(4. 2)

where p is the penetration depth of one geometry into another. $\dot{p}$ is the penetration velocity at the contact point. e is a positive real value denoting the force exponent and is termed as contact coefficient. C_{max} is the maximum damping coefficient and d_{max} is a positive real value specifying the maximum penetration to apply C_{max}. Step, the damping coefficient is a cubic polynomial step function.
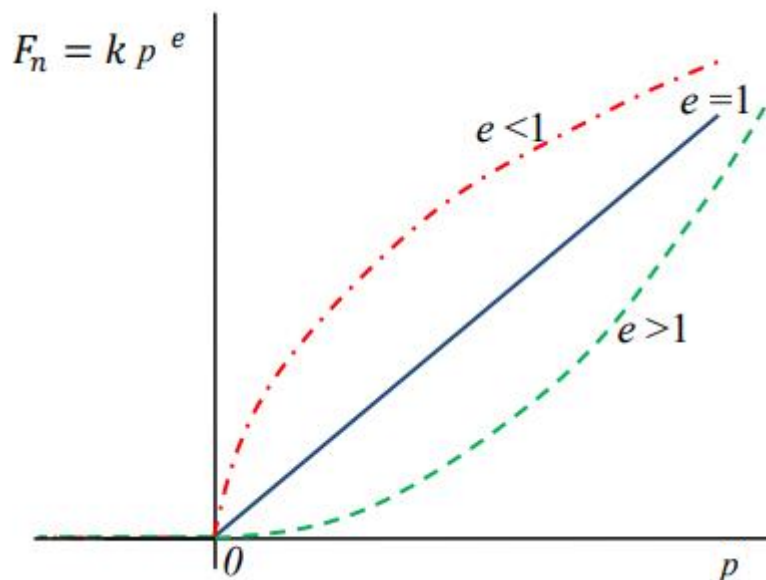

Figure 4-3. The contact force variation curve.

4.2.2   The flexibility of gear

In order to improve the accuracy of the dynamic model, the gear is modeled as a flexible body by using a finite element analysis tool. In the past, the finite element analysis (FEA) and multi-body system simulation (MBS) were used to the field of mechanical system simulation. Thereinto, FEA solvers is applied to research the elastic/plastic behavior of single deformable components, and multi-body analysis mainly focused on the non-linear dynamics of entire systems of interconnected rigid bodies. In recent years, many different software products have utilized sub-structuring techniques to combine the benefits of both MBS and FEA. In the field of multibody system simulation, the intention is the realistic representation of component level flexibility. Based on the purpose of FEA, this method can be used to derive complex dynamic loading conditions of these flexible components, but in general, it cannot be completed manually. Especially in the field of structural optimization based on finite element method, the formulation of actual boundary and loading conditions has an important impact on the final design of the structure. In this study, the flexible gear is processed by the HyperWorks software, and is exported to MNF file in the gearbox. The details of this study and implementation of these programs are discussed in this section.

An assembly of the gearbox is developed by using SolidWorks. These parts are linked together using the coincident, concentric and gear mates. The geometry of the required gear on the middle shaft is exported to make the flexible body by using HyperWorks software. The figure shows the gear solid model in the HyperWorks software.
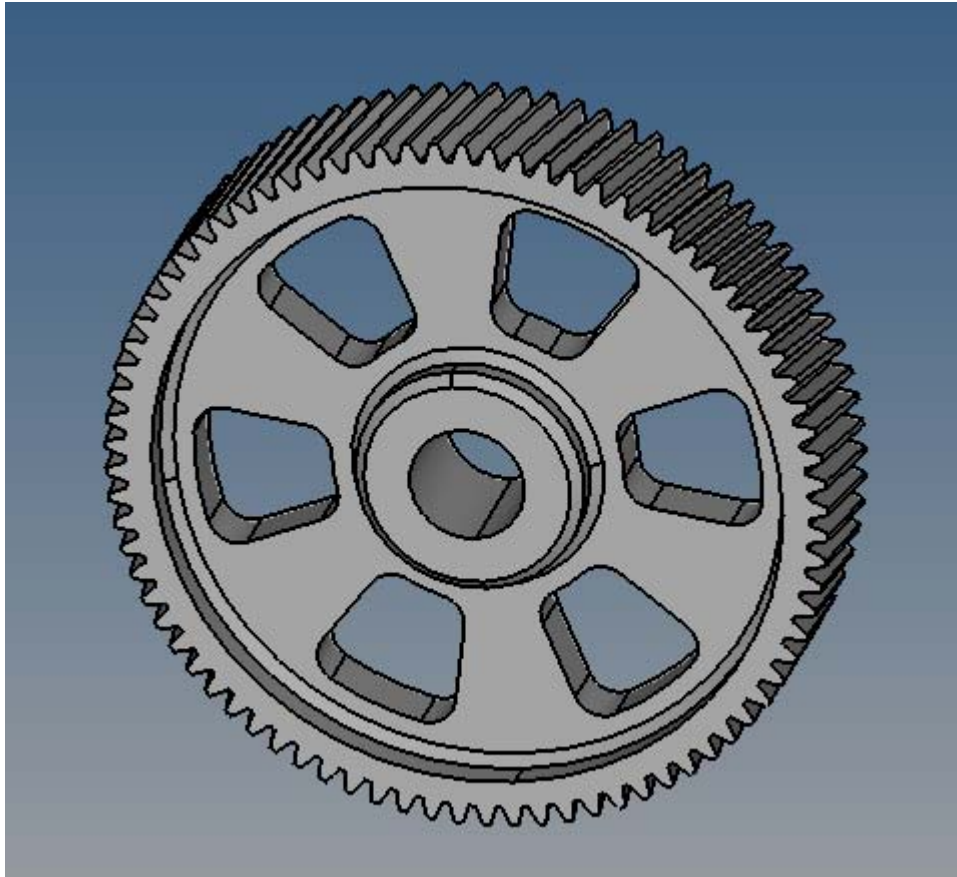
Figure 4-4. The gear solid model.

Assembly modeling in FE analysis is complex and time taking. Accuracy of the FE solution mainly depends on the Pre-processing. However, the gear of middle shaft is only processed in this study. In HyperWorks, there are extensive element libraries that provide useful tools for solving problems. Users could choose different element families to closely match their problems. One of the major distinctions between different element families is the geometry of the elements. It is because each element family was designed for different purposes and applications. For example, shell elements should be applied on structures that contain thin walls, beam elements should be considered when the structures are constructed from beams, rigid elements should only be applied to the structures that are unable to deform, etc. The following figure 4-5 contains the most commonly used element families.
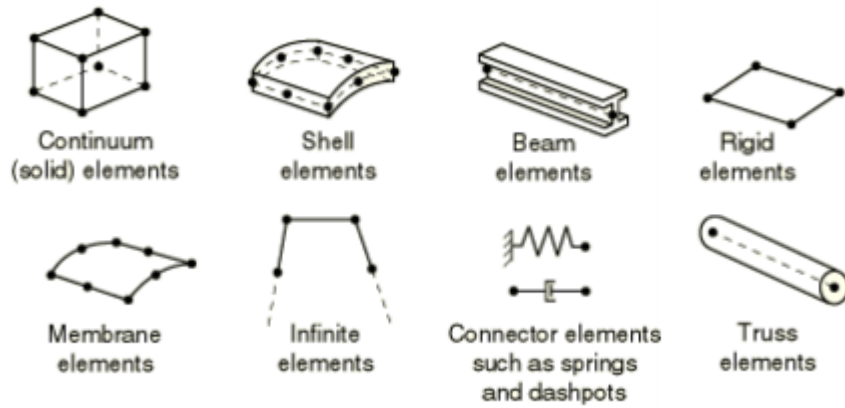
Figure 4-5. The commonly used element families.

Once the element families have been picked, it is necessary to decide what type of elements should be utilized and its dimensionality. For finite element analysis, the displacements or other degrees of freedom are calculated at the nodes of the element. The displacements are obtained by interpolating from the nodal displacements, and most often the interpolation order is determined by the number of nodes used in the element. Hence, depending on the number of nodes on the element, different interpolation methods will be applied. Trilateral (2D) and tetrahedron (3D) elements are better suited for gear solid modeling as they are the most used elements for non-linear analysis. For the gear model, tetrahedron element has been applied. The figure 4-6 shows 3D FEM model of the gear.
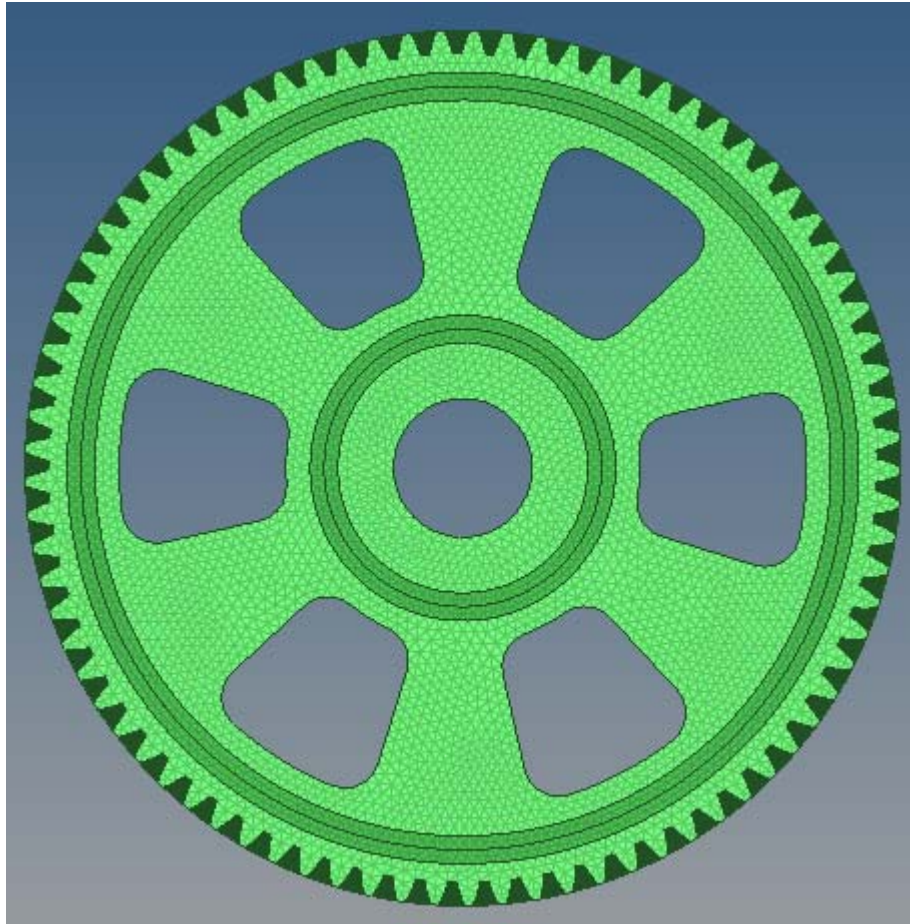
Figure 4-6. 3D FEM model of the gear.

The selected material for the gear of middle shaft is carbon steel since it is one of the most commercially use steel in the industries. The material properties of carbon steel are shown in Table 4-1.

Table 4-1. The material properties of carbon steel.

Modulus of Elasticity (Mpsi)	30
Modulus of Rigidity (Mpsi)	11.5
Poisson's Ratio	0.292
Unit Weight (lbf/in3)	0.282
Mass Density (lbf s2 /in4)	0.00073

MNF file is created by HyperWorks/MotionView, that can be used in ADAMS to use as a flexible body.

4.3 The definition of the fault gear

When gears break down, the faulty component often causes an impact, which generates impact energy. Types of gear fault include missing tooth, broken tooth, chipping tip, root crack and spalling conditions [94-96]. However, in the case of a broken tooth, the gearbox needs to change to a new gear. Therefore, in order to investigate the fault features of the helical gear, a different degree fault of breakage gear is implemented in this paper [97]. The tooth width and broken width are defined as L and B, so the degree of breakage is B/L. The breakage size is shown in figure 4-7.

(a)	*(b)*	*(c)*
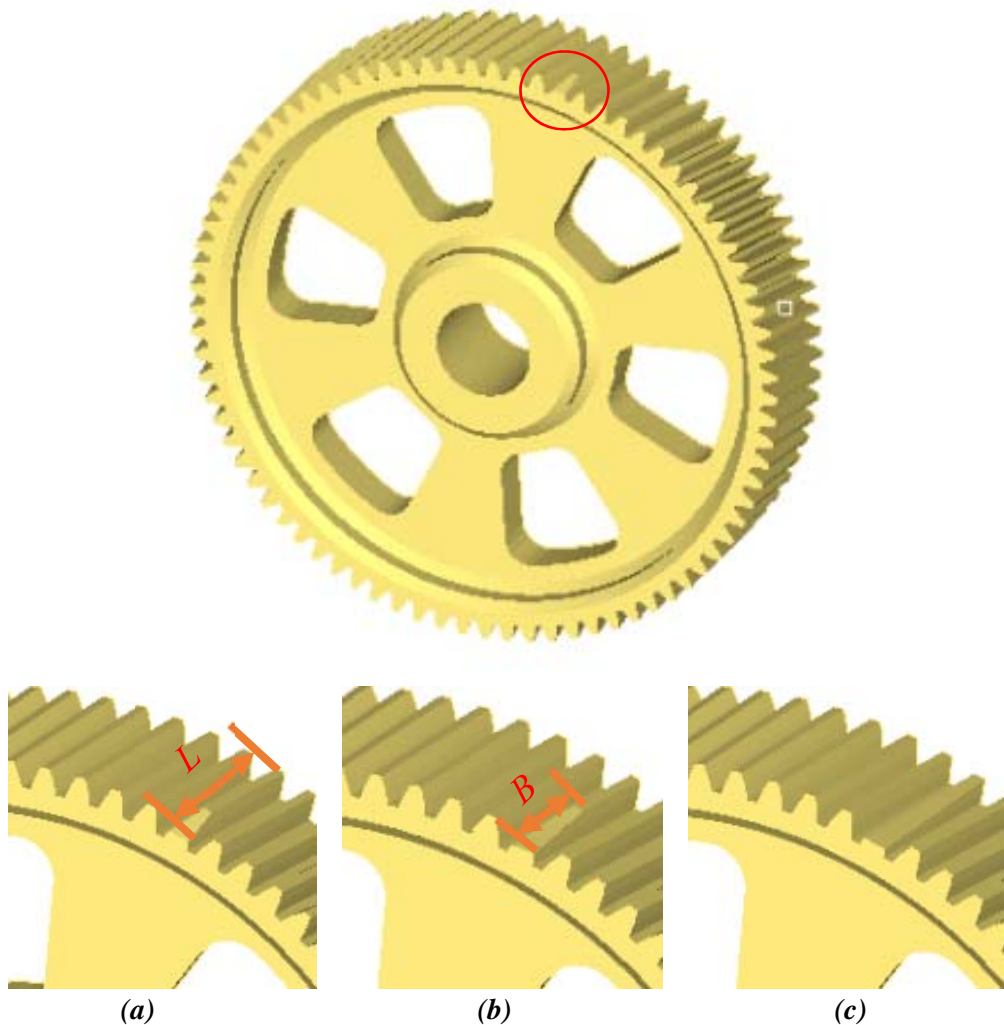
Figure 4-7. The degree of tooth breakage, (a) breakage 1/3, (b) breakage 2/3, (c) all breakage.

4.4 Conclusions

This chapter establish the multi-body dynamic model of the gearbox system with the ADAMS software. The flexibility treatment of the middle fault gear can improve the precision of the fault characteristic. At the same time, the three different breakage teeth are designed to validate the performance of the different algorithms.

Chapter 5 Results and discussions for the simulated model

5.1 Introduction

Just like chapter 4 was dedicated to describing the multi-body dynamic model of the gearbox system. The fault signal is obtained from the simulated model in the different conditions. This chapter will be dedicated to analyze the vibration characteristic of faulty gear by using the different algorithms. For the dynamical model, the input rotation speed of the gearbox is set to 2880 RPM (48Hz), and the sampling frequency is 20 kHz.

5.2 The fault analysis of different breakages

In this subsection, different gear faults are analyzed using the dynamical model of the gearbox system. A simulation experiment is first designed and performed to verify the effectiveness of the SS-AEWT method on signal feature extraction. Generally, when a defect emerges on one of the main parts of rotating machinery, such as bearing or gear, the corresponding vibration signal with periodic impulses features can be measured by the transducer [98]. Moreover, harmonic components always can be detected in the filed test vibration signal.
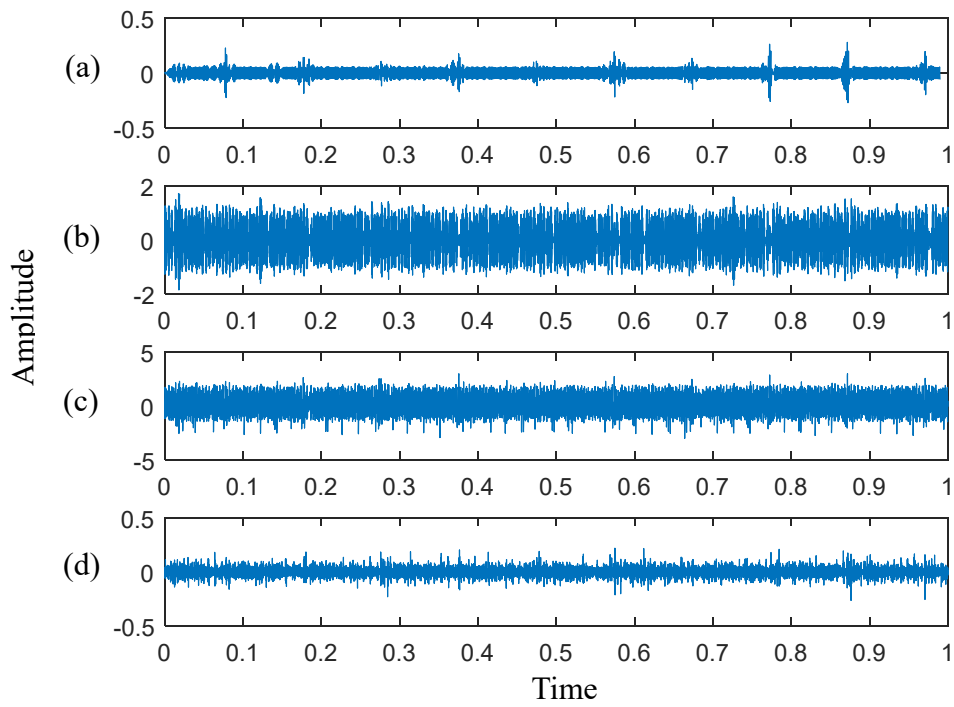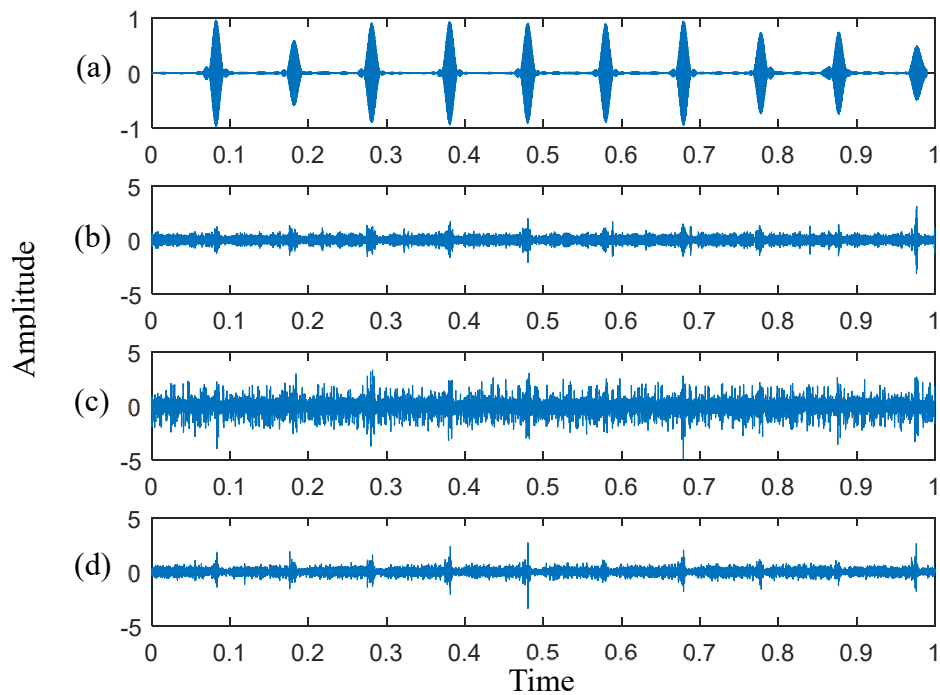
Figure 5-1. The compared results of different algorithm in 1/3 breakage tooth: (a) the proposed algorithm (b) EMD algorithm (c) LMD algorithm (d) DWT algorithm.
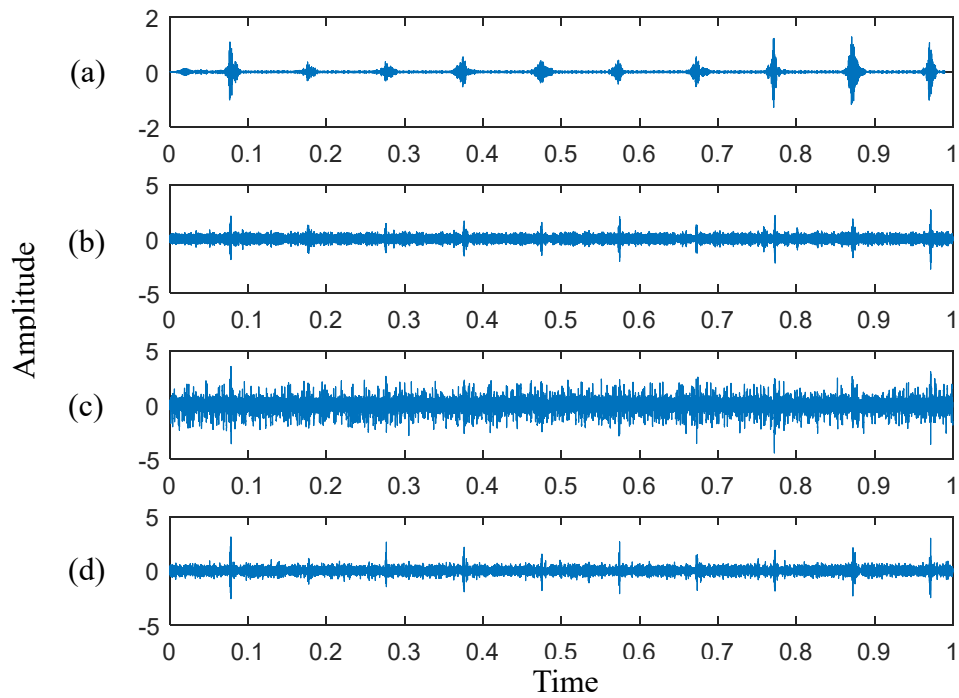
Figure 5-2. The compared results of different algorithm in 2/3 breakage tooth: (a) the proposed algorithm (b) EMD algorithm (c) LMD algorithm (d) DWT algorithm.

Figure 5-3. The compared results of different algorithm in all breakage tooth: (a) the proposed algorithm (b) EMD algorithm (c) LMD algorithm (d) DWT algorithm.

The periodic impulse features of the gear fault signal are displayed in figure 5-1, 5-2 and 5-3. The SS-AEWT method is applied to process this simulated signal. The figure 5-1 shows that the fault signal is extracted by using different algorithms in 1/3 breakage tooth condition. The SS-AEWT method can obviously extract the periodic impulse in the time domain. However, other methods have no detect the fault information. According to the result, harmonic component is identified successfully in the time domain. In order to identify and extract the side-band frequency features, the envelope analysis is applied to process the signal.
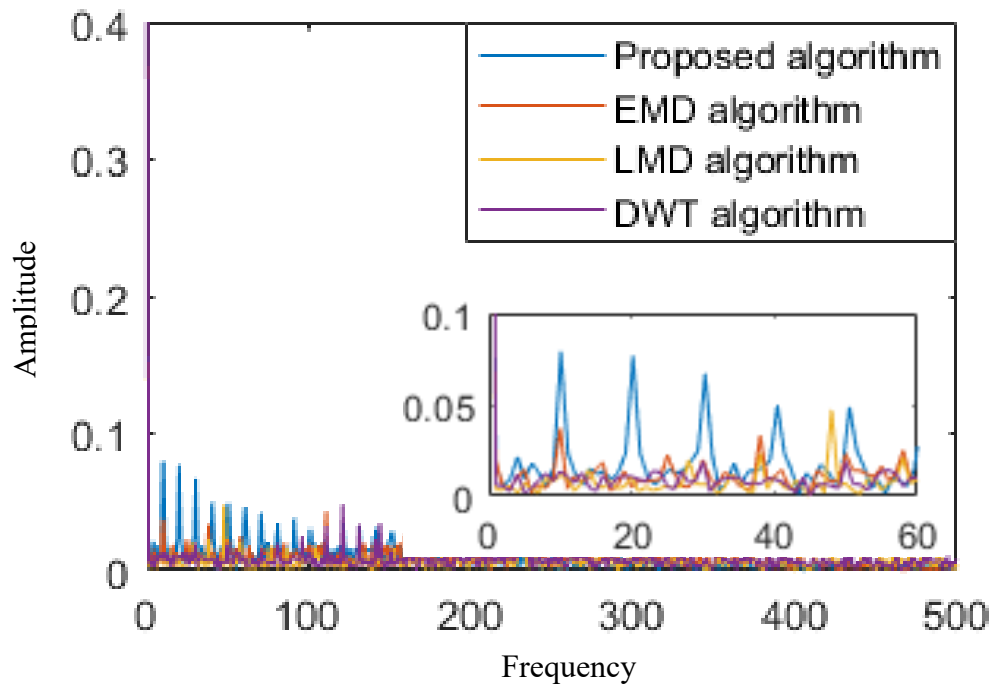
(a)
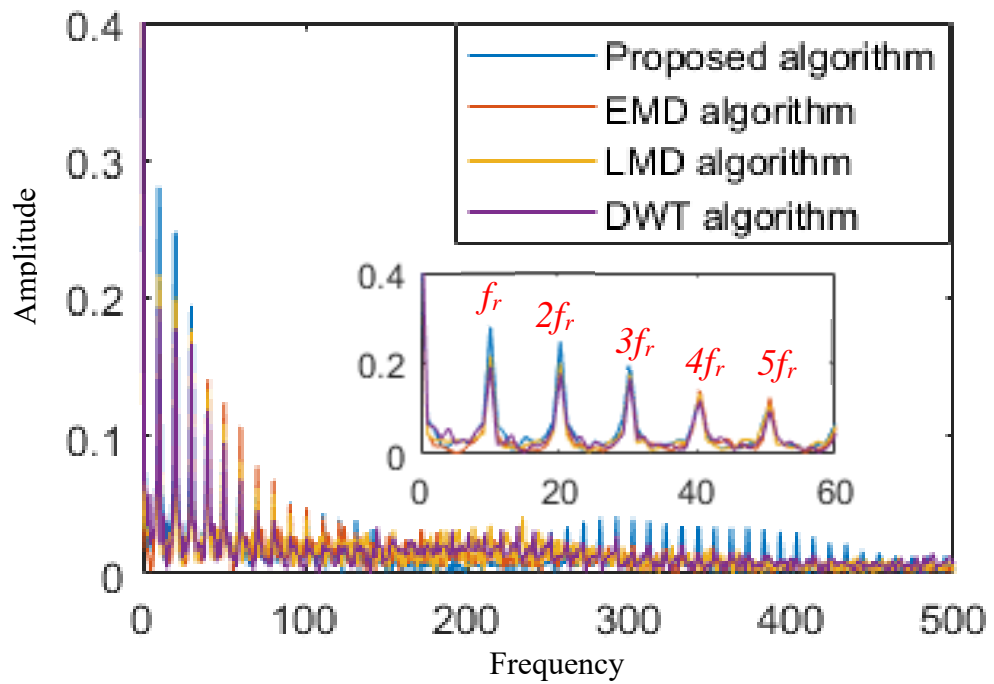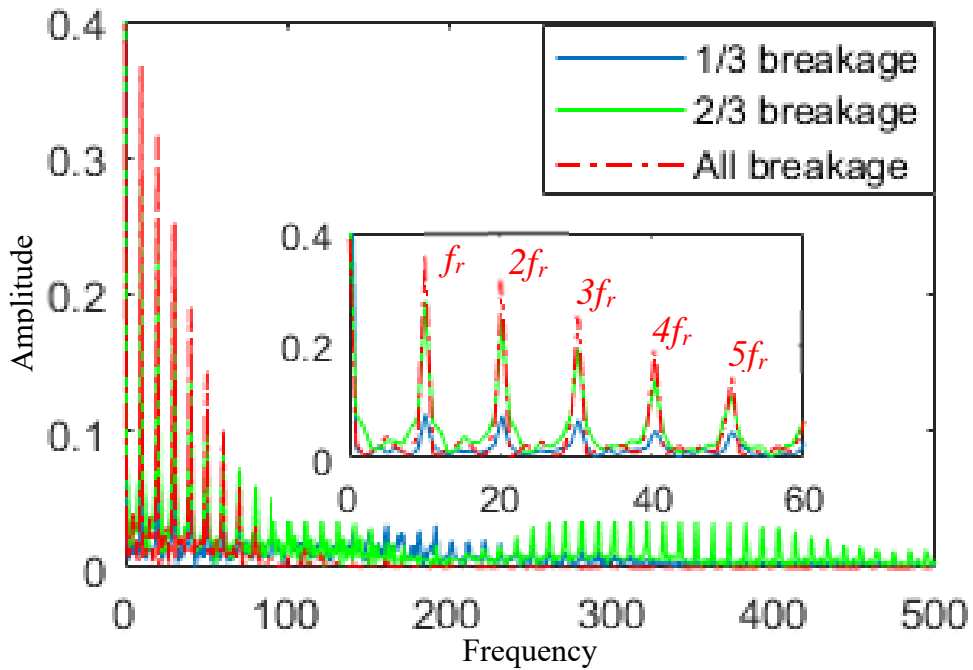

(b)
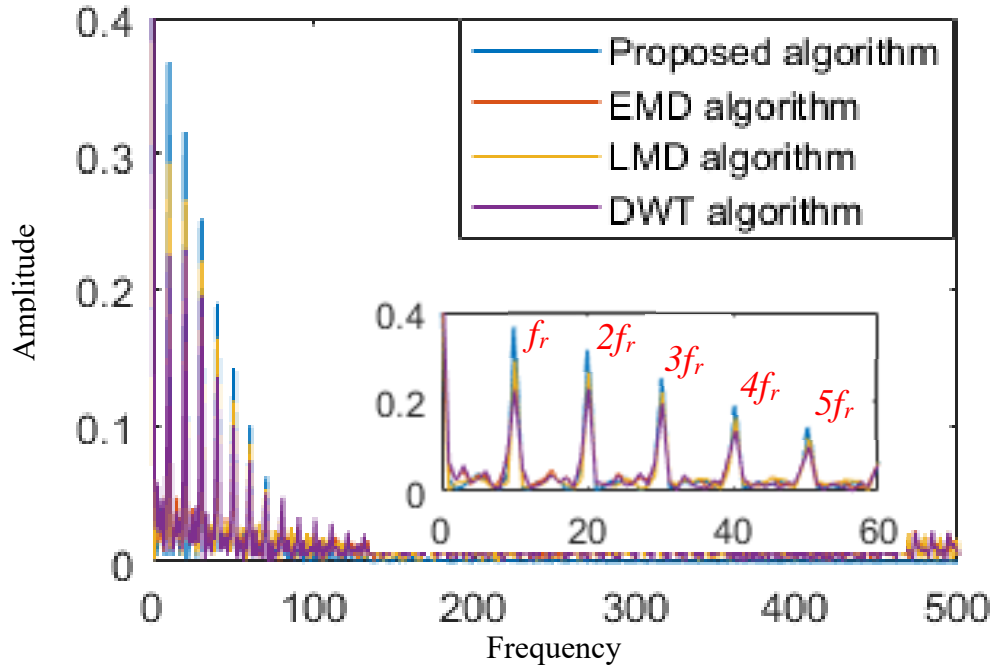
(c)

(d)

Figure 5-4. The comparison results (a) 1/3 breakage, (b) 2/3 breakage (c) All breakage (d) the SS-AEWT method with different breakage

According to the parameters of the gearbox, the rotational frequency of the faulty gear shaft is $f_r = f_{in}(Z_1/Z_2) = 48Hz*(17/81) = 10.07Hz$. The first-order frequency

value of the analytical result is 10.1Hz, which is close to the theoretical value. The variation of each order frequency amplitude is consistent with the experimental data, the comparative results are shown in figure 5-4. Hence, the dynamical model can reflect the fault characteristics of the tooth breakages. The SS-AEWT method can still clearly extract the side-band frequency feature with the 1/3 tooth breakage, but other methods have lost the ability to detect the gear fault. The result is shown in figure 5-4 (a).

Table 5-1. Comparison of the first-order frequency amplitude value of different analysis methods

| Fault type	EMD	LMD	DWT	Proposed algorithm	Percentage
1/3 breakage	0.037	0.011	0.013	0.079	53%, 86%, 84%
2/3 breakage	0.22	0.24	0.21	0.32	45%, 33%, 52%
All breakage	0.25	0.29	0.22	0.37	32%, 22%, 41%

The results from Table 2, the amplitude value of frequency feature for EMD method is much bigger than LMD and DWT method with the different tooth breakage. However, the amplitude value obtained by the SS-AEWT method is 53%, 45% and 32% higher than that of EMD with the different tooth breakage, respectively. Especially 1/3 tooth breakage, other methods are very difficult to detect the side-band frequency features. The results indicate that the SS-AEWT method can clearly extract the side-band frequency features without the external noise, and the amplitude value is enlarged with increasing tooth breakage.

5.3 The fault analysis of the SNR effect

The detection of the side-band frequency was applied to the simulated signal for 2/3 tooth breakage with different levels of noise added. Because there is no external noise, the simulated signal for the faulty gear is very a clear impulse signal, as shown in figure 5-5 (a). However, the vibration signal is weak for an early fault diagnosis of a gearbox

and often buried under background noise. Next, the simulated signal with different white noise (10 dB, 5 dB, 0 dB, -5 dB and -10 dB) was processed by the SS-AEWT method. The waveforms are shown in figure 5-5 (b-f) in the time domain. The impulse signals become increasingly misty as the SNR decreases, especially with noise under the 0 dB.
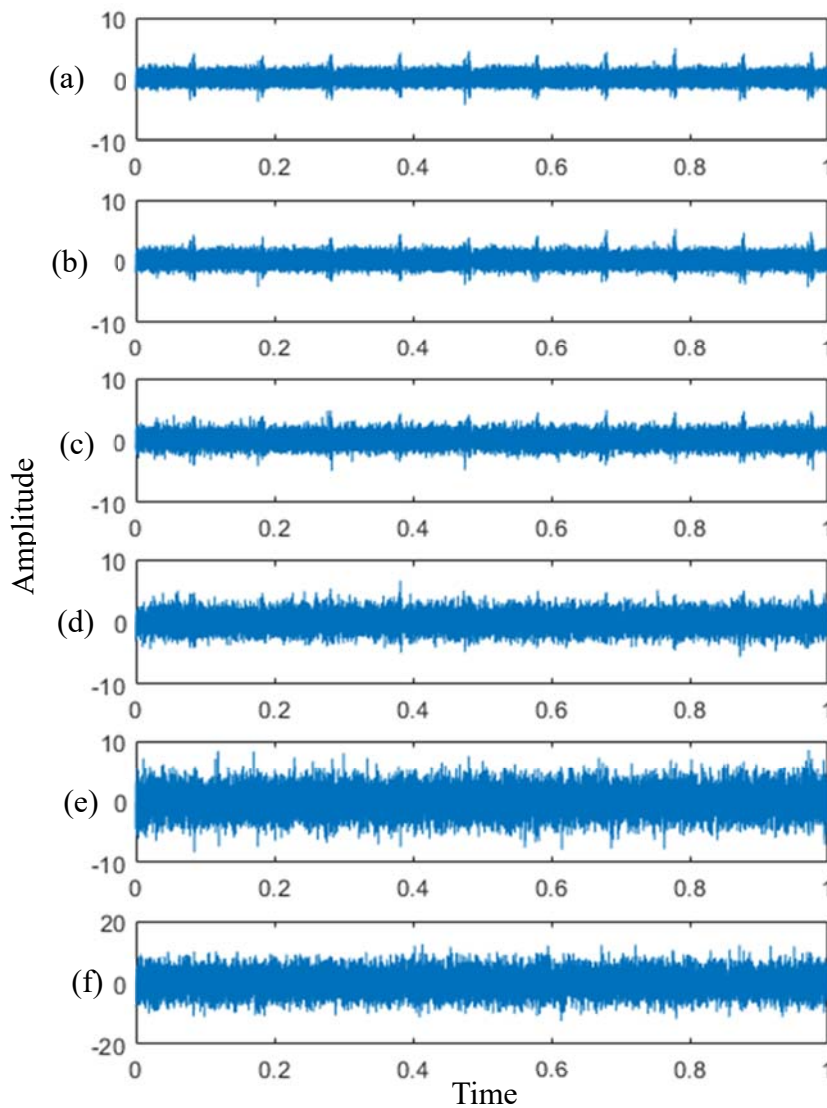

Figure 5-5. The simulated signal with added noise,

(a) no noise, (b) 10 dB, (c) 5 dB, (d) 0 dB, (e) -5 dB, and (f) -10 dB.

The corresponding waveforms and envelope spectra of the faulty component

information are extracted by using EWT and a square envelope, respectively. The results are shown in figure 5-6 and figure 5-7. The fault feature information is basically reserved above -5 dB of noise, and the side-band components are obtained by envelope analysis. This indicates that the frequency feature of the faulty component of a gear is effectively extracted by the SS-AEWT method. The fundamental frequency equals the result of the theoretical calculation, and the amplitude value of the order frequency remains stable.
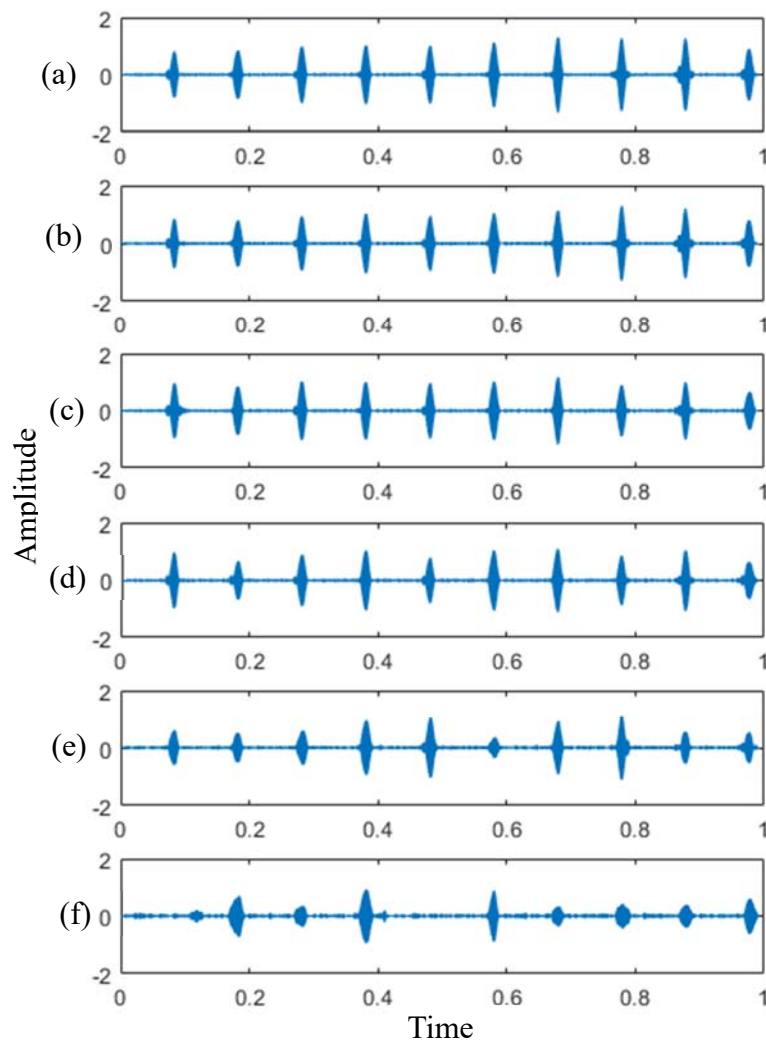
Figure 5-6. The impulse component with EWT method,

(a) no noise, (b) 10 dB, (c) 5 dB, (d) 0 dB, (e) -5 dB, and (f) -10 dB.
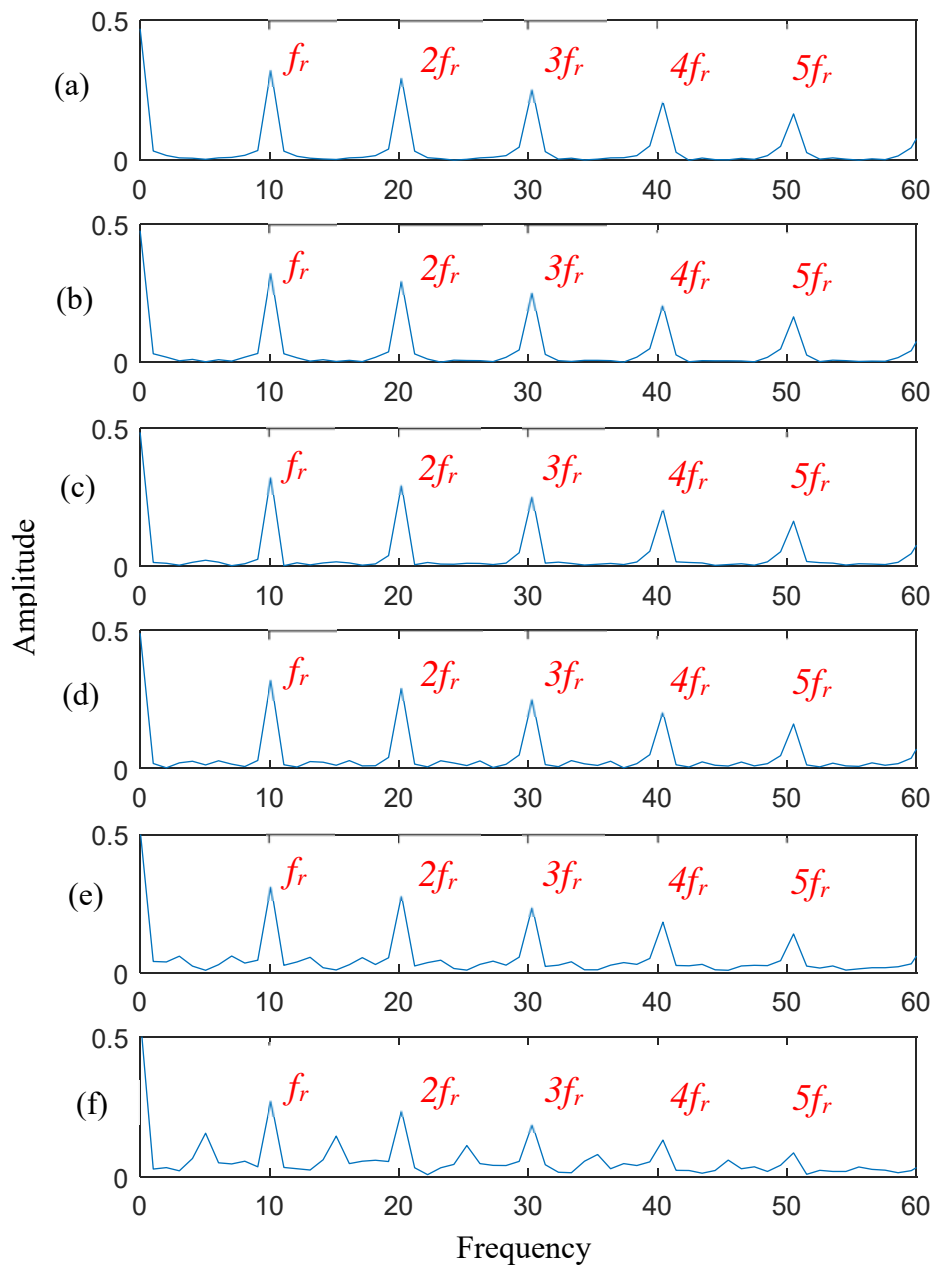
Figure 5-7. The faulty features with square envelope analysis,

*(a) no noise, (b) 10 dB, (c) 5 dB, (d) 0 dB, (e) -5 dB, and (f) -10 dB.*

In the figure 5-8, the proposed signal processing method can effectively extract the side-band frequency component, and stably obtain the fixed amplitude value where the

SNR level is low. As a result, the SS-AEWT method indicates that it can largely enhance the representation of the faulty gear component and make the amplitude of the side-band frequency more stable under the strong noise.
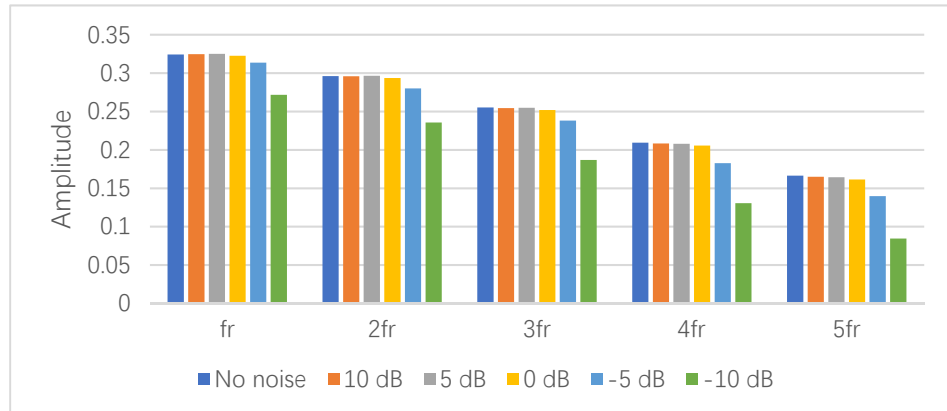
Figure 5-8. The comparison results for different noise level

5.4 Comparison of different methods

To verify the effectiveness of the SS-AEWT method, the simulated signal with 5 dB of noise was considered on the 2/3 tooth breakage situation. The frequency spectrum is obtained with the spectral subtraction method. The figure 5-9 shows that the side-band frequency under the strong noise is hardly extracted from the frequency spectrum. However, the spectral subtraction method can enhance the amplitude value of the side-band frequency region more than the gear meshing frequency region. The results are shown in the figure 5-10. The side-band frequency features are extracted by the EWT method.
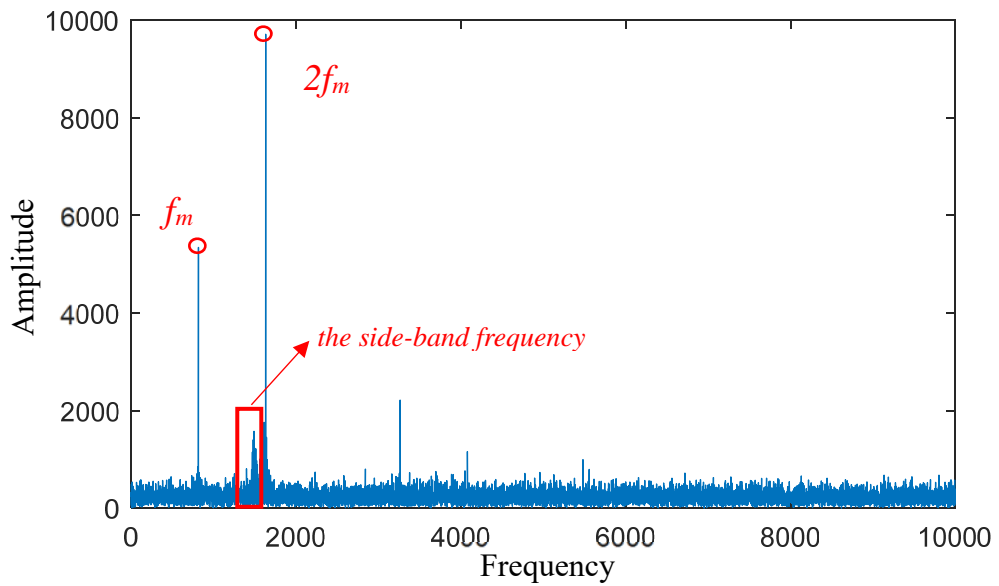
Figure 5-9. The frequency spectrum with 5dB of noise
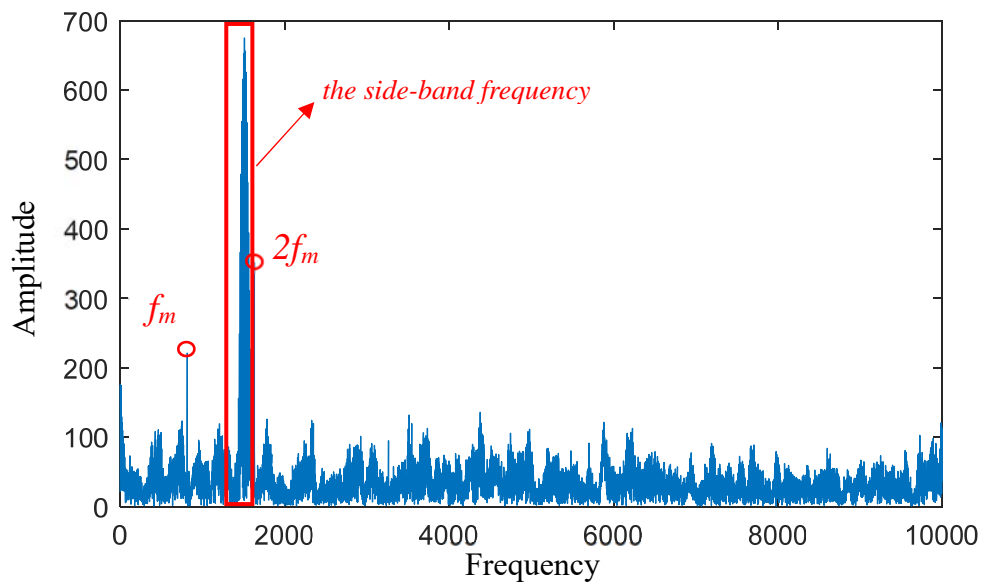
Figure 5-10. The frequency spectrum with spectral subtraction

For comparison, this subsection uses the EMD, LMD and DWT methods to decompose the simulated signal with the SNR 5 dB noise, respectively. Firstly, EMD is employed to decompose the observation signal into eight IMFs, and the result of each IMF is showed in figure 5-11. The adding noise signals are complex, so it can't directly evaluate the fault frequency with the power spectrum. The frequency characteristics of each IMF are significantly extracted with the envelope spectrum, which shows in figure

5-11 (b). The envelope spectrum of the first IMF contains the primary information of fault signal, therefore, the side band feature frequency can be identified clearly.
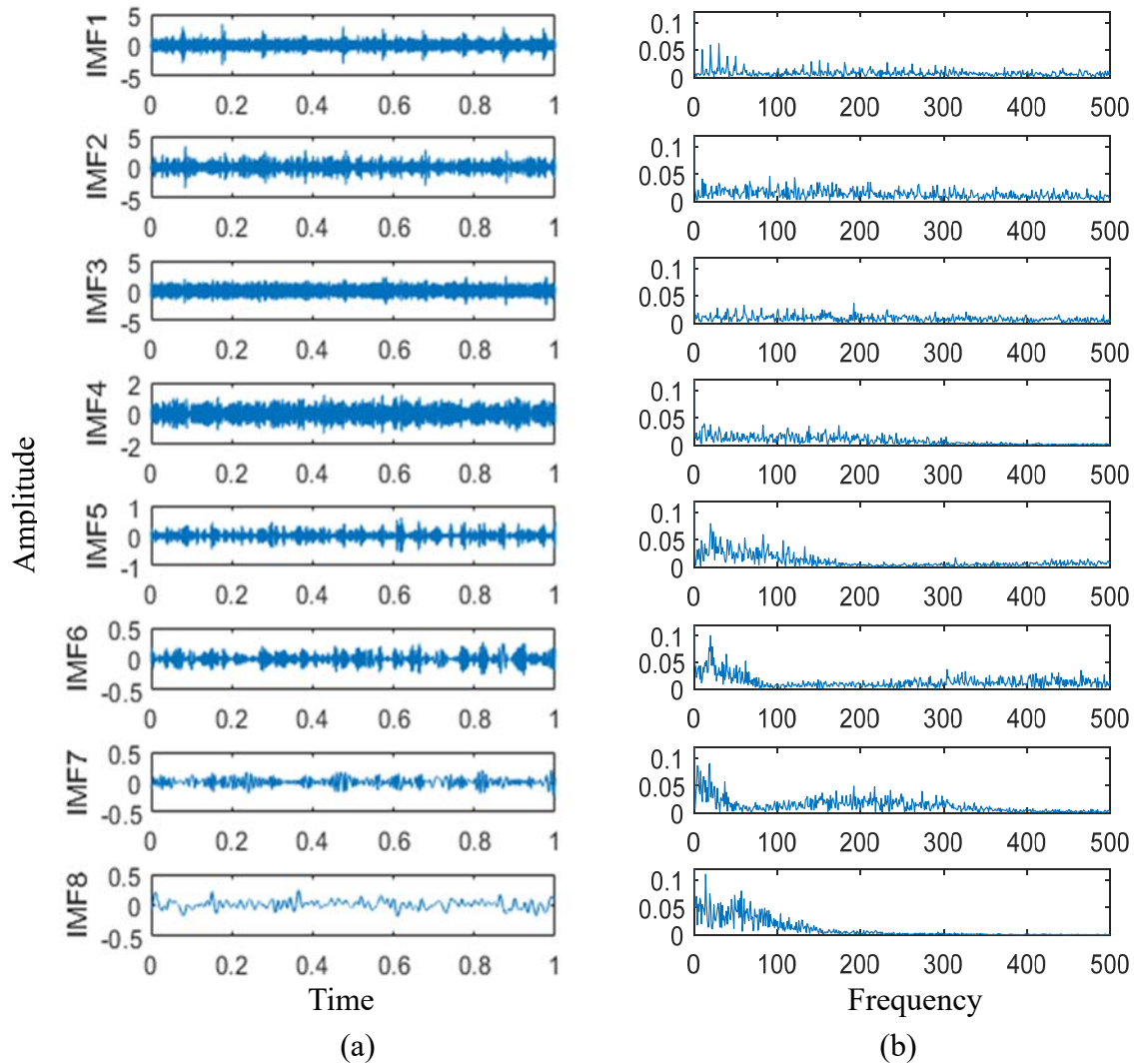
Figure 5-11. The results of EMD method

The LMD is applied to adaptively decompose the adding noise signal into several PFs from high frequency band to the low one. Several PFs can be obtained with the LMD process. The LMD decomposition results and the envelope spectrums are shown in figure 5-12. The first PF is selected for further analysis, because it has the biggest correlation coefficient value and keeps the most of information from original signal.
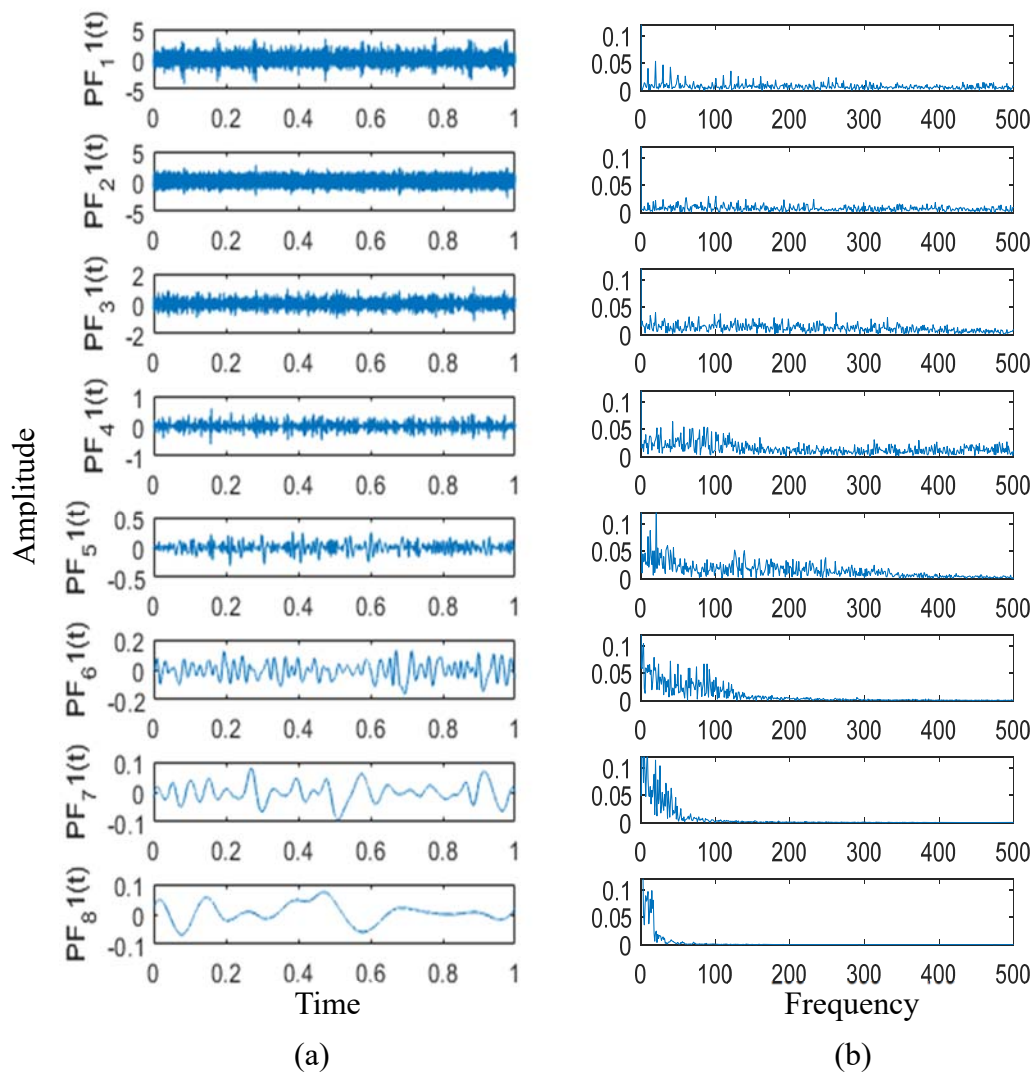
Figure 5-12. The results of LMD method

In this section, the DWT decomposes the adding noise signal to extract the main information of the fault features, and the results of DWT decomposition and the envelope analysis of each level wavelet coefficients are shown in figure 5-13. The wavelet correlation of the d_2 level is much bigger than others, so it can be used as the features of the fault information.
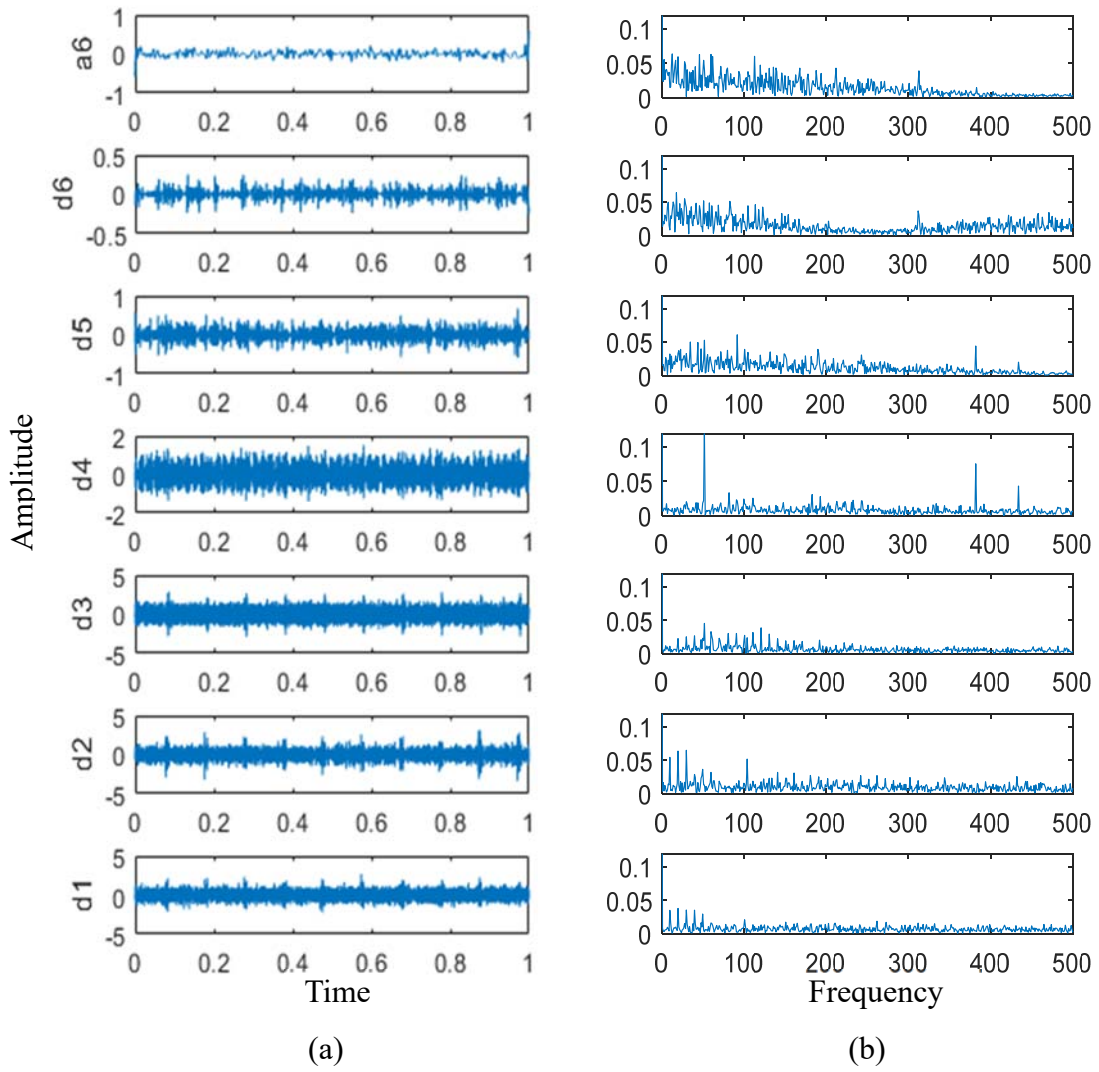
Figure 5-13. The results of DWT method
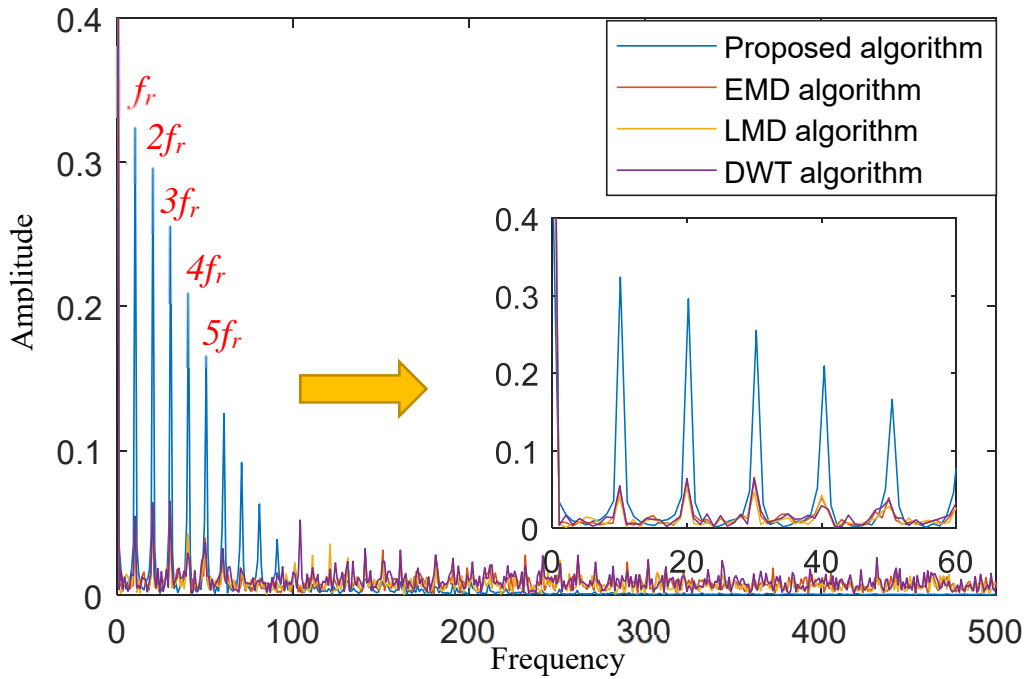
Figure 5-14. The fault features with square envelope analysis

Table 5-2. The side-band amplitudes for different analysis method

Analysis type	Amplitude of fr	Amplitude of 2fr	Amplitude of 3fr	Amplitude of 4fr	Amplitude of 5fr
EMD algorithm	0.051	0.0595	0.0619	0.0392	0.0393
LMD algorithm	0.0402	0.0533	0.0465	0.0425	0.0279
DWT algorithm	0.0546	0.0639	0.0651	0.0288	0.0365
Proposed algorithm	0.3251	0.2965	0.2548	0.2078	0.1642

The figure 5-14 and table 5-2 shows the side-band features calculated from the square envelope analysis. The proposed algorithm has significantly better performance for the feature extraction of the side-band information of the faulty gear. The noise energy has been obviously reduced by the SS-AEWT method, which is efficient for fault feature extraction.

Table 5-3. The amplitude value of first-order frequency for different analysis methods and SNR

SNR	EMD	LMD	DWT	Proposed algorithm	Percentage
10 dB	0.0965	0.0518	0.0675	0.3247	236%, 527%, 381%
5 dB	0.0510	0.0401	0.0351	0.3251	537%, 711%, 826%
0 dB	0.0266	0.0343	0.0156	0.3225	1112%, 840%, 1967%
-5 dB	0.0109	0.0138	0.0067	0.3136	2777%, 2172%, 4581%
-10 dB	0.0036	0.0016	0.0063	0.2716	7444%, 16875%, 4211%

Table 5-3 shows that EMD, LMD and DWT method can extract the side-band frequency features except noise -5dB and -10dB. Their performance for extracting the side-band feature reached a limit when the noise exceeded -5dB. However, the SS-AEWT method can more clearly extract the side-band feature under different background noise, and its amplitude value remains stable. Therefore, the SS-AEWT method is feasible for reducing strong noise and effectively extracting the faulty features.

5.5 Signal vibration for the low rotational speed

In this section, the low rotational speed of the gearbox system is considered in 2/3 breakage tooth condition, and input shaft speed is 1000 rpm. The vibration signal is obtained from the simulated model, the original signal is shown in the figure 5-15. The original signal of faulty tooth has three impacts in a second. The impulse information is submerged in the vibration signal. Therefore, the extraction of impulse signal from the complex vibration signal is very necessary.
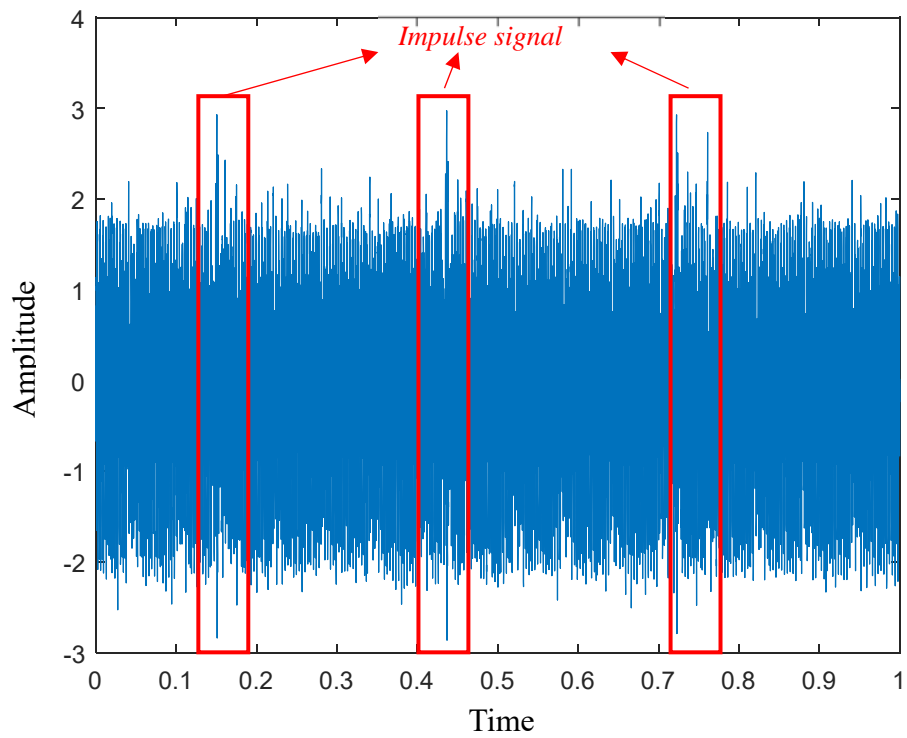
Figure 5-15. The original signal of the gear fault in time domain.
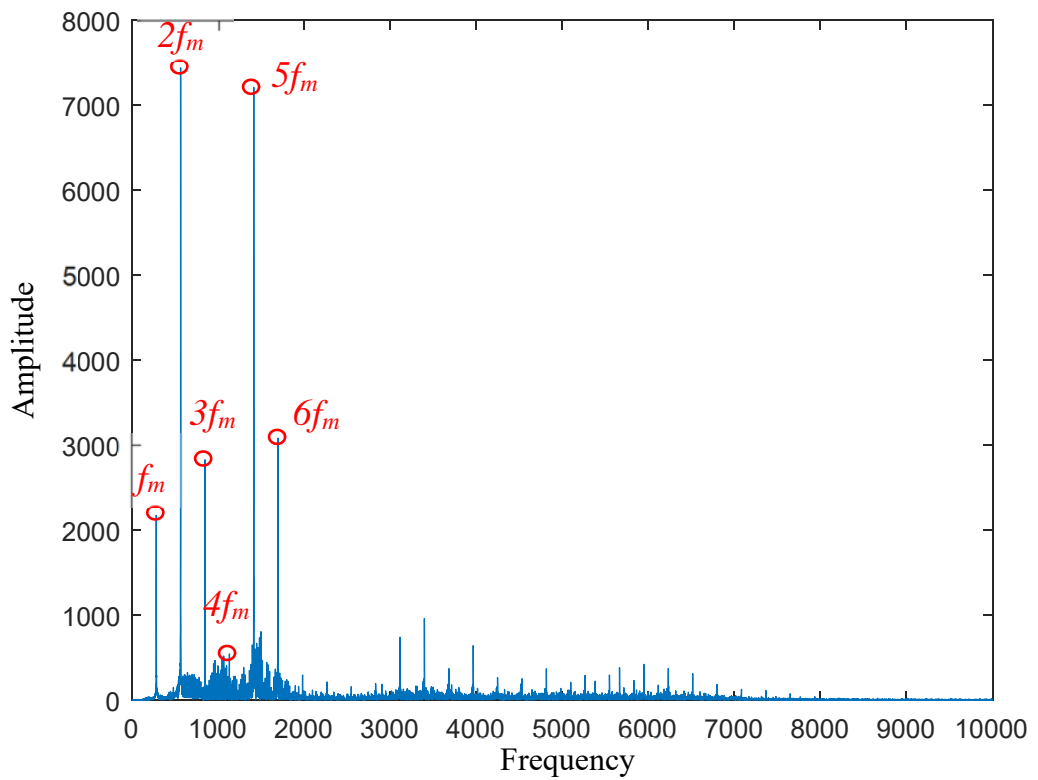
Figure 5-16. The frequency spectrum results.

The figure 5-16 shows the frequency spectrum of the fault signal. The peaks of the spectrum are primarily the meshing frequency of the gear train, but the amplitude value of fault signal features is very small. The different methods are used to extract the fault information as below.
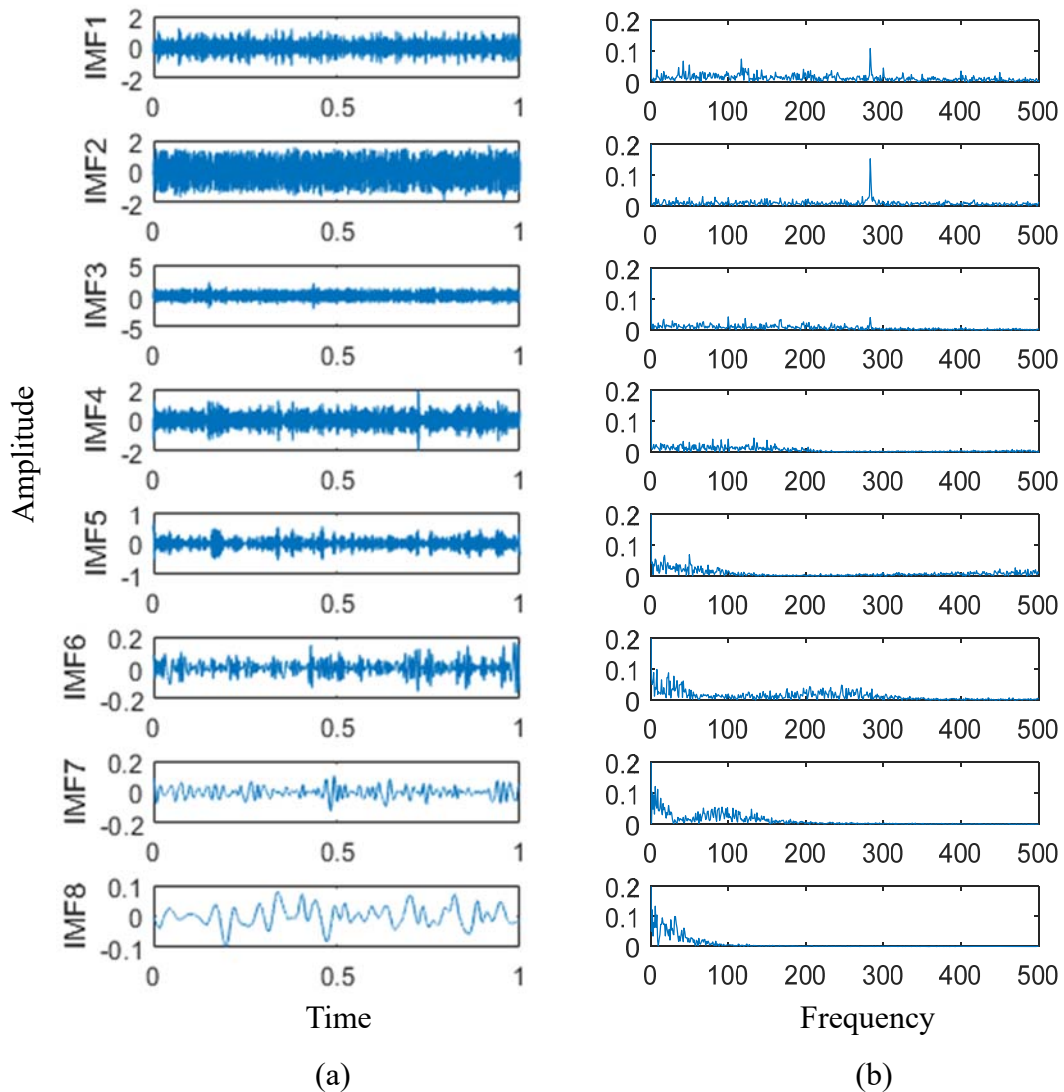
Figure 5-17. The analysis results with EMD algorithm.

The figure 5-17 shows the results of EMD method. The frequency spectrum of each IMF is extracted with the envelope analysis, which shows in figure 5-17 (b). The EMD method is very difficult to extract the side-band frequency features from the envelope spectrum of each IMF. Therefore, this algorithm is limited to extract the fault features

in low rotational speed.
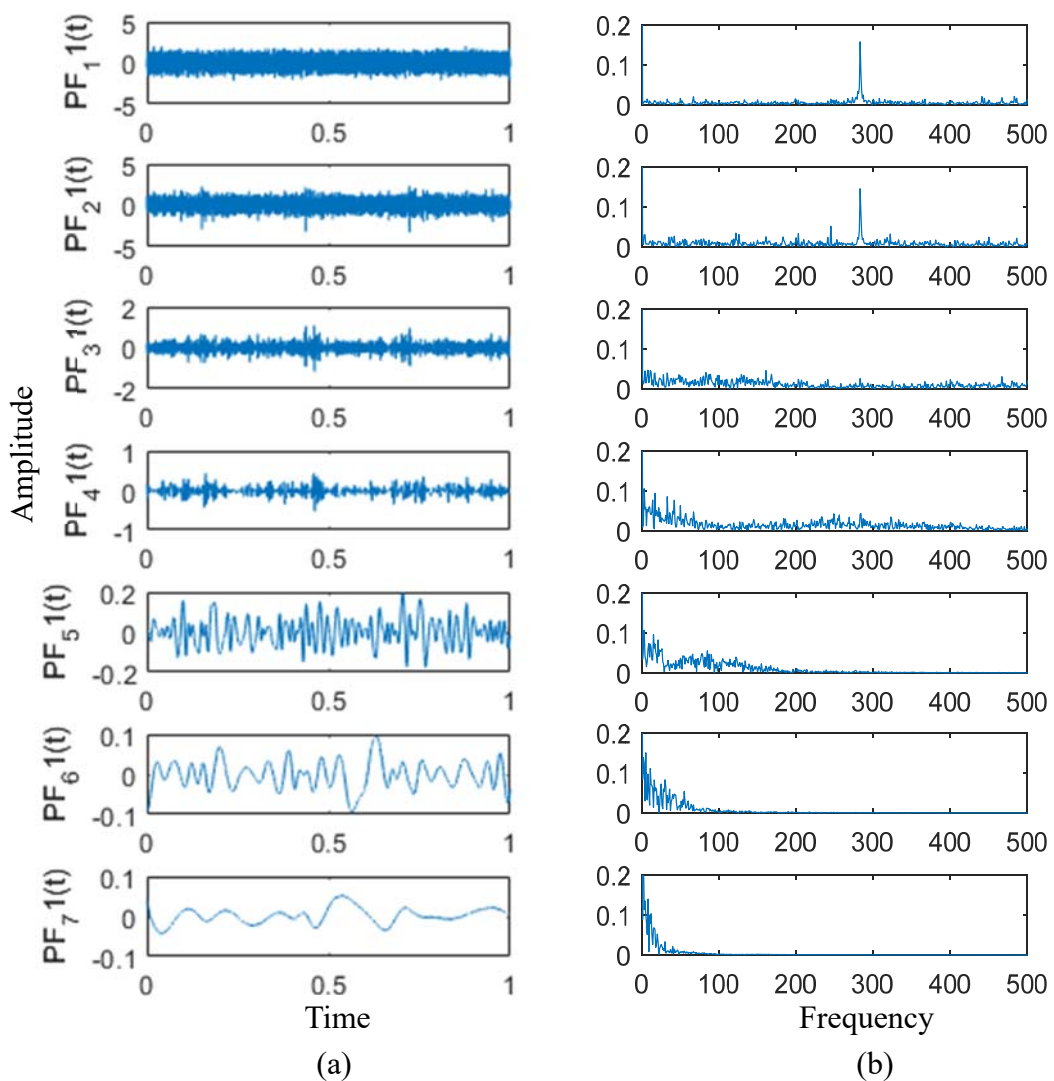
Figure 5-18. The analysis result with LMD algorithm.

The LMD is applied to adaptively decompose the signal into several PFs from high frequency band to the low one. Several PFs can be obtained with the LMD method. The LMD decomposition results and the envelope spectrums are shown in figure 5-18. Each PF doesn't contain the fault information, so LMD technique cannot the extract the sideband frequency features.
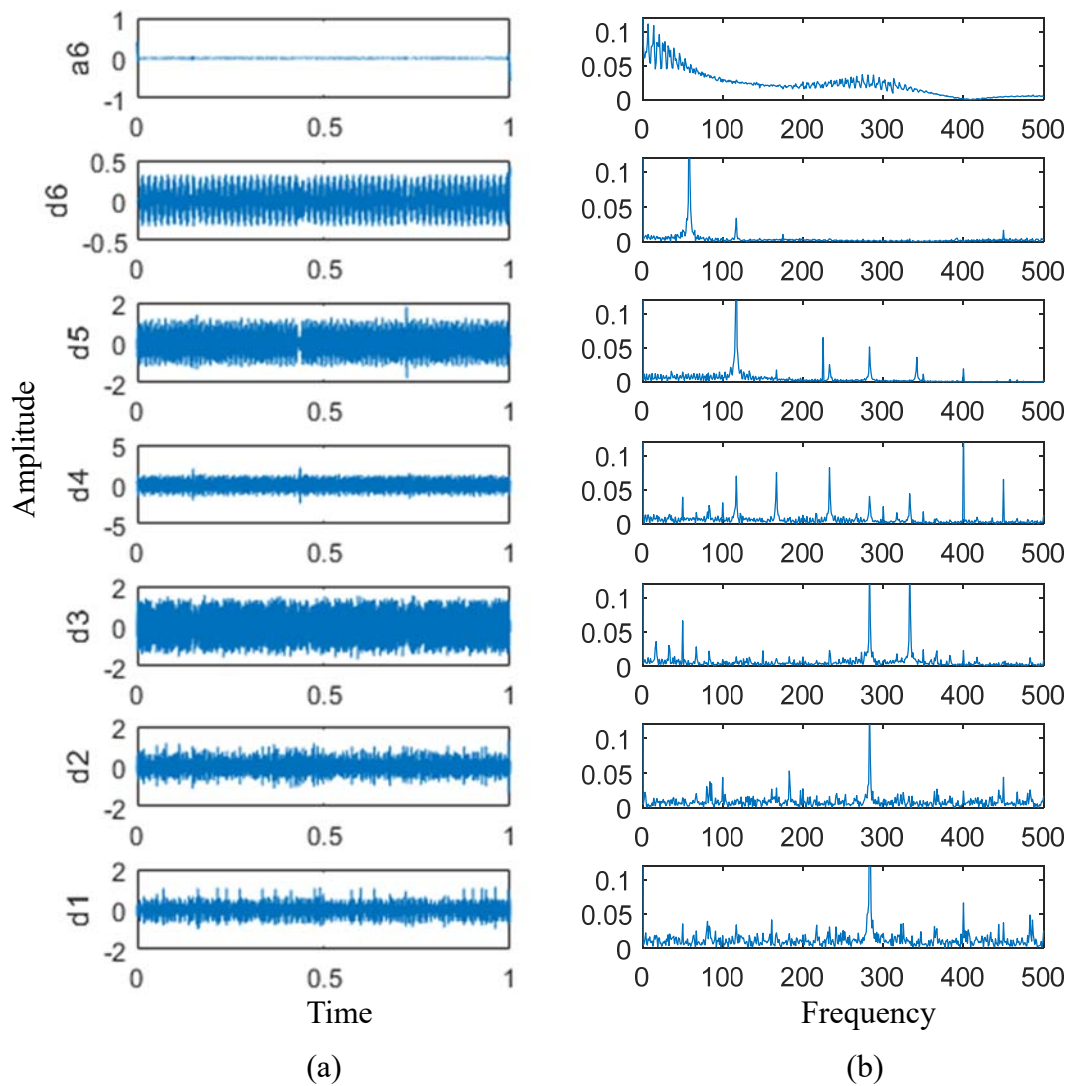
Figure 5-19. The result with DWT algorithm.

The DWT decomposes the signal to extract the main information of the fault features, and the results of DWT decomposition and the envelope analysis of each level wavelet coefficients are shown in figure 5-19. The wavelet correlation of each level is very small and the fault information is not obvious, so the DWT technique cannot also be used to extract the fault characteristics.
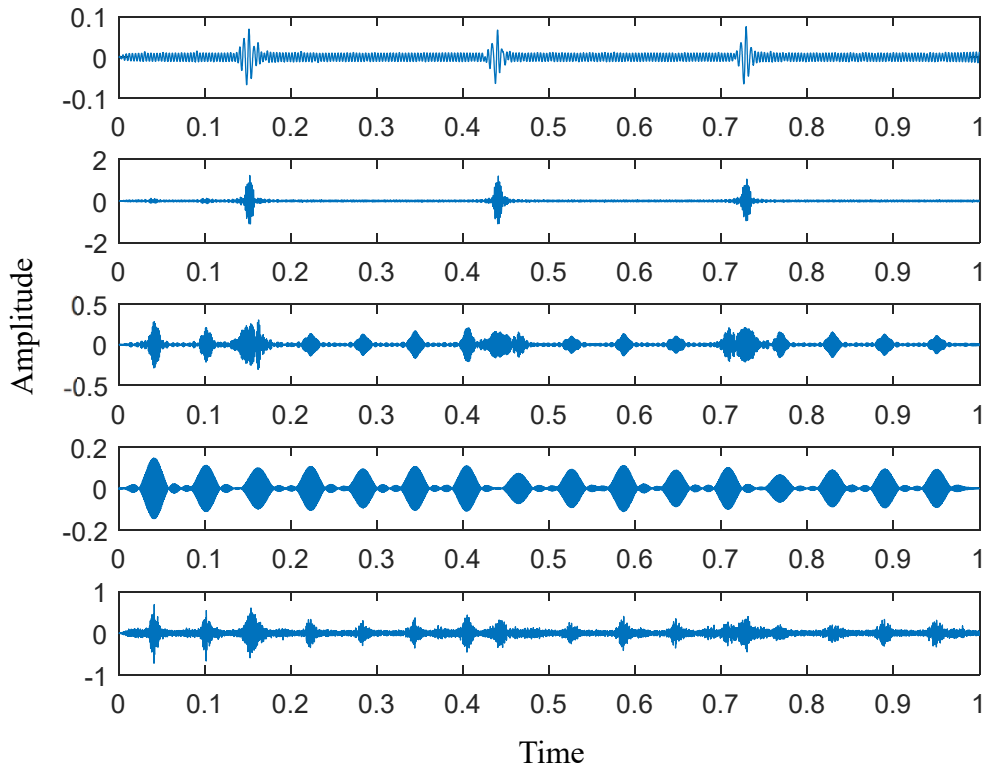
Figure 5-20. The result with EWT algorithm.
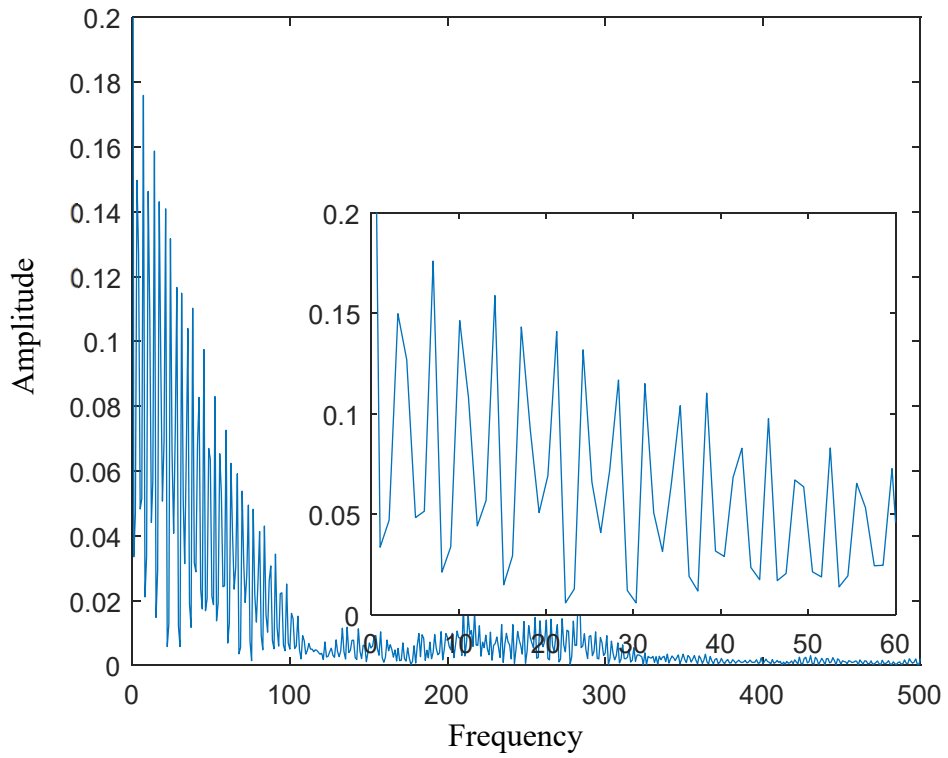
Figure 5-21. The side-band frequency with envelope spectrum.

The figure 5-20 shows the decomposition results of EWT technique. The first and second level wavelet coefficient can obviously display the fault impulse information of gear. Therefore, the side-band frequency features of the second level wavelet coefficient is obtained with the envelope spectrum analysis, which is shown in figure 5-21. The first order frequency is 3.53 Hz. According the theoretical calculation, the rotational frequency of the middle shaft is 3.5 Hz. Hence, the performance of the SS-AEWT method is better than other methods on low rotation speed.

5.6 Conclusions

A novel signal processing method was proposed to detect the diagnosis of gearbox system in the different conditions. According the results of multi-body dynamics model with the different breakage tooth, the different signal processing methods are effectively verified. The performance of the SS-AEWT method is better than EMD, LMD and DWT method in the different conditions, such as breakage tooth, external noise and rotational speed. The simulated results indicate that the SS-AEWT method cannot only maintain the stability of algorithm performance, but also can detect the side-band frequency features of the gear fault information.

Chapter 6 Conclusions

6.1 Conclusions

The research work of this dissertation mainly focuses on the fault diagnosis of gearbox system under the different conditions. The gearbox system model can be established using the Euler-Lagrange method in ADAMS software. The spectral subtraction method can be applied to gearbox fault diagnosis to remove partial additive noise. The EWT technique is adopted in this present work to determine the segment boundaries accurately and improve the fault-detection performance. Therefore, this paper has proposed the adaptive EWT technique combined with the spectral subtraction method for fault diagnosis of a gearbox system. Firstly, the side-band frequency features are extracted to verify the effectiveness of the algorithms with the experimental data when the gear breaks down. The results indicate that the performance of the SS-AEWT method is better than other methods. Then the multi-body dynamics model of the gearbox system is established after gear flexibility treatment. The different tooth breakages are designed by the dynamical model. The experimental results indicate that the dynamical model can satisfy the gear fault characteristics, and it can be used to validate the algorithm performance. For smaller tooth breakage, the SS-AEWT method can more clearly detect the fault features than EMD, LMD, and DWT techniques. When the fault features are not extracted by EMD, LMD, and DWT techniques at a noise above −5dB, the SS-AEWT method can still discern the side-band frequency features.

The spectral subtraction technique can eliminate the strong noise to enhance the faulty component. Then, the EWT method can effectively extract the transient impulse component, and the side-band frequency features are significantly obvious. The multi-body dynamics model of the gearbox system after gear flexibility treatment is helpful for establishing the gearbox fault. Furthermore, it can be used to design multiple faults

of the gearbox and provide much data for predicting gearbox faults.

REFERENCES

1. J.L. Chen, Y.Y. Zi, Z.J. He, Compound faults detection of rotating machinery using improved adaptive redundant lifting multiwavelet, Mech. Syst. Signal Process. 1 (5) (2013) 36e54.

2. Sun, R.; Yang, Z.; Chen, X.; Tian, S.; Xie, Y. Gear fault diagnosis based on the structured sparsity time-frequency analysis, Mechanical Systems and Signal Processing 102 (2018) 346–363.

3. Beardmore, Roy. "Gears- Gearboxes." RoyMech. N.p., 6 Oct. 2012. Web. 30 Aug. 2014.

4. Budynas, Richard G., J. Keith. Nisbett, and Joseph Edward. Shigley. Shigley's Mechanical Engineering Design. New York: McGraw-Hill, 2011. Print.

5. Different Types of Gears. 2006. gearsandstuff.com. Different Types of Gear, 5 Oct. 2013

6. H. Ding, A. Kahraman , Interactions between nonlinear spur gear dynamics and surface wear, J. Sound Vib. 307 (3) (2007) 662–679.

7. X. Liu, Y. Yang, J. Zhang, Investigation on coupling effects between surface wear and dynamics in a spur gear system, Tribol. Int. 101 (2016) 383–394.

8. A. Flodin, Wear of spur and helical gears, Ph.D. Thesis, KTH Stockholm, in: Royal Institute of Technology, Stockholm, 2000.

9. C. Hu, et al. , Development of a gear vibration indicator and its application in gear wear monitoring, Mech. Syst. Signal Process. 76 (2016) 319–336.

10. F. Choy, V. Polyshchuk, J. Zakrajsek, R. Handschuh, D. Townsend, Analysis of the effects of surface pitting and wear on the vibration of a gear trans-mission system, Tribol. Int. 29 (1996) 77–83.

11. H. Ding, Dynamic wear models for gear systems, PhD DISSERTATION, The Ohio State University, 2007.

12. O.D. Mohammed, M. Rantatalo, J.-O. Aidanpää, Dynamic modelling of a one-stage spur gear system and vibration-based tooth crack detection analysis,Mech. Syst. Signal Process. 54 (2015) 293–305.

13. S. Wu, M.J. Zuo, A. Parey, Simulation of spur gear dynamics and estimation of fault growth, J. Sound Vib. 317 (3) (2008) 608–624.

14. Z. Tian, M.J. Zuo, S. Wu, Crack propagation assessment for spur gears using model-based analysis and simulation, J. Intell. Manuf. 23 (2) (2012) 239–253.

15. Z. Chen, Y. Shao, Dynamic simulation of spur gear with tooth root crack propagating along tooth width and crack depth, Eng. Fail. Anal. 18 (8) (2011) 2149–2164.

16. Lu, D.; Gong, X.; Qiao, W. Current-based diagnosis for gear tooth breaks in wind turbine gearboxes. In Proceedings of the 2012 IEEE Energy Conversion Congress and Exposition (ECCE), Raleigh, NC, USA, 15–20 September 2012.

17. Chaari, F.; Baccar, W.; Abbes, M.S.; Haddar, M. Effect of spalling or tooth

breakage on gearmesh stiffness and dynamic response of a one-stage spur gear transmission. Eur. J. Mech. A Solids 2008, 27, 691–705.

18. Jia, S.; Howard, I. Comparison of localised spalling and crack damage from dynamic modelling of spur gear vibrations, Mech. Syst. Signal Process. 20 (2) (2006) 332–349.

19. Pandya, Y.; Parey, A. Failure path based modified gear mesh stiffness for spur gear pair with tooth root crack, Eng. Fail. Anal. 27 (2013) 286–296.

20. Brethee, K.F.; Zhen, D.; Gu, F.; Ball, A.D. Helical gear wear monitoring: Modelling and experimental validation, Mechanism and Machine Theory 117 (2017) 210–229.

21. Inalpolat, M.; Kahraman, A. A theoretical and experimental investigation of modulation sidebands of planetary gear sets, Journal of Sound and Vibration 323 (2009) 677–696.

22. Wang, L.; Shao, Y.; Cao, Z. Optimal demodulation subband selection for sun gear crack fault diagnosis in planetary gearbox, Measurement 125 (2018) 554-563.

23. Behzad M, Bastami A R, Mba D. A new model for estimating vibrations generated in the defective rolling element bearings. ASME Transactions on Journal of Vibration and Acoustics, 2011, 133 (4), 041101.

24. Liu J, Shao Y M, Lim T C. Vibration analysis of ball bearings with a localized defect applying piecewise response function. Mechanical and Machine Theory, 2012, 56: 156-169.

25. Muir D, Howe B. On-line oil debris monitor (ODM) for the advanced tactical fighter engines. SAEP Paper No. 961308, May 1996.

26. Hong H, Liang M. A fractional calculus technique for no-line detection of oil debris. Measurement Science and Technology, 2008, 19 (5): 1-14.

27. Yoshioka T, Korenaga A, Mano M, et al. Diagnosis of rolling bearing by measuring time interval of acoustic emission generation. ASME Transactions on Journal of Tribology, 1999, 121 (3): 468-472.

28. Jamaludin N, Mba D. Monitoring extremely slow rolling element bearing Part 1. NDT&E International, 2002, 35 (6): 349-358.

29. Mba D, Rao R B K N. Development of acoustic emission technology for condition monitoring and diagnosis of rotating machines: bearings, pumps, gearboxes, engines and rotating structures. The shock and vibration digest, 2006, 38 (1): 3-16.

30. Hong H, Liang M. K-Hybrid. A kurtosis-based hybrid thresholding method mechanical signal denoising. ASME Transactions on Journal of Vibration and Acoustics, 2007, 129 (4): 458-470.

31. Braun S. The extraction of periodic waveforms by time domain averaging. Acoustics, 1975, 32 (2): 69-77.

32. McFadden P D. Examination of a technique for the early detection of failure in gears by signal processing of the time domain average of the meshing vibration. Mechanical Systems and Signal Processing, 2000, 14 (6): 891-906.

33. McCormick A C, Nandi A K. Bispectral and trispectral features for machine

condition diagnosis. IEE Proceedings-vision Image and Signal Processing, 1999, 146 (5): 229-234.

34. Fonollosa J R, Nikias C L. Wigner higher-order moment spectra: definitions, properties, computation and applications to transient signal detection. IEEE Transaction on Signal Processing, 1993, 42 (1): 245-266.

35. Barker R W, Klute G A, Hinich M J. Monitoring rotating tool wear using high order spectral features. ASME Transactions on Journal of Engineering for industry, 1993, 115: 23-29.

36. Wang W J, McFadden P D. Early detection of gear failure by vibration analysis – I: Calculation of the time-frequency distribution. Mechanical Systems and Signal Processing, 1993, 7 (3): 193-203.

37. Stazewski W J, Tomlinson G R. Local tooth fault detection in gearboxes using a moving window procedure. Mechanical Systems and Signal Processing, 1997, 11 (3): 331-350.

38. Meng Q F, Qu L S. Rotating machinery fault diagnosis using Wigner distribution. Mechanical Systems and Signal Processing, 1991, 5 (5): 155-166.

39. Chillaz M, Favre B. Engine noise characterization with Wigner-Ville time-frequency analysis. Mechanical Systems and Signal Processing, 1993, 7 (5): 375-400.

40. Baydar N, Ball A. A comparative study of acoustic and vibration signals in detection of gear failure using Wigner-Ville distribution. Mechanical Systems and Signal Processing, 2001, 15 (6): 1091-1107.

41. Lin J, Qu L S. Feature extraction based on Morlet wavelet and its application for mechanical fault diagnosis. Journal of Sound and Vibration. 2000, 234 (1): 135-148.

42. Peng Z K, Chu F L, He Y Y. Vibration signal analysis and feature extraction based on reassigned wavelet scalogram. Journal of Sound and Vibration. 2000, 253 (5): 1087-1100.

43. Cheng J S, Yu D J, Yang Y. Application of an impulse response wavelet to fault diagnosis of rolling bearings. Mechanical Systems and Signal Processing. 2007, 21 (2): 920-929.

44. Fan X F, Zuo M J. Gearbox fault detection using Hilbert and wavelet packet transform. Mechanical Systems and Signal Processing. 2006, 20 (4): 966-982.

45. W Loutridis S J. Instantaneous energy density as a feature for gear fault detection. Mechanical Systems and Signal Processing. 2006, 20 (5): 1239-1253.

46. Yu D J, Cheng J S, Yang Y. Application of EMD method and Hilbert spectrum to the fault diagnosis of roller bearings. Mechanical Systems and Signal Processing. 2005, 19 (2): 259-270.

47. Yang Y, Yu D J, Cheng J S. A fault diagnosis approach for roller bearing based on IMF envelope spectrum ans SVM. Measurement. 2007, 40 (9): 943-950.

48. Huang N E, Wu M-L C, Long S R, et al. A confidence limit for the empirical mode decomposition and Hilbert spectral analysis. Proceeding of the Royal Society of London A. 2003, 459: 2317-2345.

49. Boashash B. Estimating and interpreting the instantaneous frequency of a

signal-part 1: Fundamentals. Proceedings of the IEEE, 1992, 80 (4): 520-538.

50. Boashash B. Estimating and interpreting the instantaneous frequency of a signal-part 2: Algorithms and applications. Proceedings of the IEEE, 1992, 80 (4): 540-568.

51. Smith J S. The local mean decomposition and its application to EEG perception data. Journal of the Royal Society Interface. 2005, 2 (5): 443-454.

52. Cheng J S, Zhang K, Yang Y. An order tracking technique for the gear fault diagnosis using local mean decomposition method. Mechanism and Machine Theory. 2012, 55 (9): 67-76.

53. Wu Z H, Huang N E. Ensemble empirical mode decomposition: A noise-assisted data analysis method. Advances in Adaptive Data Analysis. 2009, 1 (1): 1-41.

54. Oyague F., 2009, Gearbox Modeling and Load Simulation of a Baseline 750-kW Wind Turbine Using State-of-the- Art Simulation Codes, Golden, Colorado.

55. Helsen J., Vandepitte D., and Desmet W., 2010, "Flexible modelling of wind turbine gearboxes with special focus on shaft flexibilities," Proceedings of 10th international conference on recent advances in structural dynamics (RASD).

56. Peeters J. L. M., Vandepitte D., and Sas P., 2006, "Analysis of internal drive train dynamics in a wind turbine," Wind Energy, 9(1-2), pp. 141–161.

57. Peeters J., 2006, "Simulation of Dynamic Drive Train Loads in a Wind Turbine," Katholieke Universiteit Leuven.

58. Musial W., Butterfield S., and McNiff B., 2007, "Improving wind turbine gearbox reliability," European Wind Energy Conference, Milan, Italy.

59. Crowther A., Ramakrishnan V., Zaidi N. A., and Halse C., 2011, "Sources of time-•varying contact stress and misalignments in wind turbine planetary sets," Wind Energy, 14(5), pp. 637–651.

60. Puigcorbe J., and De-Beaumont A., 2010, "Wind Turbine Gearbox Reliability: The impact of rotor support," Renewable Energy World Magazine.

61. Zimmerman G., 2010, "Tuned to the forces of nature," Mechanical Engineering, 132(5), pp. 46–49.

62. G. Dalpiaz, A. Rivola, R. Rubini, Effectiveness and sensitivity of vibration processing techniques for local fault detection in gears, Mechanical System and Signal Processing 14 (3) (2000) 387–412.

63. Yu, G.; Mallat, S.; Bacry, E. Audio denoising by time-frequency block thresholding. IEEE Trans. Signal Process. 2008, 56, 1830–1839.

64. Ephraim, Y.; Malah, D. Speech enhancement using a minimum mean square short-time spectral amplitude estimator. IEEE Trans. Acoust. Speech Signal Process. 1984, 32, 1109–1121.

65. Boll, S. Suppression of acoustic noise in speech using spectral subtraction. IEEE Trans. Acoust. Speech Signal Process. 1979, 27, 113–120.

66. Li, S.; Wan, M.X.; Wang, S.P. Multi-band spectral subtraction method for electrolarynx speech enhancement. Algorithms 2009, 2, 550–564.

67. N. E. Huang, Z. Shen, S. R. Long, M. C. Wu, H. H. Shih, Q. Zheng, N.-C. Yen, C. C. Tung, and H. H. Liu, "The empirical mode decomposition and the hilbert spectrum for nonlinear and non-stationary time series analysis," Proceedings of

the Royal Society of London. Series A: Mathematical, Physical and Engineering Sciences, vol. 454, no. 1971, pp. 903–995, 1998.

68. Nastaran R. Empirical Mode Decomposition and Analysis of Non-Stationary Cardiac Signals. Department of Electrical and Computer Engineering Ryerson University Toronto, Ontario, Canada. Aug 2013.

69. K.-M. Chang, "Ensemble empirical mode decomposition for high frequency ecg noise reduction," Biomedizinische Technik/Biomedical Engineering, vol. 55, no. 4, pp. 193–201, 2010.

70. B. Ghoraani, S. Krishnan, R. Selvaraj, and V. Chauhan, "Adaptive time-frequency matrix features for t wave alternans analysis," in Engineering in Medicine and Biology Society, 2009. EMBC 2009. Annual International Conference of the IEEE, pp. 39–42, IEEE, 2009.

71. Han, M. and J. Pan, A fault diagnosis method combined with LMD, sample entropy and energy ratio for roller bearings. Measurement, 2015. 76: p. 7-19.

72. Tian, Y., et al., Rolling bearing fault diagnosis under variable conditions using LMD-SVD and extreme learning machine. Mechanism and Machine Theory, 2015. 90: p. 175-186.

73. Guo, W., et al., Elimination of end effects in local mean decomposition using spectral coherence and applications for rotating machinery. Digital Signal Processing, 2016. 55: p. 52-63.

74. Cheng, J., Y. Yang, and Y. Yang, A rotating machinery fault diagnosis method based on local mean decomposition. Digital Signal Processing, 2012. 22(2): p. 356-366.

75. Huang, D., J. Zhao, and J. Su, Practical implementation of the Hilbert-Huang transform algorithm. Acta Oceanologica Sinica, 2002. 25(1): p. 1-11.

76. Gai, Q., X.-J. Ma, and H.-Y. Zhang, New method for processing end effect in local wave method. JOURNAL-DALIAN UNIVERSITY OF TECHNOLOGY, 2002. 42(1): p. 115-117.

77. [100] Yong-jun, D., et al., Comments and modifications on EMD method. Chinese Science Bulletin, 2001. 46(3): p. 257-263.

78. Guo, W., et al., Elimination of end effects in local mean decomposition using spectral coherence and applications for rotating machinery. Digital Signal Processing, 2016. 55: p. 52-63.

79. Wang, Y., Z. He, and Y. Zi, A demodulation method based on improved local mean decomposition and its application in rub-impact fault diagnosis. Measurement Science and Technology, 2009. 20(2): p. 025704.

80. Prabhakar, S., A.R. Mohanty, and A.S. Sekhar, Application of discrete wavelet transform for detection of ball bearing race faults. Tribology International, 2002. 35(12): p. 793-800.

81. Chen, J., et al., Wavelet transform based on inner product in fault diagnosis of rotating machinery: A review. Mechanical Systems and Signal Processing, 2016. 70: p. 1-35.

82. Lin, J. and L.S. Qu, Feature extraction based on Morlet wavelet and its application for mechanical fault diagnosis. Journal of Sound and Vibration,

2000. 234(1): p. 135-148.

83. Liu, H., A.N. Cartwright, and C. Basaran, Moiré interferogram phase extraction: a ridge detection algorithm for continuous wavelet transforms. Applied Optics, 2004. 43(4): p. 850-857.

84. Liu, Z., et al., A hybrid fault diagnosis method based on second generation wavelet de-noising and local mean decomposition for rotating machinery. ISA Transactions, 2016. 61: p. 211-220.

85. Yang, D.-M. Induction motor bearing fault detection with non-stationary signal analysis. in 2007 IEEE International Conference on Mechatronics. 2007. IEEE.

86. Zhi, Q., Sound Quality Improvement for Vehicle Noise Based on A Delayless Narrowband Active Sound Quality Equalizer Algorithm, in Department of Mechanical and Automotive Engineering. 2014, University of Ulsan.

87. Vikas Sharman, Anand Parey. Frequency domain averaging based experimental evaluation of gear fault without tachometer for fluctuating speed conditions. Mechanical Systems and Signal Processing 85 (2017) 278–295.

88. Bendat, J.S., The Hilbert Transform and Applications to Correlation Measurements, Brüel and Kjær Application Note BT0008-11.

89. Van der Pol, B., "The Fundamental Principles of Frequency Modulation", Journal of the IEE (London), Vol 93, pp. 153-158, 1946.

90. The Centre des Etudes Techniques des Industries Mécaniques de Senlis. Gear Data Center Test Seeded Fault Testdata. Available online: http://161.3.130.30/unecampagne.php?reference=13&langue=en&onglet=3 (accessed on 17 January 2011 Day Month Year).

91. MSC Software. ADAMS. http://www.mscsoftware.com/Contents/Products/CAE-Tools/ Adams.aspx.

92. MSC, 2012, "Adams 2012 Products Manual."

93. Johnson K. L., 1985, Contact Mechanics, Cambridge University Press.

94. "MSC Sim Companion-3-Example of using Hertzian Contact Theory to estimate contact stiffness."

95. Zhang, S.; Tang, J. Integrating angle-frequency domain synchronous averaging technique with feature extraction for gear fault diagnosis. Mech. Syst. Signal Process. 2018, 99, 711–729.

96. Li, Y.; Cheng, G.; Liu, C.; Chen, X. Study on planetary gear fault diagnosis based on variational mode decomposition and deep neural networks. Measurement 2018, 130, 94–104.

97. Sharma, V.; Parey, A. Frequency domain averaging based experimental evaluation of gear fault without tachometer for fluctuating speed conditions. Mech. Syst. Signal Process. 2017, 85, 278–295.

98. Cerrada, M.; Zurita, G.; Cabrera, D.; Sánchez, R.-V.; Artés, M.; Li, C. Fault diagnosis in spur gears based on genetic algorithm and random forest. Mech. Syst. Signal Process. 2016, 70–71, 87–103.

99. J.L. Chen, Y.Y. Zi, Z.J. He, Compound faults detection of rotating machinery using improved adaptive redundant lifting multiwavelet, Mech. Syst. Signal Process. 1 (5) (2013) 36e54.